KINETICS OF RAPID REACTIONS INVOLVING TWO PAIRS OF CONSECUTIVE SECOND ORDER STEPS

By H. G. Higgins* and E. J. Williams†

[*Manuscript received February* 20, 1953]

Summary

An examination is made of the kinetics of the reaction between A and B, where both reactants are capable of unifunctional behaviour, and A is also capable of bifunctional behaviour, for the general case in which the two reactive sites on A are not equivalent. Solutions are given of the appropriate rate equations for the two pairs of consecutive stages, and it is shown that the final concentrations of reactants and products can be related to given values of the initial concentrations and the velocity constants of the four second order stages. Relatively simple relations are established between the final concentrations and the ratio of the velocity constants for the case in which reaction at one position on A does not affect the reactivity of the other position. Some special cases of interest are considered. The results are related to the authors' earlier treatment of the case in which the initial reactivity of the two positions on A is initially the same. The theory is applied, by way of example, to the coupling of histidine with *p*-diazobenzenesulphonic acid, which appears to conform to the assumption of the same initial reactivity. The implications of the method in the correlation of molecular structure and reactivity are briefly discussed.

I. Introduction

In a previous paper (Higgins and Williams 1952) a kinetic treatment was presented appropriate to rapid reactions involving two consecutive second order steps, and relations were derived, for the final state, between the concentrations of the reactants and products and the ratio of the velocity constants of the two stages. The treatment was limited by the assumption that the reactivity of the two positions on the potentially bifunctional molecule was initially the same. In the more general case the reaction may be considered as taking place irreversibly in two *pairs* of consecutive stages :

$$(1) \quad A + B \xrightarrow{k_1} AB,$$

$$(2) \quad AB + B \xrightarrow{k_2} BAB,$$

$$(3) \quad A + B \xrightarrow{k_3} BA,$$

$$(4) \quad BA + B \xrightarrow{k_4} BAB,$$

where the reactants A and B are both capable of unifunctional behaviour, and A is also capable of bifunctional behaviour, and where k_1, k_2, k_3, and k_4 are the velocity constants of the stages shown. A can react initially with B at either

* Division of Forest Products, C.S.I.R.O., Melbourne.

† Section of Mathematical Statistics, C.S.I.R.O., at Division of Forest Products, C.S.I.R.O., Melbourne.

of two *non-equivalent* positions to produce the isomers AB and BA, both of which are capable of reacting with another molecule of B at the remaining position to produce BAB.

In the present paper general solutions are given of the appropriate rate equations for this type of reaction, and relatively simple relations are established between the final concentrations and the ratio of the velocity constants for the case where reaction at one position on molecule A does not affect the reactivity of the other position.

Although it is not possible to evaluate the velocity constants by means of the methods described, it should be possible in suitable circumstances to obtain reliable estimates of their ratios and to relate them to basic electronic phenomena. The method bears some analogies to the " competition method " instituted by Ingold and Shaw (1927) for determining the effect of a substituent on aromatic reactivity. From the overall relative rates of reaction of the substituted benzene with respect to benzene itself, Ri and Eyring (1940) calculated the charges on the nuclear carbon atoms of several monosubstituted benzenes by applying the theory of absolute reaction rates (see review by Ferguson 1952). The basic problem of theoretical organic chemistry is posed by Dewar (1951) as the prediction of the way in which a given change in the structure of a molecule will influence its reactivity, and any experimental method should be of use which can help to provide data against which different methods of correlating structure and reactivity can be tested.

Since the completion of the present manuscript, recent papers by Stephukovich and Timonin (1951), Schwemer and Frost (1951), and Frost and Schwemer (1952) have come to the authors' attention. These deal with aspects of the theory of the kinetics of consecutive second order reactions, but do not anticipate the treatment given below.

II. Theory

(*a*) *General*

Let c with appropriate subscript denote the molar concentrations at time t, and x_1, x_2, x_3, x_4 denote the fall in the concentrations of A, AB, A, and BA respectively in time t due to the individual reactions 1, 2, 3, and 4. The initial concentrations of A and B are a and b respectively and of AB, BA, and BAB are zero. (C will subsequently be used for corresponding final concentrations.)

Then

$$a-(x_1+x_3)=c_A, \quad \ldots\ldots\ldots\ldots\ldots (1)$$

$$b-(x_1+x_2+x_3+x_4)=c_B, \quad \ldots\ldots\ldots\ldots\ldots (2)$$

$$x_1-x_2=c_{AB}, \quad \ldots\ldots\ldots\ldots\ldots (3)$$

$$x_3-x_4=c_{BA}, \quad \ldots\ldots\ldots\ldots\ldots (4)$$

and

$$x_2+x_4=c_{BAB}. \quad \ldots\ldots\ldots\ldots\ldots (5)$$

From the law of mass action

$$dx_1/dt=k_1(a-x_1-x_3)(b-x_1-x_2-x_3-x_4), \quad \ldots\ldots\ldots (6)$$

$$dx_2/dt=k_2(x_1-x_2)(b-x_1-x_2-x_3-x_4), \quad \ldots\ldots\ldots (7)$$

$$dx_3/dt=k_3(a-x_1-x_3)(b-x_1-x_2-x_3-x_4), \quad \ldots\ldots\ldots (8)$$

and

$$dx_4/dt = k_4(x_3 - x_4)(b - x_1 - x_2 - x_3 - x_4). \quad \ldots\ldots\ldots (9)$$

Eliminating t from these equations

$$\frac{x_1}{k_1} = \frac{x_3}{k_3}, \quad \ldots\ldots\ldots (10)$$

$$\frac{dx_2}{dx_3} = \frac{k_2}{k_3}\,\frac{(k_1x_3 - k_3x_2)}{(k_3a - (k_1+k_3)x_3)}, \quad \ldots\ldots\ldots (11)$$

$$\frac{dx_4}{dx_3} = k_4\frac{(x_3 - x_4)}{k_3a - (k_1+k_3)x_3}. \quad \ldots\ldots\ldots (12)$$

For (11), the integrating factor is

$$[k_3a - (k_1+k_3)x_3]^{-k_2/(k_1+k_3)},$$

giving

$$-k_3[k_3a - (k_1+k_3)x_3]^{-k_2/(k_1+k_3)}dx_2$$

$$+k_2(k_1x_3 - k_3x_2)[k_3a - (k_1+k_3)x_3]^{-1-k_2/(k_1+k_3)}dx_3 = 0,$$

provided $k_1+k_3 \neq k_2$. Hence, with the constant inferred from the initial conditions $x_2 = x_3 = 0$, we have

$$(k_1x_3 - k_3x_2)[k_3a - (k_1+k_3)x_3]^{-k_2/(k_1+k_3)} + \frac{k_1[k_3a - (k_1+k_3)x_3]^{1-k_2/(k_1+k_3)}}{k_1+k_3-k_2}$$

$$= \frac{k_1(k_3a)^{1-k_2/(k_1+k_3)}}{k_1+k_3-k_2}. \quad \ldots\ldots\ldots (13)$$

For (12), the integrating factor is

$$[k_3a - (k_1+k_3)x_3]^{-k_4/(k_1+k_3)},$$

giving

$$-[k_3a - (k_1+k_3)x_3]^{-k_4/(k_1+k_3)}dx_4 + k_4(x_3 - x_4)[k_3a - (k_1+k_3)x_3]^{-1-k_4/(k_1+k_3)}dx_3 = 0.$$

The integral is

$$(x_3 - x_4)[k_3a - (k_1+k_3)x_3]^{-k_4/(k_1+k_3)} + \frac{[k_3a - (k_1+k_3)x_3]^{1-k_4/(k_1+k_3)}}{k_1+k_3-k_4}$$

$$= \frac{(k_3a)^{1-k_4/(k_1+k_3)}}{k_1+k_3-k_4}. \quad \ldots\ldots\ldots (14)$$

These general solutions may be expressed as

$$k_3(k_1+k_3-k_2)x_2 = k_1k_3a - k_1k_2x_3 - k_1(k_3a)^{1-[k_2/(k_1+k_3)]}[k_3a - (k_1+k_3)x_3]^{k_2/(k_1+k_3)}, \quad \ldots\ldots\ldots (15)$$

and as

$$(k_1+k_3-k_4)x_4 = k_3a - k_4x_3 - (k_3a)^{1-k_4/(k_1+k_3)}[k_3a - (k_1+k_3)x_3]^{k_4/(k_1+k_3)}. \quad \ldots\ldots\ldots (16)$$

(b) Final State

(i) When $a < b/2$: Here the initial concentration of B is sufficient for each molecule of AB and BA formed to be finally converted to BAB, so that $x_1 = x_2$, $x_3 = x_4$, and $x_1 + x_3 = a$.

The final concentrations, C, are then given, from equations (1) to (5), by

$$C_A=C_{AB}=C_{BA}=0\,;\quad C_B=b-2a\,;\quad C_{BAB}=a. \quad \ldots\ldots\ldots (17)$$

These solutions are the same as for the simpler treatment (Higgins and Williams 1952) and it is only when $a>b/2$ that the more general solutions which emerge, involving the ratios of the velocity constants, differ in form from the previous treatment.

(ii) When $a>b/2$: Here the final concentrations of AB, BA, and BAB will depend on the ratios of the velocity constants, since B must react with A to produce AB and BA, then with AB and BA to produce BAB. As A is present in sufficient concentration initially for all the molecules of B to react eventually, the substances present finally will be A, AB, BA, and BAB. Thus

$$x_1+x_2+x_3+x_4=b, \quad \ldots\ldots\ldots\ldots\ldots\ldots (18)$$

and $C_B=0$. Since equations (10), (15), and (16) hold at all times, the final state condition (18) would provide a value of x_3 corresponding to given values of a, b, and k's. From the values of x's so determined the final concentrations could be found by means of equations (1), (3), (4), and (5).

From observation of a, b, and the final concentrations it is similarly possible to derive relationships between the velocity constants. The large number of variables, however, makes it difficult to tabulate the ratios of the velocity constants in terms of the final concentrations, nor can the relationships be expressed in readily accessible graphical form, as was done for the simpler case previously treated.

We may, however, obtain more easily manageable results in certain other special cases of interest, one of which is considered below.

(c) *Reaction at Independent Positions*

Probably no two reactive positions on molecule A can be regarded as altogether independent, in the sense that reaction with B at one position will not affect the velocity constant for reaction at the other. However, in certain circumstances, dependent on such factors as the distance between the reacting sites on A, the extent of their electronic insulation from each other and the extent to which steric hindrance by the first B group accepted affects the accessibility of the second position, virtual independence may be achieved. In this case the following special conditions would be expected to hold:

$$k_1=k_4\,;\qquad k_2=k_3.$$

Since the ratios of the velocity constants, rather than their absolute values, determine the concentrations at times inversely proportional to the rate constants, we may, without loss of generality, put $k_1=1$ and $k_2=K$, so that $K=k_2:k_1$. Then, from (15),

$$Kx_2=K(a-x_3)-(Ka)^{1/(1+K)}[Ka-(1+K)x_3]^{K/(1+K)},$$

or, on expressing x_3 in terms of x_1,

$$x_2=a-Kx_1-a^{1/(1+K)}[a-(1+K)x_1]^{K/(1+K)}, \quad \ldots\ldots (19)$$

and, from (16),

$$Kx_4=Ka-x_3-(Ka)^{K/(1+K)}[Ka-(1+K)x_3]^{1/(1+K)},$$

or

$$x_4 = a - x_1 - a^{K/(1+K)}[a-(1+K)x_1]^{1/(1+K)}. \quad \ldots\ldots\ldots (20)$$

Upon applying the final condition (18) for $a > b/2$, we get

$$b = 2a - a^{1/(1+K)}[a-(1+K)x_1]^{K/(1+K)} - a^{K/(1+K)}[a-(1+K)x_1]^{1/(1+K)}. \quad \ldots (21)$$

Now, substituting from (10) in (1)

$$C_A = a-(1+K)x_1, \quad \ldots\ldots\ldots\ldots\ldots (22)$$

so that (21) becomes

$$b = 2a - a^{1/(1+K)}C_A^{K/(1+K)} - a^{K/(1+K)}C_A^{1/(1+K)}. \quad \ldots\ldots\ldots (23)$$

Upon dividing by a

$$\frac{b}{a} = 2 - \left(\frac{C_A}{a}\right)^{K/(1+K)} - \left(\frac{C_A}{a}\right)^{1/(1+K)}. \quad \ldots\ldots\ldots\ldots (24)$$

Thus we may tabulate b/a in terms of C_A/a and K, and hence, in conformity with the method of presentation previously used, we may tabulate, or plot, corresponding values of a/b and C_A/b for given values of K. Observation of C_A when a and b are known will then permit K to be determined.

It may be more convenient to determine the final concentrations of the products AB, BA, and BAB than the residual concentration of A, which is then given from equations (1), (3). (4), and (5) by

$$C_A = a - (C_{AB} + C_{BA} + C_{BAB}), \quad \ldots\ldots\ldots\ldots (25)$$

when all the products are determined. However, individual determinations of C_{AB}, C_{BA}, or C_{BAB} will also permit K to be found. For, from (3) and (19),

$$C_{AB} = x_1(1+K) - a + a^{1/(1+K)}[a-(1+K)x_1]^{K/(1+K)},$$

whence

$$\frac{C_{AB}}{a} = \left(\frac{C_A}{a}\right)^{K/(1+K)} - \frac{C_A}{a}, \quad \ldots\ldots\ldots\ldots\ldots (26)$$

and, from (4) and (20)

$$\frac{C_{BA}}{a} = \left(\frac{C_A}{a}\right)^{1/(1+K)} - \frac{C_A}{a}. \quad \ldots\ldots\ldots\ldots\ldots (27)$$

From (5) and the steps leading to (26) and (27)

$$\frac{C_{BAB}}{a} = 1 - \left(\frac{C_A}{a}\right)^{K/(1+K)} - \left(\frac{C_A}{a}\right)^{1/(1+K)} + \left(\frac{C_A}{a}\right). \quad \ldots. (28)$$

The values of C_{AB}/a, C_{BA}/a, and C_{BAB}/a corresponding to C_A/a can now be tabulated for the same series of K values as used above, and since corresponding values of a/b are available from (24), the corresponding values of C_{AB}/b, C_{BA}/b, and C_{BAB}/b can be derived from them. Thus we may plot the various final concentrations in terms of a/b for any given value of K.

Conforming still to the conditions of the above section (final state, independent positions) we may consider a special case which defines certain limits of the above solutions and which does not readily emerge from the equations. This is when one of the two positions on molecule A is very much more reactive than the other, so that K is either very small or very large, but not zero or ∞, that is, when $k_1 \gg k_2$ or $k_2 \gg k_1$.

(i) $k_1 \gg k_2$: Since stage 1 of the reaction takes place very much faster than stage 3, a molecule of B may be considered to react with A to form AB in preference to BA until either A or B is exhausted, and AB proceeds to the formation of BAB only when molecules of B are available surplus to the requirements of stage 1, that is, when $a<b$. Stages 3 and 4 are eliminated and the remainder of the reaction proceeds according to stage 2.

Hence, when $a>b$,

$$C_{AB}=b\,;\quad C_A=a-b\,;\quad C_{BA}=C_{BAB}=C_B=0,\quad \ldots\ldots\ (29)$$

and when $b>a>b/2$.

$$C_{BAB}=b-a\,;\quad C_{AB}=a-(b-a)=2a-b\,;\quad C_A=C_B=C_{BA}=0.\quad \ldots\ (30)$$

(ii) $k_2 \gg k_1$: The solutions are the same as (29) and (30) with AB and BA interchanged.

The theoretical final concentrations of the reactants and products have now been defined for all cases (except that in which either or both pairs of equal velocity constants are zero, the solution of which is almost self-evident), and in Figures 1–3 the relationship between these final concentrations and the initial values of the reactants are shown for specific values of $k_2 : k_1$.

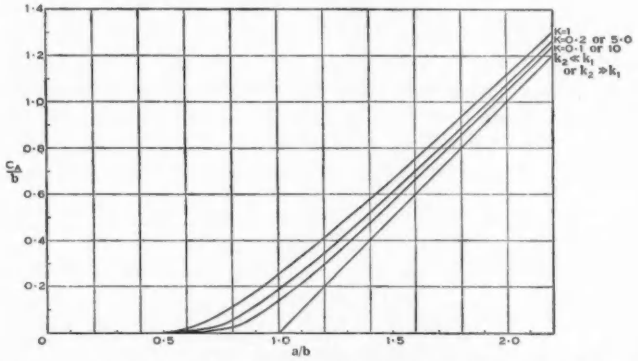

Fig. 1.—Relation between initial and final concentrations of A for various ratios of velocity constants.

It follows also from equations (26), (27), and (28) that C_{AB}/a, C_{BA}/a, or C_{BAB}/a can be plotted as functions of C_A/a for specific values of K, and that K can therefore be determined even when a/b is unknown, provided the assumption of independence is known to be justified. This procedure may be useful in cases in which one of the reactants has first to be formed from another substance in an undetermined yield.

(*d*) *Relation between Ratio of Velocity Constants and Final Concentrations When* a/b *is Constant*

It can be seen from Figures 1 and 3 that, as K is varied, the final concentrations of A and BAB have a rather small range for a given value of a/b. The maximum range, one-quarter of the initial concentration of B, occurs when

$a/b=1$. It will therefore be of advantage, particularly when using C_A or C_{BAB} to determine K, to be able to express their relationships directly for constant values of a/b, and similar expressions for C_{AB} and C_{BA} will also be useful.

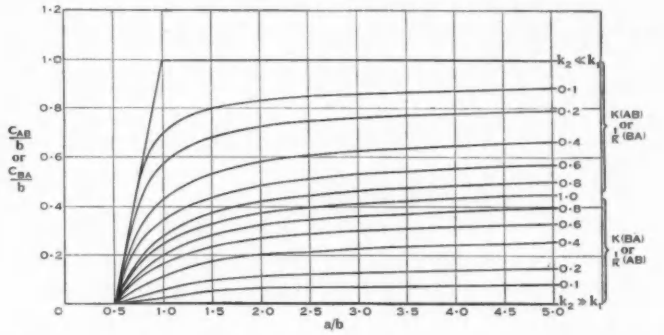

Fig. 2.—Dependence of final concentrations of AB and BA on initial concentration of A for various ratios of velocity constants.

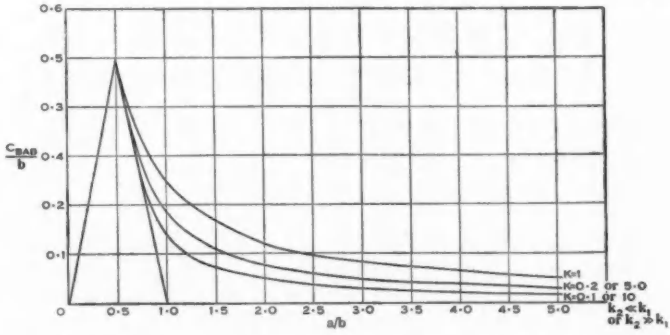

Fig. 3.—Dependence of final concentration of BAB on initial concentration of A for various ratios of velocity constants.

If we put

$$\left(\frac{C_A}{a}\right)^{1/(1+K)}=y\ ;\quad \frac{C_A}{a}=y^{1+K},$$

then, from (**24**),

$$y^K=2-\frac{b}{a}-y,$$

so that

$$\frac{C_A}{a}=y\left(2-\frac{b}{a}-y\right), \quad \ldots\ldots\ldots\ldots\ldots\ldots (31)$$

and

$$K=\frac{\log\left(2-\frac{b}{a}-y\right)}{\log y}. \quad \ldots\ldots\ldots\ldots (32)$$

Further, from (26), (27), and (28),

$$\frac{C_{AB}}{a}=2-\frac{b}{a}-y-\frac{C_A}{a}, \quad \ldots\ldots\ldots\ldots (33)$$

$$\frac{C_{BA}}{a}=y-\frac{C_A}{a}, \quad \ldots\ldots\ldots\ldots (34)$$

$$\frac{C_{BAB}}{a}=\frac{C_A}{a}+\frac{b}{a}-1, \quad \ldots\ldots\ldots\ldots (35)$$

By assuming a series of values of y, for any constant value of a/b, a series of corresponding values of C_A/a, and hence C_A/b, and K may be tabulated from (31) and (32), and the corresponding final concentrations of the other constituents may then readily be calculated from (33), (34), and (35). When $a=b$, the above equations reduce to very simple terms, and the dependence of the final concentrations on K is as shown in Figure 4. In this case $C_A=C_{BAB}$.

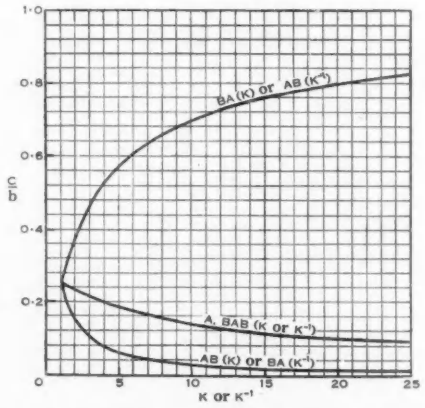

Fig. 4.—Dependence of final concentrations on ratio of velocity constants for independent positions when $a=b$; $(K=k_2:k_1)$.

(e) Coincidence of Functions Resulting from Different Physical Assumptions

One situation exists in which ambiguous conclusions may be drawn from apparent conformity with either the assumption of the same initial reactivity of the two positions (Higgins and Williams 1952) or that of the independence of the two reactive positions. Physically this is the case in which

$$k_1=k_2=k_3=k_4,$$

that is, the reactivity of each *position*, regardless of the state of the other, is the same. The overall reactivity of the molecule A is reduced by half upon reaction at one position, so that a value for k_2/k_1 of $\frac{1}{2}$ is obtained by assuming the same initial reactivity, whereas a value for k_2/k_1 of 1 is obtained by assuming independence of the positions. This may be readily confirmed mathematically. By inserting the value $\frac{1}{2}$ for k_2/k_1 in equation (**12**) of the 1952 paper, we get

$$\frac{b}{a}=2-2\sqrt{\frac{C_A}{a}}, \quad \ldots\ldots\ldots\ldots\ldots\ldots \quad (36)$$

and from equations (**13**) and (**14**) of the same paper

$$\frac{C_{AB}}{a}=2-\frac{b}{a}-2\frac{C_A}{a}, \quad \ldots\ldots\ldots\ldots\ldots\ldots \quad (37)$$

and

$$\frac{C_{BAB}}{a}=\frac{b}{a}-1+\frac{C_A}{a}. \quad \ldots\ldots\ldots\ldots\ldots\ldots \quad (38)$$

By inserting the value 1 for k_2/k_1 in equation (**24**) of the present paper, we get equation (**36**), and in equations (**26**), (**27**), and (**28**) we get, upon substituting from (**36**)

$$\frac{C_{AB}}{a}=\frac{C_{BA}}{a}=1-\frac{b}{2a}-\frac{C_A}{a}, \quad \ldots\ldots\ldots\ldots\ldots\ldots \quad (39)$$

so that

$$\frac{C_{AB}+C_{BA}}{a}=2-\frac{b}{a}-2\frac{C_A}{a},$$

as in (**37**), and

$$\frac{C_{BAB}}{a}=\frac{b}{a}-1+\frac{C_A}{a},$$

as in (**38**).

The significance of these equations is that they represent the only circumstances (apart from limiting cases) in which the form of the functions coincides for the assumptions of same initial reactivity and of independence of the positions. On the basis of the first concept, however, the velocity constant k_1, referring to the whole molecule A, is clearly twice the value of the k_1 which refers, on the basis of the second concept, to only one reactive position.

III. Application to Coupling of Histidine with *p*-Diazobenzenesulphonic Acid

It has been shown by Higgins and Fraser (1952) that the widely used coupling reaction of Pauly (1905) between histidine and *p*-diazobenzenesulphonic acid may lead to the formation of either mono- or bisazo-derivatives with absorption maxima at 380 and 490 mμ respectively. Diazotization of sulphanilic acid by means of nitrous acid is followed by coupling under alkaline conditions of the diazotized sulphanilic acid with histidine. A series of azo-derivatives was prepared, the concentration of sulphanilic acid being kept constant and that of the histidine varied over a wide range. Reagents and procedure were the same

as described previously (Higgins and Fraser 1952) except for initial concentrations of histidine and of sulphanilic acid. The extinctions were measured at 380 and 490 mμ, and are shown in Figure 5 as functions of the initial histidine concentration ; the initial concentration of sulphanilic acid was kept constant at 0·32 g/l. Histidine can be identified with the substance *A* of the kinetic treatment developed in this paper and the *p*-diazobenzenesulphonic acid which is formed in the acid solution with the substance *B*. The theory demands quite generally, regardless of the relations between the four velocity constants, that when $a/b=0\cdot5$ the final concentrations of *BAB* (in this case the bisazo-derivative) should reach its maximum value of $b/2$ and that at the same value of a/b the final concentrations of the intermediates should be zero.

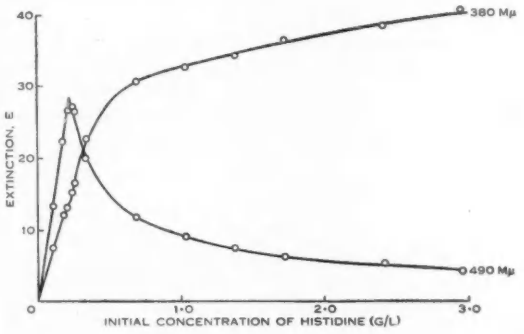

Fig. 5.—Observed extinctions, attributable to azo-derivatives of histidine.

The spectrophotometric studies of the coupling reaction (Higgins and Fraser 1952) revealed the presence of only one monoazo-derivative. Since *AB* and *BA* are not readily distinguishable spectrophotometrically, absorbing at the same wavelength, it will be assumed that their molecular extinction coefficients are also equal. If this is so the extinction *E* of the system is given by

$$E=C_{BAB}\varepsilon_{BAB}+C_{AB}\varepsilon_{AB}, \quad \ldots\ldots\ldots\ldots\ldots\ldots (40)$$

where ε denotes the molecular extinction coefficient and where C_{AB} now refers to the sum of the final concentrations of *AB* and *BA*. When $a/b=0\cdot5$, we now have

$$E_{380}=13\cdot8,\ E_{490}=28\cdot6,\ C_{BAB}/b=0\cdot5,\ C_{AB}/b=0,$$

so that from (40)

$$b\varepsilon^{490}_{BAB}=\frac{E_{490}}{C_{BAB}/b}=57\cdot2,$$

and

$$b\varepsilon^{380}_{BAB}=\frac{E_{380}}{C_{BAB}/b}=27\cdot6.$$

As $a/b \to \infty$, $C_{AB}/b \to 1$ and $C_{BAB}/b \to 0$, again regardless of the relations between the velocity constants. By extrapolation the limiting values of the extinctions are

$$E_{380} \to 41 \cdot 5, \quad E_{490} \to 2 \cdot 66,$$

so that from (**40**)

$$b\varepsilon_{AB}^{380} = \frac{E_{380}}{C_{AB}/b} = 41 \cdot 5,$$

and

$$b\varepsilon_{AB}^{490} = \frac{E_{490}}{C_{AB}/b} = 2 \cdot 66.$$

Equation (**40**) now takes the simultaneous form

$$E_{380} = 27 \cdot 6\frac{C_{BAB}}{b} + 41 \cdot 5\frac{C_{AB}}{b},$$

$$E_{490} = 57 \cdot 2\frac{C_{BAB}}{b} + 2 \cdot 66\frac{C_{AB}}{b},$$

giving

$$\frac{C_{BAB}}{b} = 10^{-3}(-1 \cdot 16E_{380} + 18 \cdot 0E_{490}), \quad \ldots\ldots\ldots \quad (41)$$

$$\frac{C_{AB}}{b} = 10^{-3}(24 \cdot 9E_{380} - 12 \cdot 0E_{490}). \quad \ldots\ldots\ldots\ldots \quad (42)$$

Solution of these equations for the values of E given in Figure 5 yields the values of C_{AB}/b and C_{BAB}/b which are shown in Figure 6 (curves 2 and 5) as functions of a/b. The values of a/b were calculated from the initial histidine

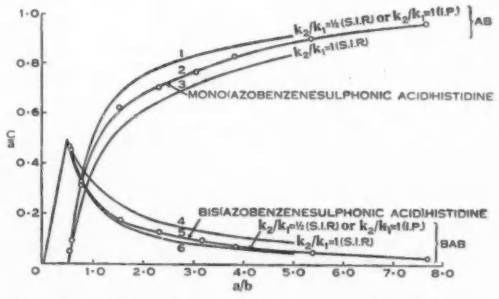

Fig. 6.—Observed relations between final concentrations of mono- and bis-(azobenzenesulphonic acid)histidine and initial concentration of histidine, compared with theoretical curves for *AB* and *BAB*. (The assumption of the same initial reactivity is denoted by S.I.R. and that of independent positions by I.P.)

concentrations by taking the maximum in the curve for the extinction at 490 mμ (Fig. 5) as $a/b = 0 \cdot 5$. The theoretical curves also shown for C_{AB} and C_{BAB} refer to values for k_2/k_1 of $\frac{1}{2}$ and 1 in the 1952 treatment (same initial reactivity of two positions), and it can be seen that all the experimental points fall between

these two lines, suggesting that the data support the assumptions upon which this treatment is based and that the reactivity of the imidazole ring of histidine after accepting the first diazonium group is only about 0·7 times its initial reactivity. This means that the reactivity of an individual position is *increased* by twice this factor.

The data do not conform to the case in which the independence of the two reactive positions is assumed. The curves for $k_2/k_1=1$ on this assumption are the same, as shown in Section III (*e*), as those for $k_2/k_1=\frac{1}{2}$ on the assumption of the same initial reactivity. The deviation from this special case, however, expressed for example by curves 5 and 6 of Figure 6, is sufficiently small to permit the possibility of a considerable degree of independence between the two positions.

The conclusion that the two positions are not completely independent is in agreement with the evidence provided by the absorption spectra themselves, which show a large displacement in the wavelength of maximum absorption when the second reactive position on the imidazole ring is occupied by a diazonium group.

IV. Acknowledgments

The assistance of Mr. K. J. Harrington and of the computing staff of the Section of Mathematical Statistics is acknowledged with thanks. Helpful comments on the manuscript have been made by Dr. K. L. Sutherland and Mr. D. E. Bland. Dr. S. J. Leach has suggested that the treatment might be applicable to peptide hydrolysis and peptide synthesis.

V. References

Dewar, M. J. S. (1951).—*Ann. Rep. Progr. Chem.* **48**: 112.
Ferguson, L. N. (1952).—*Chem. Rev.* **50**: 47.
Frost, A. A., and Schwemer, W. C. (1952).—*J. Amer. Chem. Soc.* **74**: 1268.
Higgins, H. G., and Fraser, D. (1952).—*Aust. J. Sci. Res.* A **5**: 736.
Higgins, H. G., and Williams, E. J. (1952).—*Aust. J. Sci. Res.* A **5**: 572.
Ingold, C. K., and Shaw, F. R. (1927).—*J. Chem. Soc.* **1927**: 2918.
Pauly, H. (1905).—*Hoppe-Seyl. Z.* **44**: 159.
Ri, T., and Eyring, H. (1940).—*J. Chem. Phys.* **8**: 433.
Schwemer, W. C., and Frost, A. A. (1951).—*J. Amer. Chem. Soc.* **73**: 4541.
Stephukovich, A. D., and Timonin, L. M. (1951).—*J. Phys. Chem., Moscau* **25** (2): 143.

DETERMINATION OF ACTIVITY COEFFICIENTS FROM TOTAL PRESSURE MEASUREMENTS

By J. A. Barker*

[*Manuscript received March* 12, 1953]

Summary

A method of least squares is described for calculating activity coefficients from results of total vapour pressure measurements.

I. Introduction

The present paper describes a procedure, based on the method of least squares, for calculating activity coefficients for solutions from total vapour pressures. Although several methods are described in the literature (see, for example, Musil and Schramke 1949*a*, 1949*b*; Redlich and Kister 1949), there is no systematic method capable of extracting the best results from given experimental data, with due allowance for vapour phase non-ideality.

The author believes that activity coefficients derived from total pressure measurements can be comparable in accuracy with those derived from the more difficult partial pressure measurements, particularly for solutions of high relative volatility where the difficulty of obtaining a vapour sample in true equilibrium with the liquid is most marked. This belief is supported by the example worked below. A general discussion of the relative advantages of total and partial pressure measurements is given by Scatchard (1952).

The activity coefficients and excess chemical potentials are given by the equations (Scatchard and Raymond 1938):

$$\left.\begin{aligned}\mu_1^E &= RT \ln \gamma_1 \\ &= RT \ln (Py_1/P_1x_1) + (V_1-\beta_{11})(P_1-P) + P\delta_{12}y_2^2, \\ \mu_2^E &= RT \ln \gamma_2 \\ &= RT \ln (Py_2/P_2x_2) + (V_2-\beta_{22})(P_2-P) + P\delta_{12}y_1^2.\end{aligned}\right\} \quad \ldots\ldots\ldots\ldots \quad (1)$$

Here μ_1^E and μ_2^E are the changes in chemical potentials in excess of the changes for an ideal solution, P is the total pressure, P_1 and P_2 are the vapour pressures of the pure components, x and y are liquid and vapour mole fractions respectively, γ_1 and γ_2 are activity coefficients, V_1 and V_2 are liquid molar volumes, β_{11}, β_{22}, and β_{12} are second virial coefficients in the equations of state of the pure and mixed vapours, and $\delta_{12}=2\beta_{12}-\beta_{11}-\beta_{22}$.

It follows from equations (1) that the total pressure is given by

$$P=\gamma_1 p_1' + \gamma_2 p_2', \quad \ldots\ldots\ldots\ldots\ldots\ldots\ldots\ldots \quad (2)$$

$$p_1' = x_1 P_1 \exp [(V_1-\beta_{11})(P-P_1)/RT - P\delta_{12}y_2^2/RT], \quad \ldots\ldots \quad (3)$$

$$p_2' = x_2 P_2 \exp [(V_2-\beta_{22})(P-P_2)/RT - P\delta_{12}y_1^2/RT]. \quad \ldots\ldots \quad (4)$$

* Division of Industrial Chemistry, C.S.I.R.O., Melbourne.

The symbols p_1' and p_2', introduced for brevity and defined by equations (3) and (4), represent the values the partial pressures would have if the liquid solution were ideal but the vapour phase remained non-ideal.

It has been usual in the past to assume that the mixture virial coefficient β_{12} is the arithmetic mean of β_{11} and β_{22}, so that δ_{12} is zero. This assumption does not lead to serious error for solutions of non-polar components, but Scatchard and Ticknor (1952) showed that it could be a serious source of error for solutions containing associated liquids. In describing the method we shall therefore not assume that δ_{12} is zero.

We assume that the concentration dependence of the excess free energy of mixing can be described by the equation (Scatchard 1949)

$$\begin{aligned} G_x^E &= x_1\mu_1^E + x_2\mu_2^E \\ &= x_1x_2[a + b(x_1-x_2) + c(x_1-x_2)^2 + \dots]. \end{aligned} \quad \dots\dots\dots\dots \quad (5)$$

If $b=c=\dots=0$, equation (5) has the form appropriate for a regular solution. An equation of the form (5), with sufficient terms, can represent measured values of G_x^E with any desired accuracy.

Equation (5) implies that the activity coefficients are given by

$$\left.\begin{aligned} \ln\gamma_1 &= Al_1 + Bm_1 + Cn_1 + \dots, \\ \ln\gamma_2 &= Al_2 + Bm_2 + Cn_2 + \dots, \end{aligned}\right\} \quad \dots\dots\dots\dots\dots\dots \quad (6)$$

where

$$\left.\begin{aligned} l_1 &= x_2^2,\ m_1 = -x_2^2(1-4x_1),\ n_1 = x_2^2(1-8x_1+12x_1^2), \\ l_2 &= x_1^2,\ m_2 = +x_1^2(1-4x_2),\ n_2 = x_1^2(1-8x_2+12x_2^2), \end{aligned}\right\} \quad \dots\dots \quad (7)$$

and

$$A = a/RT,\ B = b/RT,\ C = c/RT. \quad \dots\dots\dots\dots \quad (8)$$

II. Description of Method

We determine the constants A, B, C by a process of successive approximations. To find a first approximation we assume that the solution behaves like a regular solution, so that B and C are zero. If we neglect the corrections for vapour phase non-ideality, then A is given by

$$A = 4\ln\left(\frac{2P^*}{P_1+P_2}\right),$$

where P^* is the pressure for the equimolar mixture, which can be estimated graphically. Using this value of A we can calculate approximate vapour concentrations which are sufficiently accurate to use in the small correction term $P\delta_{12}y^2/RT$ in equations (3) and (4).

We now calculate p_1', p_2' for the experimental liquid compositions. Using the first approximation for A, we calculate γ_1 and γ_2 by equations (6), P by equation (2), the pressure residuals $R = P_{\text{expt.}} - P_{\text{calc.}}$, and the derivatives dP/dA, dP/dB, dP/dC, which are given by

$$\left.\begin{aligned} dP/dA &= l_1\gamma_1p_1' + l_2\gamma_2p_2', \\ dP/dB &= m_1\gamma_1p_1' + m_2\gamma_2p_2', \\ dP/dC &= n_1\gamma_1p_1' + n_2\gamma_2p_2', \end{aligned}\right\} \quad \dots\dots\dots \quad (9)$$

We determine the changes δA, δB, δC in A, B, C which will most nearly reduce the pressure residuals to zero, by fitting by least squares to the equation

$$(dP/dA)\delta A+(dP/dB)\delta B+(dP/dC)\delta C=R. \quad \ldots\ldots\ldots (10)$$

That is, we solve the equations

$$\left.\begin{aligned}
\delta A\Sigma(dP/dA)^2+\delta B\Sigma(dP/dA)(dP/dB)+\delta C\Sigma(dP/dA)(dP/dC) &= \Sigma R(dP/dA),\\
\delta A\Sigma(dP/dA)(dP/dB)+\delta B\Sigma(dP/dB)^2+\delta C\Sigma(dP/dB)(dP/dC) &= \Sigma R(dP/dB),\\
\delta A\Sigma(dP/dA)(dP/dC)+\delta B\Sigma(dP/dB)(dP/dC)+\delta C\Sigma(dP/dC)^2 &= \Sigma R(dP/dC),
\end{aligned}\right\}$$
$$\ldots\ldots\ldots\ldots\ldots\ldots (11)$$

where the summations Σ are taken over all the experimental points.

Adding these increments to the initial values of A, B, C we find improved approximations. Since the second derivatives of P with respect to A, B, C are not zero, these are not necessarily the best values, and it may be necessary to repeat the process until A, B, C do not change significantly. In practice, it is not necessary to recalculate the derivatives dP/dA etc. at each stage.

We illustrate the method using the data of Brown (1952) on the system benzene+n-heptane at 80 °C. The second virial coefficients used were those given by Brown ; in particular δ_{12} was assumed to be zero. In Table 1 we give

TABLE 1

SUCCESSIVE APPROXIMATIONS TO A, B, AND C

x_1	$P_{\text{expt.}}$ (mm)	Pressure residuals, $P_{\text{expt.}}-P_{\text{calc.}}$ (mm)			$y_{1\text{calc.}}$	$y_{1\text{expt.}}$
		$A=0\cdot3859$ $B=C=0$	$A=0\cdot3592$ $B=0\cdot0845$ $C=0\cdot0366$	$A=0\cdot3620$ $B=0\cdot0891$ $C=0\cdot0261$		
0·0464	454·62	−3·35	−0·48	−0·11	0·0993	0·0988
0·0861	476·25	−5·73	−0·60	−0·15	0·1734	0·1729
0·2004	534·38	−7·30	+0·25	+0·31	0·3463	0·3473
0·2792	569·49	−7·04	−0·11	−0·42	0·4409	0·4412
0·3842	613·53	−3·27	+1·08	+0·44	0·5458	0·5464
0·4857	650·16	−2·72	+1·07	+0·39	0·6310	0·6304
0·5824	679·74	+1·51	−0·33	−0·87	0·7016	0·7009
0·6904	708·78	+4·37	+0·15	−0·14	0·7749	0·7759
0·7842	729·77	+5·29	+0·32	+0·21	0·8363	0·8384
0·8972	748·46	+3·95	+0·41	−0·05	0·9148	0·9149

experimental liquid compositions and total pressures, the pressure residuals found with first, second, and third (final) approximations to A, B, and C, the calculated vapour compositions, and finally the measured vapour compositions (which were, of course, not used in the calculations). The agreement between the two sets of values of vapour compositions is very satisfactory.

Our values of the constants a, b, c in the equation for G_x^E, together with those determined by Brown from total pressures and vapour concentrations, are shown in Table 2. The values of G_x^E found with the two sets of constants are

TABLE 2

CONSTANTS IN EQUATION FOR G_x^E

	a (cal/mol)	b (cal/mol)	c (cal/mol)
From total pressure ..	253·9	62·5	18·3
From total pressure and vapour composition ..	254·3	64·3	12·3

shown in Table 3. Since the estimated experimental error in Brown's G_x^E values was 3 cal/mol, the two sets of values are in remarkable agreement.

TABLE 3

VALUES OF G_x^E

x_1	0·1	0·2	0·3	0·4	0·5	0·6	0·7	0·8	0·9
G_x^E (total pressure)	19·4	35·7	48·7	58·1	63·5	64·1	59·2	47·7	28·4
G_x^E (total pressure and vapour composition)	19·0	35·2	48·4	58·1	63·6	64·2	59·2	47·6	28·2

III. REFERENCES

BROWN, I. (1952).—*Aust. J. Sci. Res.* **A 5**: 530.

MUSIL, A., and SCHRAMKE, E. (1949*a*).—*Acta Phys. Austr.* **3**: 137.

MUSIL, A., and SCHRAMKE, E. (1949*b*).—*Acta Phys. Austr.* **3**: 309.

REDLICH, O., and KISTER, A. T. (1949).—*J. Amer. Chem. Soc.* **71**: 505.

SCATCHARD, G. (1949).—*Chem. Rev.* **44**: 7.

SCATCHARD, G. (1952).—*Ann. Rev. Phys. Chem.* **3**: 269.

SCATCHARD, G., and RAYMOND, C. L. (1938).—*J. Amer. Chem. Soc.* **60**: 1278.

SCATCHARD, G., and TICKNOR, L. B. (1952).—*J. Amer. Chem. Soc.* **74**: 3724.

ON THE MECHANISM OF THE POLAROGRAPHIC REDUCTION OF OXYGEN

By S. Hacobian*

[*Manuscript received March* 17, 1953]

Summary

Investigations of the A.C. and D.C. polarography of oxygen in neutral and alkaline media have shown that the reduction process is univalent and reversible. It has also been shown experimentally that hydrogen peroxide is reversibly oxidized to oxygen in the presence of alkali. In order to explain the nature of the A.C. and D.C. polarograms thus obtained, a one electron reduction mechanism involving the hydroxyl radical and either the oxygen atom or the oxygen molecule is discussed.

I. Introduction

The first wave in the D.C. polarographic reduction of oxygen in neutral and alkaline media has been postulated to be the result of the reaction (Heyrovsky 1927, 1931 ; Varasova 1930 ; Raýman 1931) :

$$O_2+2H_2O+2\varepsilon \rightarrow H_2O_2+2OH^- . \quad \ldots\ldots\ldots\ldots \quad (1)$$

It was thought that two electrons are required for the reduction. The process itself was regarded as irreversible and requiring a large overvoltage. (Stackelberg 1939 ; Kolthoff and Lingane 1941 ; Kolthoff and Miller 1941). No inference regarding the number of electrons involved could be drawn from the log plot [log $(i_d-i)/i$ *v.* E] since the Nernst equation is not valid for irreversible processes.

It is the object of the present paper to show that in contradistinction to the findings reported in the previous paragraph, the polarographic reduction of oxygen is reversible in neutral and alkaline solutions. This follows from the occurrence of an oxidation and a reduction step at identical potentials (Fig. 3) and from the fact that A.C. polarograms of oxygen reduction are obtained in neutral and alkaline media. As pointed out in previous work (Breyer and Gutmann 1946, 1947 ; Breyer, Gutmann, and Hacobian 1950*a*, 1950*b* ; Breyer and Hacobian 1952*a*, 1952*b*) A.C. polarograms are obtained only in cases where the electrode process is not irreversible. The present paper shows also how far the mechanism of the reduction of oxygen can be established with the help of the combined techniques of A.C. and conventional D.C. polarography.

II. A.C. and D.C. Polarographic Reduction of Oxygen in Neutral, Alkaline, and Acid Media

A.C. and D.C. polarograms of oxygen in various concentrations of sodium perchlorate are shown in Figure 1. In 0·1M and higher concentrations of $NaClO_4$, no oxygen maximum appears, and well-defined D.C. polarographic steps are obtained. That the first oxygen wave represents a reversible reduction

* Physico-Chemical Laboratories, Faculty of Agriculture, University of Sydney.

of O_2 to H_2O_2 is clearly shown by the presence of an A.C. polarogram whose summit potential (E_s) coincides with the half-step potential ($E_{\frac{1}{2}}$) of the D.C. polarographic step. Analysis of the D.C. polarogram gives a linear log plot of 62 mV slope, indicating a one electron process.

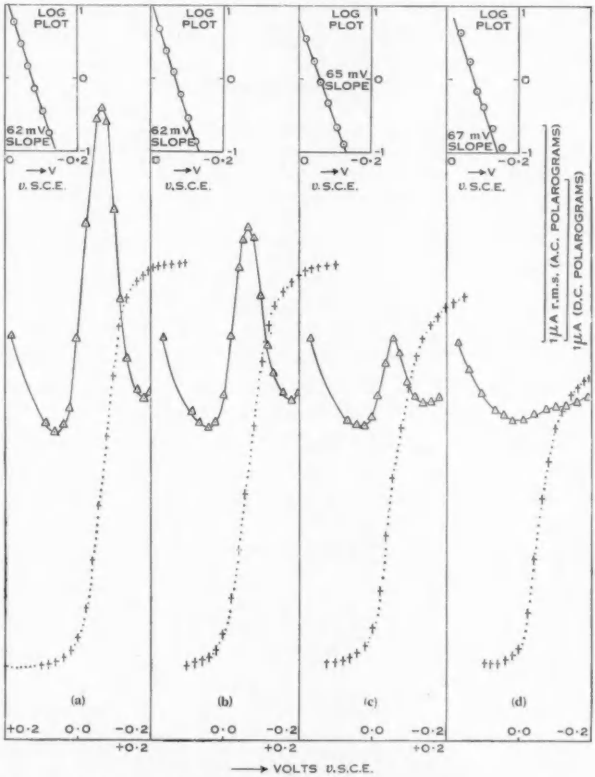

Fig. 1.—A.C. and D.C. polarograms of oxygen in varying concentrations of $NaClO_4$. Superimposed A.C. voltage, 15 mV r.m.s.; T, 20 °C. Capillary characteristics: m, 1·6 mg/sec, t, 3·5 sec.

(a) 0·1M $NaClO_4$ (saturated with air).
(b) 0·2M $NaClO_4$ (saturated with air).
(c) 0·5M $NaClO_4$ (saturated with air).
(d) 1·0M $NaClO_4$ (saturated with air).

△——△ A.C. polarograms.
+....+ D.C. polarograms.

It was originally thought by the author that the A.C. wave might be tensammetric (cf. Breyer and Hacobian 1952*c*) rather than polarographic and possibly due to the adsorption of mercuric hydroxide produced at the electrode as a

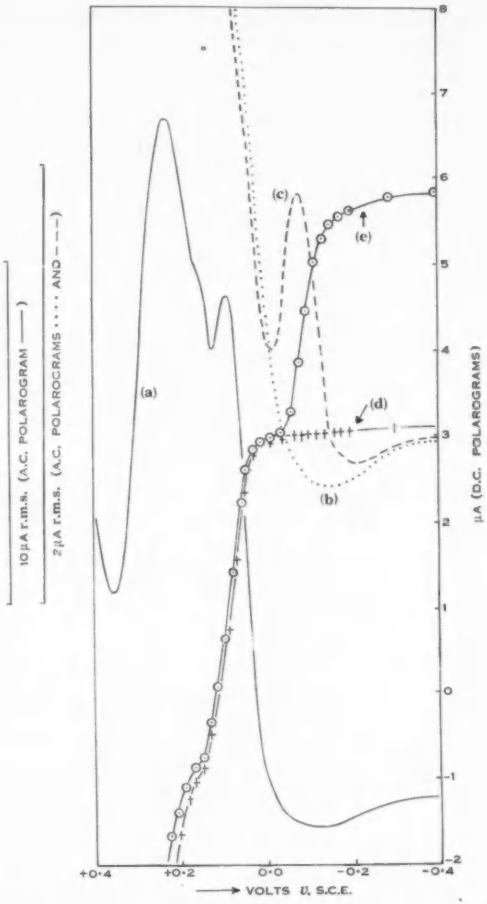

Fig. 2.—A.C. and D.C. polarograms of 0·1M $NaClO_4 + 10^{-3}$M OH^- and approximately $0{\cdot}5 \times 10^{-3}$M $HgCl_2$ in presence and absence of air. A.C. voltage, 15 mV r.m.s.; T, 20 °C. Capillary characteristics: m, 1·6 mg/sec, t, 3·5 sec.

(a) A.C. polarogram of above solution in the absence of air.
(b) As in (a) using a higher sensitivity range.
(c) As in (b) and in the presence of air.
(d) D.C. polarogram corresponding to (a).
(e) As in (d) and in the presence of air.

result of oxidation of mercurous ions by H_2O_2 in the presence of OH^- ions. The resulting mercuric hydroxide could then have given rise to a tensammetric or transition-type of wave (Breyer and Hacobian 1953). This hypothesis, however, was ruled out by the following experiments:

(i) A.C. polarography of an air-free solution of 0·1M $NaClO_4$ in the presence of Hg^{++} and OH^- ions showed the presence of two waves between 0 and +0·4 V *v.* the saturated calomel electrode (S.C.E.) (cf. A.C. polarograms *a* and *b* in Fig. 2). No A.C. wave was produced in the region of the oxygen discharge between 0 and −0·2 V. D.C. polarography also showed the presence of two steps corresponding to the A.C. waves (polarogram *d*, Fig. 2); the first cathodic step represents the reduction of Hg^{++} to mercury whereas the anodic step is due to the presence of OH^- and Cl^- ions (cf. Kolthoff and Lingane 1941, pp. 323–6).

(ii) A.C. and D.C. oxygen waves appeared, however, when the above solution was saturated with air (polarograms *c* and *e*, Fig. 2). The E_s and $E_{\frac{1}{2}}$ values of the respective waves were identical with those obtained in pure 0·1M $NaClO_4$ solution saturated with air.

TABLE 1

A.C. AND D.C. POLAROGRAPHIC REDUCTION OF OXYGEN IN 0·1M $NaClO_4$ AND IN THE PRESENCE OF VARIOUS AMOUNTS OF $HClO_4$

Solution	i_d (μA)	$i_{d\sim}$ (μA r.m.s.)	Log Plot of D.C. Polarogram (mV)
1. 0·1M $NaClO_4$ saturated with air	2·85	1·60	62
1.plus 5×10^{-4}M $HClO_4$ ..	2·40	0·7	65
1.plus 10^{-3}M $HClO_4$ ..	2·40	*	Non-linear
1.plus 10^{-2}M $HClO_4$ ..	2·40	*	Non-linear

* No A.C. wave obtained.

That the A.C. oxygen wave was definitely polarographic and not tensammetric in nature was further shown by the fact that the E_s values did not change with changes in oxygen concentration. If the waves were tensammetric an appreciable shift of the summit potential with changes in concentration would be expected according to the log c/E_s rule (Breyer and Hacobian 1952*c*).

The combined A.C. and D.C. polarography of oxygen in dilute supporting electrolytes other than $NaClO_4$ (for example, in 0·1M Na_2SO_4 and 0·1M KNO_3) was also investigated and similar results were obtained.

The effect of the increase of concentration of the supporting electrolyte on the A.C. and D.C. polarographic waves is shown in Figures 1 (*a*)–(*d*). The log plot of the respective D.C. steps becomes increasingly non-linear, whilst at the same time the A.C. wave gradually disappears. No A.C. wave is seen in M $NaClO_4$ solutions and correspondingly a non-linear log plot of the respective D.C. polarogram is obtained.

Increasing irreversibility in the reduction of oxygen is also effected by the presence of small amounts of acid. Table 1 shows that the oxygen reduction becomes irreversible when the acid content reaches 10^{-3} molar.

Just as in the case of neutral solutions oxygen is also reversibly reduced in the presence of alkali.* Two A.C. waves were observed: the anodic one corresponding to the discharge of OH^- ions (Breyer and Hacobian 1951) and the cathodic one to the reduction of oxygen.

III. A.C. and D.C. Polarographic Oxidation of Hydrogen Peroxide in Alkaline Media

Curve *e* in Figure 3 shows the D.C. polarogram obtained with an air-free solution of 0·1M $NaClO_4$ containing $2{\cdot}5\times10^{-4}$M hydrogen peroxide; curve *h* is that obtained with an air-free solution of 0·1M $NaClO_4$ containing $2{\cdot}5\times10^{-4}$M OH^- ions. As expected polarogram *e* shows only the reduction step of H_2O_2, whereas polarogram *h* shows only the anodic step of the OH^- ion discharge.

If, however, both H_2O_2 and OH^- are present simultaneously, a new anodic step appears between 0 and −0·2 V (polarogram *f*). This anodic step corresponds in height, slope, and half step potential to the cathodic step obtained by reduction of oxygen in 0·1M $NaClO_4$ (polarogram *d*). It can be reasonably concluded, therefore, that this anodic step is the counterpart to the cathodic one obtained in the reduction of O_2 to H_2O_2. It is thus due to the oxidation of H_2O_2 to O_2 and it follows that the polarographic reduction of oxygen in alkaline solution is a reversible process.

The following is a summary of the observations made when solutions containing both H_2O_2 and OH^- ions were subjected to either D.C. or A.C. polarography.

1. Solution of $2{\cdot}5\times10^{-4}$M $H_2O_2+2{\cdot}5\times10^{-4}$M OH^- in 0·1M $NaClO_4$ (air-free).
   - (i) A large drawn-out step between −0·6 and −1·2 V is observed representing the reduction of H_2O_2 to water (irreversible; absence of A.C. wave, cf. polarogram *e*, Fig. 3).
   - (ii) A large well-defined anodic step is observed between 0 and −0·1 V representing the oxidation of H_2O_2 to oxygen in the presence of OH^- ions (reversible; presence of corresponding A.C. wave, cf. polarograms *a* and *f*, Fig. 3).
   - (iii) A small well-defined anodic step follows between +0·1 and +0·2 V representing the discharge of OH^- ions (reversible; presence of corresponding A.C. wave, cf. polarograms *a* and *f*, Fig. 3).
2. Solution as in (1) after standing for 1 hr in the absence of air.
   - (i) The D.C. polarographic step between −0·6 and −1·2 V has decreased as a result of partial decomposition of the added hydrogen peroxide (cf. polarogram *g*, Fig. 3).
   - (ii) The D.C. polarographic step occurring between 0 and −0·1 V is now partly cathodic and its total height has decreased. The cathodic part of the step is due to the polarographic reduction of oxygen formed

* It should be kept in mind, however, that OH^- ions are formed in the reduction of O_2, so that the space near the electrode will always be alkaline (cf. for example, Kolthoff and Miller 1941).

from H_2O_2 on standing in alkaline solution. This peroxide decomposition is also the reason why the anodic part of the step (due to the oxidation of H_2O_2) is substantially lowered (cf. polarogram *g*, Fig. 3).

(iii) There is an increase in height of the OH^- ion step (polarogram *g*, Fig. 3). This increase in step height is explained by the fact that the

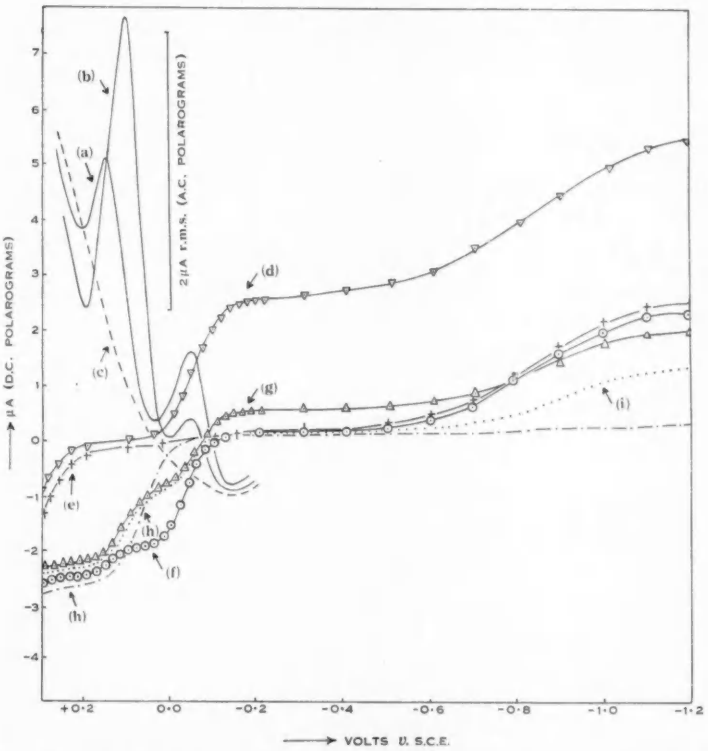

Fig. 3.—A.C. and D.C. polarograms of H_2O_2 in the presence and absence of alkali. A.C. voltage, 15 mV r.m.s.; T, 20 °C. Capillary characteristics: *m*, 1·6 mg/sec, *t*, 3·5 sec. (*a*) A.C. polarogram of approximately $2{\cdot}5\times10^{-4}$M $H_2O_2+2{\cdot}5\times10^{-4}$M NaOH in 0·1M $NaClO_4$ in absence of air. (*b*) As in (*a*) after standing for 1 hr. (*c*) A.C. polarogram of 0·1M $NaClO_4$ in the absence of air. (*d*) D.C. polarogram of 0·1M $NaClO_4$ in the presence of air. (*e*) D.C. polarogram of 0·1M $NaClO_4$+approx. $2{\cdot}5\times10^{-4}$M H_2O_2 (absence of air). (*f*) D.C. polarogram of 0·1M $NaClO_4$+approx. $2{\cdot}5\times10^{-4}$M $H_2O_2+2{\cdot}5\times10^{-4}$M NaOH (absence of air). (*g*) As in (*f*) after standing for 1 hr. (*h*) D.C. polarogram of 0·1M $NaClO_4+2{\cdot}5\times10^{-4}$M NaOH. (*i*) As in (*g*) and after passing nitrogen.

hydroxyl ions participate in two different reactions, namely, (*a*) in the normal cathodic discharge of OH^- ions, and (*b*) in the reaction with H_2O_2 to produce O_2. With decreasing H_2O_2 concentration, fewer

hydroxyl ions are used in reaction (*b*), thus making more available for the discharge process (*a*) resulting in an increased OH^- ion step height.

3. Solution as in (2) after passing nitrogen.

The D.C. polarogram is identical with that obtained before passing nitrogen as in (2) except that the cathodic oxygen step has disappeared, proving that the cathodic part of polarogram *g* is due to oxygen reduction (polarogram *i*, Fig. 3).

IV. Discussion

From the experimental results it can be concluded that: (i) oxygen is reduced reversibly at the dropping mercury electrode in neutral and alkaline media to hydrogen peroxide and hydroxyl ions; and (ii) one electron is involved in the reduction process.

On this basis, either of two electrochemical processes is possible:

(*a*) A one electron process involving the oxygen molecule.

(*b*) A one electron process involving the oxygen atom.

The following sections deal with the merits of each of the two possible reduction processes.

(*a*) *A One Electron Transfer via Oxygen Molecule*

Considering the oxygen molecule as the reactant, the following reduction mechanism can be postulated:

$$O_2+2H_2O+\varepsilon\rightarrow 1\tfrac{1}{2}H_2O_2+OH^-. \quad \ldots\ldots\ldots\ldots \quad (2)$$

Equation (2) represents the overall reaction and necessarily involves a number of subsidiary steps. Thus, for instance, the existence of free radicals, such as $OH^{\cdot}$, $HO_2^{\cdot}$, and HO_2^- in aqueous solutions of H_2O_2, has been proved by a number of workers (Taylor 1926; Urey, Dawsey, and Rice 1929; Franck and Haber 1931; Haber and Willstatter 1931; Haber and Weiss 1932, 1934). Gorin (1940) stipulated a one electron reduction of oxygen to oxygen ion:

$$O_2+\varepsilon\rightarrow O_2^-. \quad \ldots\ldots\ldots\ldots\ldots\ldots \quad (3)$$

This oxygen ion could then react with water first to give HO_2^- and $OH^{\cdot}$ radicals and finally hydrogen peroxide according to:

$$O_2^-+H_2O\rightarrow HO_2^-+OH^{\cdot}, \quad \ldots\ldots\ldots\ldots \quad (4)$$

$$HO_2^-+H_2O\rightarrow OH^-+H_2O_2, \quad \ldots\ldots\ldots\ldots \quad (5)$$

$$OH^{\cdot}+OH^{\cdot}\rightarrow H_2O_2. \quad \ldots\ldots\ldots\ldots\ldots \quad (6)$$

The experimental results reported in this paper show that hydrogen peroxide is oxidized to oxygen and water in the presence of OH^- ions. It can be assumed that this process leads over a number of intermediate steps such as:

$$H_2O_2+OH^-\rightarrow H_2O+HO_2^-, \quad \ldots\ldots\ldots\ldots\ldots \quad (7)$$

$$HO_2^-+H_2O_2\rightarrow HO_2^{\cdot}+OH^{\cdot}+OH^-, \quad \ldots\ldots\ldots \quad (8)$$

$$HO_2^{\cdot}\rightarrow H^++O_2^-, \quad \ldots\ldots\ldots\ldots\ldots \quad (9)$$

$$O_2^- \rightarrow O_2 + \varepsilon, \quad \ldots\ldots\ldots\ldots\ldots\ldots \quad (10)$$

$$H^+ + OH^- \rightarrow H_2O, \quad \ldots\ldots\ldots\ldots\ldots\ldots \quad (11)$$

$$OH\cdot + OH\cdot \rightarrow H_2O_2, \quad \ldots\ldots\ldots\ldots\ldots\ldots \quad (12)$$

to the overall reaction :

$$1\tfrac{1}{2}H_2O_2 + OH^- \rightarrow O_2 + 2H_2O + \varepsilon, \quad \ldots\ldots\ldots\ldots\ldots \quad (13)$$

which is the reverse of reaction (**2**). Reactions (**8**) (Uri 1952), (**9**) (Evans, Hush, and Uri 1952), and (**10**) (Gorin 1940) all involve fairly low heat, free energy, and entropy changes. Reactions (**7**), (**11**), and (**12**) are exothermic and involve heat changes of approximately 10 kcal (reactions (**7**) and (**11**)) and 50 kcal (reaction (**12**)) per mole respectively (in aqueous solution).

According to equations (**3**) and (**10**) the electron-transfer process involves the oxygen molecule and not the oxygen atom. This mechanism seems more probable from the energetic point of view because of the relatively small activation energy and heat changes involved. On the other hand, the step height obtained in polarography of oxygen seems to indicate that the reaction via the oxygen atom is the more likely one. As shown by Kolthoff and Lingane (1941) the concentration of dissolved oxygen in dilute salt solution exposed to air is about $2{\cdot}5 \times 10^{-4}$M. If, now, the diffusion current of oxygen is compared with that obtained with a cadmium salt solution, it is found that it corresponds to that of a 5×10^{-4}M solution of Cd^{++}. Assuming that the one electron transfer mechanism of O_2 holds, the diffusion coefficient for the oxygen molecule then results as being 15 times greater than that of the Cd^{++} ion. This value seems unduly large in view of the following considerations : the diameter of the hexaquo Cd^{++} ion is roughly twice that of the unsolvated oxygen molecule ; applying now the Stokes-Einstein equation, the calculated value of the diffusion coefficient of oxygen results to be only about twice as large as that for the solvated cadmium ion. Hence the one electron reduction of *molecular* oxygen seems unlikely. The second and more feasible alternative is that of an oxygen molecule being split into oxygen atoms at the electrode surface and subsequently reduced according to the overall reaction :

$$\tfrac{1}{2}O_2 \rightarrow O + \varepsilon + H_2O \rightarrow \tfrac{1}{2}H_2O_2 + OH^-. \quad \ldots\ldots\ldots \quad (14)$$

When the diffusion coefficient of the oxygen molecule is calculated on this basis, it is found to be approximately four times as large as that of Cd^{++} (that is, about $2{\cdot}8 \times 10^{-5}$ cm^2 sec), in perfect agreement with the experimental results obtained by Kolthoff and Miller (1941).

(*b*) *A One Electron Transfer via the Oxygen Atom*

The initial step in the reaction, involving the separation of oxygen molecules into oxygen atoms, requires a large dissociation energy (approximately 118 kcal/mol). It should not be forgotten, however, that this type of process will be appreciably facilitated at the Hg/electrolyte boundary, be it because of adsorption forces, or be it for the electrical field present at the interface. Thus, for instance, Hinshelwood (1940) quoting from Langmuir, says that " the

adsorption of such gases as oxygen . . . by metals is probably accompanied by the resolution of the molecules into atoms ". It seems reasonable to assume, furthermore, that in the case of electrodes the process of dissociation is further assisted by what Hardy (1925) calls " an electric field of prodigious intensity " at the boundary phase.

Assuming thus the change

$$O_2 \xrightarrow[\text{electrode}]{\text{Hg}} 2O, \quad \ldots\ldots\ldots\ldots\ldots (15)$$

to be the first step, the following reactions could subsequently occur:

$$O + H_2O + \varepsilon \rightarrow OH^- + OH^{\cdot}, \quad \ldots\ldots\ldots\ldots (16)$$

$$OH^{\cdot} + OH^{\cdot} \rightarrow H_2O_2, \quad \ldots\ldots\ldots\ldots\ldots (17)$$

giving the overall reaction:

$$O + H_2O + \varepsilon \rightarrow \tfrac{1}{2}H_2O_2 + OH^-. \quad \ldots\ldots\ldots\ldots (18)$$

As to the oxidation of hydrogen peroxide in alkaline solutions, which probably also involves the interfacial forces at the Hg/solution boundary, it can be represented by

$$H_2O_2 \xrightarrow[\text{electrode}]{\text{Hg}} OH^{\cdot} + OH^{\cdot} \quad \ldots\ldots\ldots\ldots\ldots (19)$$

$$OH^{\cdot} + OH^- \rightarrow O + H_2O + \varepsilon, \quad \ldots\ldots\ldots\ldots (20)$$

giving the overall reaction

$$\tfrac{1}{2}H_2O_2 + OH^- \rightarrow O + H_2O + \varepsilon \quad \ldots\ldots\ldots\ldots\ldots (21)$$

which is the reverse of reaction (18). This is followed by

$$2O \rightarrow O_2, \quad \ldots\ldots\ldots\ldots\ldots\ldots (22)$$

the reverse of reaction (15). Although the dissociation energy of the process $O_2 \rightarrow 2O$ is high, the free energy change of the overall reaction resulting from the combination of processes (15) and (18) is small (about 10 kcal/mol), making its occurrence the more probable.

The reversibility of the proposed reaction mechanism is shown by the presence of an anodic D.C. polarographic wave corresponding to the cathodic oxygen wave. In the absence of hydroxyl ions, however, reaction (20) cannot occur and hence no oxygen wave appears.

V. Acknowledgments

The author is much indebted to Dr. B. Breyer for suggesting this research problem, as well as for his constant advice and criticism. Thanks are also due to the Trustees of the Science and Industry Endowment Fund for financial assistance, to Mr. H. Bauer for checking some of the manuscript, and to Miss M. Ford for repeating some of the experimental results.

VI. References

Breyer, B., and Gutmann, F. (1946).—*Trans. Faraday Soc.* **42**: 645.

Breyer, B., and Gutmann, F. (1947).—*Disc. Faraday Soc.* **1**: 19.

Breyer, B., Gutmann, F., and Hacobian, S. (1950*a*).—*Aust. J. Sci. Res.* A **3**: 558.

Breyer, B., Gutmann, F., and Hacobian, S. (1950*b*).—*Aust. J. Sci. Res.* A **3**: 567.

Breyer, B., and Hacobian, S. (1951).—*Aust. J. Sci. Res.* A **4**: 610.

Breyer, B., and Hacobian, S. (1952*a*).—*Aust. J. Sci.* **14**: 118.

Breyer, B., and Hacobian, S. (1952*b*).—*Aust. J. Sci.* **14**: 153.

Breyer, B., and Hacobian, S. (1952*c*).—*Aust. J. Sci. Res.* A **5**: 500.

Breyer, B., and Hacobian, S. (1953).—*Aust. J. Chem.* **6**: 186.

Evans, M. G., Hush, N. S., and Uri, N. (1952).—*Quart. Rev. Chem. Soc. Lond.* **6**: 186.

Franck, J., and Haber, F. (1931).—*S.B. preuss. Akad. Wiss.* **13**: 250.

Gorin, H. H. (1940).—*Ann. N.Y. Acad. Sci.* **40**: 123.

Haber, F., and Weiss, J. (1932).—*Naturwissenschaften* **20**: 948.

Haber, F., and Weiss, J. (1934).—*Proc. Roy. Soc.* A **147**: 332.

Haber, F., and Willstatter, R. (1931).—*Ber. dtsch. chem. Ges.* **64**: 2844.

Hardy, W. (1925).—*J. Chem. Soc.* **127**: 1207.

Heyrovsky, J. (1927).—*Cas. čsl Lék.* **7**: 242. (*Chem. Abstr.* **22**: 4344 (1928).)

Heyrovsky, J. (1931).—*Arh. Hem. Farm.* **5**: 162 (Czech); p. 171-3 (English). (*Chem. Abstr.* **26**: 1542 (1932).)

Hinshelwood, C. N. (1940).—"The Kinetics of Chemical Change." p. 231. (Oxford Univ. Press.)

Kolthoff, I. M., and Lingane, J. J. (1941).—"Polarography." 1st Ed. p. 307. (Interscience Publishers Inc.: New York.)

Kolthoff, I. M., and Miller, C. S. (1941).—*J. Amer. Chem. Soc.* **63**: 1013.

Raýman, B. (1931).—*Coll. Trav. Chim. Tchécosl.* **3**: 314.

Stackelberg, M. V. (1939).—*Z. Elektrochem.* **45**: 482.

Taylor, H. S. (1926).—*Z. phys. Chem.* A **120**: 183.

Urey, H. C., Dawsey, L. H., and Rice, F. O. (1929).—*J. Amer. Chem. Soc.* **51**: 1371.

Uri, N. (1952).—*Chem. Rev.* **50**: 375.

Varasova, E. (1930).—*Coll. Trav. Chim. Tchécosl.* **2**: 8.

TRANSIENT RATES OF GAS SORPTION

I. MEASUREMENT OF RAPID GAS UPTAKE BY OXIDE CATALYSTS

By M. E. WINFIELD*

[*Manuscript received March* 16, 1953]

Summary

The rate of gas uptake by a porous solid in a constant volume system was determined by measuring the decrease in pressure, using a capacitance-type glass diaphragm manometer. Techniques are described for admitting gas to adsorbent quickly, and for measuring rapid changes at low pressures and high temperatures.

For water and alcohols the rates of uptake by thoria and alumina at 110–200 °C were found to have a negative temperature coefficient. Rates were first order with respect to initial pressure. Three types of rate dependence on mass of adsorbent were found—first, zero, and second order or exponential.

I. INTRODUCTION

The rate at which a gas is taken up by a solid adsorbent has seldom been studied under conditions closely related to those which prevail in practice in catalytic reactions. Under these conditions gas transport and sorption take place so rapidly that visual measurements are inadequate, and special methods must be devised for automatically tracing the course of high-speed adsorption and distribution processes.

The first of two techniques which we have used for this purpose is described in the present paper. It is applicable to what may be called the millisecond range, that is, to phenomena whose half-life is a few milliseconds or more. Attempts to work in the microsecond range are hindered by the difficulty of admitting gas phase to solid phase quickly.

Since the principal object of measuring rapid sorption and desorption is to dissect catalytic reactions into their component steps, it is often necessary to work at high temperatures. It is also desirable to work at low pressures. A number of the reasons are given by Wicke (1939). These two factors, and the speed requirement, dictate the design of apparatus.

In the method to be described, gas uptake is measured by the change in pressure which accompanies adsorption in a constant volume system. This technique is complementary to the one in which adsorption is followed by measuring changes in electrical conductivity of the adsorbent (see, for example, Garner, Gray, and Stone 1949). Restrictions of the latter method are that it is insensitive to gas transport processes, and cannot readily be used to study the effect of bed geometry, or size of aggregates or granules.

* Division of Industrial Chemistry, C.S.I.R.O., Melbourne.

The chief disadvantage of constant volume systems is that the equations to represent the relation between time and amount adsorbed are not as simple as for constant pressure. For this reason many of the experimental results which we have obtained cannot yet be interpreted satisfactorily. Certain results which are relevant to the kinetics of dehydration catalysis are presented in Part I of this series. A mathematical treatment of the types of process which can be operative in these experiments follows in Part II. Calculated and experimental rates are compared in Part III.

II. Experimental Procedure

(*a*) *Measurement of Pressure*

The sensitive element of the manometer was a Pyrex glass diaphragm with an effective diameter of 2·5 cm and thickness 0·015 cm. Its upper surface

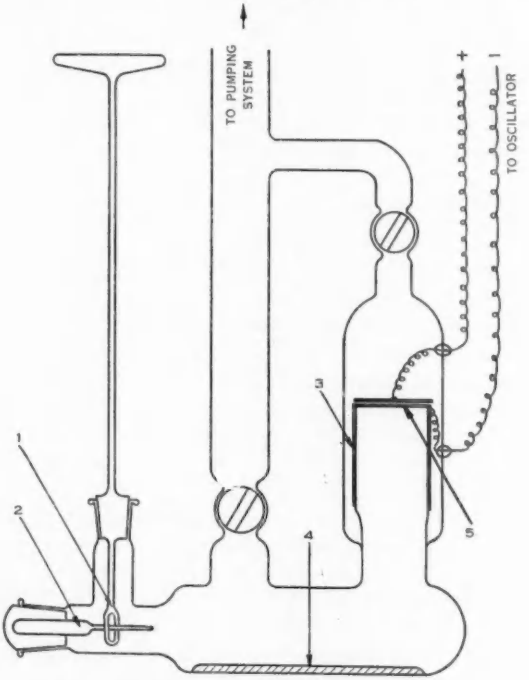

Fig. 1.—Schematic diagram of adsorption cell.
1, break-seal; 2, ampoule containing adsorbate; 3, silver coating on manometer tube and diaphragm (5); 4, adsorbent; 5, glass diaphragm.

was silvered, to form the negative plate of a capacitor, and separated by a mica spacing ring 0·025 cm thick from a rigid brass disk, which acted as the positive plate. This manometer is shown schematically in Figure 1, while details of construction for a more recent version are given in Figure 2.

Increase in pressure moved the diaphragm upwards towards the fixed plate, thus increasing the capacitance, which in turn was made to alter the frequency of a tuned oscillator circuit. By means of a discriminator, the frequency change was converted into a change in voltage, which was amplified and fed to a cathode ray tube. The circuit was similar to that used by Muncey (1948).

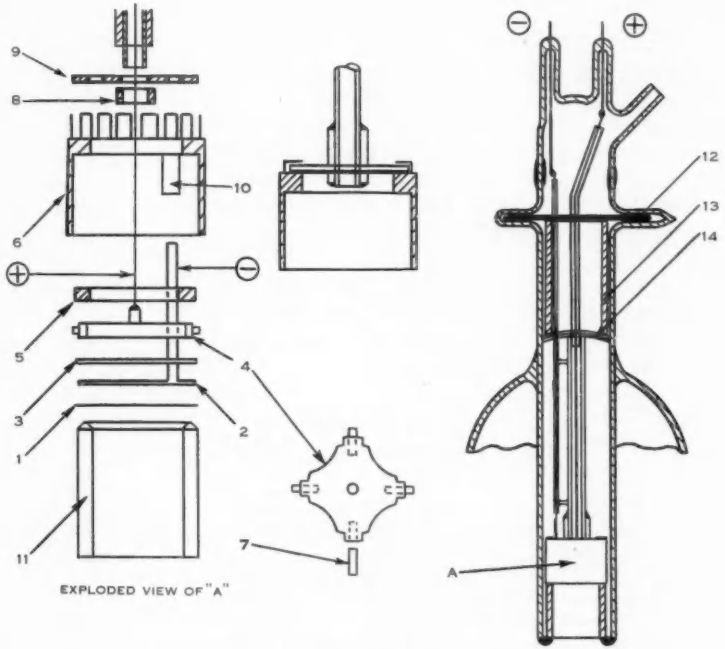

Fig. 2.—Details of manometer construction.
1, gold-plated glass diaphragm (negative electrode). Effective diameter 1·25 cm; thickness 0·004 cm; 2, platinum washer with tag (negative electrode), thickness 0·002 cm; 3, glass spacing ring, thickness 0·01 cm; 4, brass plate (positive electrode); 5, mica washer; 6, electrode assembly holder; 7, glass fibre insulators; 8, glass collar; 9, perforated mica disk; 10, slot for exit of negative lead; 11, glass tube with ground and bevelled end; 12, arrangement of pin (12), glass sleeve (13), and mica spring (14) to compress electrode assembly.

A record of pressure change as a function of time was provided by a 35 mm continuous-film camera attached to the oscillograph. In most of the experiments the film speed was 55 cm/sec. A hot-cathode mercury discharge lamp operated on 50 cycle A.C. was used to project a time marker on to the edge of the film. Figure 3 shows film records obtained using the manometer in Figure 2. Curves shown in other figures were obtained by replotting on a more convenient scale.

For most experiments the manometer sensitivity corresponded to full-scale deflection when the pressure change was 2 mm Hg. By altering the tuning and amplification, the pressure range could be varied from about 0·1 to 20 mm without changing the diaphragm. The natural frequency of vibration of the diaphragm in Figure 1 was 1200 c/s, which determined the speed of response. Although less sensitive, the smaller and more rugged diaphragm shown in Figure 2 proved to be adequate for the 2 mm range, and was appreciably faster in response.

(*b*) *Calibration of Manometer*

The oscillograph trace was photographed after each of a series of admissions of dry air to the lower side of the diaphragm, while the pressure on the upper

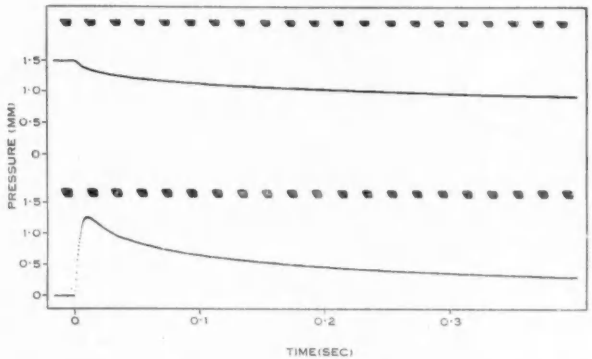

Fig. 3.—Film records representative of the two types of sorption-rate experiment.

Upper curve from experiment with 0·3 g of γ-alumina contained in the ampoule. Adsorbate, water vapour; temperature, 30° C; initial pressure, 1·5 mm Hg.

Lower curve from experiment with water vapour contained in the ampoule. Adsorbent, 0·3 g of thoria; temperature, 140 °C; initial pressure, 1·5 mm Hg. Dots in lower curve correspond to the natural frequency of vibration of the diaphragm.

side was kept below 10^{-3} mm. Immediately prior to taking each photograph, compensation for oscillator and amplifier drift was carried out by a standardized tuning procedure. The calibration pressures were measured with either an oil or a mercury manometer, connected through a liquid-air trap.

(*c*) *Design of Adsorption Cell*

As shown in Figure 1 the adsorption cell had a large flat bottom 7 cm in diameter over which the adsorbent was usually spread in a thin layer. In experiments to determine the influence of bed geometry and porosity, a dense uniform layer was obtained by evaporation after introducing the solid as an alcoholic suspension.

The adsorbate was contained in a glass ampoule with a thin neck which, in order to admit vapour to adsorbent, was broken by a break-seal of the type described by Winfield (1950). It was operated from above the cover of the furnace; so also was the stopcock for isolating the adsorption cell from the pumping system. Silicone high-vacuum grease was used as lubricant, which limited the usefulness of the instrument to temperatures below 210 °C.

Rapid degassing of cell and contents was made possible by a high-speed pumping system, with manifolds and stopcocks of large bore.

(*d*) *Temperature Control*

To eliminate the need for a stirrer, which introduced troublesome vibration, the adsorption cell was heated in a radiation furnace in which the temperature distribution was shown to be independent of stirring. It consisted of a vertical tube, 22 cm in diameter, of thick blackened brass, continuously heated by external windings. The variable component of the total heat input was provided internally, by a vertical infra-red lamp with a 750 W filament which stretched from top to bottom of the furnace. Since the heat output of the lamp was almost entirely radiation (the filament being in a vacuum) and the mass of the filament was small, with a correspondingly small time-constant, temperature control to $\pm 0{\cdot}2$ °C was possible using only a 5-junction thermocouple and a "Micromax" recorder-controller. This was considered adequate control for sorption-rate measurements.

The heat of adsorption liberated during an experiment was too small, at the low pressures employed, to raise appreciably the temperature within the cell.

(*e*) *Adsorbents and Adsorbates*

Preparation of the catalytically active thorium oxide followed the method given by Winfield (1945). The alumina monohydrate was a commercial grade of "activated alumina", used without purification, while the γ-alumina was formed from it by heating under vacuum at 300 °C. Surface areas determined by the B.E.T. method were $24{\cdot}3$ m^2/g for thoria, $51{\cdot}1$ for alumina monohydrate and 201 for γ-alumina. Whereas the thoria was in the form of soft agglomerates of fine particles, the aluminas consisted of small hard granules. Pore dimensions are given in Part III of this series.

Adsorbate liquids were purified and stored under vacuum in sealed tubes as described previously (Winfield 1950). Each of these, after being broken in a thoroughly degassed flask, provided the vapour for filling a number of the ampoules used in the sorption experiments. A finished ampoule contained an amount of vapour that was calculated to give a standard pressure p_0 when released in the adsorption cell if no sorption were to occur. This ensured that the pressure at zero time, p_0, was the same in each of a series of rate experiments carried out at different temperatures.

To fill an ampoule, vapour was admitted to a vessel of known volume and temperature to a predetermined pressure, read on a high quality air-speed indicator which had been recalibrated in mm Hg. The vapour in the manometer

came in contact only with the interior of a small metal capsule, and it was isolated from the filling system as soon as the pressure had been measured. The known volume included that of the ampoule to be filled (determined with a hypodermic syringe) but not the manometer. By cooling the tip of the ampoule in liquid oxygen, the vapour was quantitatively condensed into it. After sealing off from the filling system, the residual pressure in the latter was measured with a Pirani gauge. This was usually less than 0·005 mm, corresponding to a loss of 0·1 per cent. during the filling operation.

(*f*) *Experiment Schedule*

A weighed amount of adsorbent was placed in the adsorption cell, and an ampoule containing the adsorbate vapour. The cell was degassed at 200 °C for 4 hr at less than 10^{-4} mm pressure.

After isolating the cell from the pumps the temperature was reduced rapidly to that chosen for the experiment. The by-pass valve, which when open equalized the pressures on the two sides of the diaphragm, was closed. The oscillator was then tuned to standard sensitivity, and the oscillograph spot brought to a standard position on the cathode ray tube, corresponding to zero pressure. Immediately afterwards the camera was set in motion and the ampoule broken. Usually an experiment was allowed to proceed until the spot appeared to be stationary.

At the temperatures generally employed, namely 110–200 °C, the vapour emerged from the ampoule rapidly, under an initial pressure gradient of about an atmosphere. Since the pressure gradient declined with time, and the neck of the ampoule was narrow, several milliseconds elapsed before the vapour was largely discharged, although 75 per cent. was discharged in less than a millisecond. This constituted a weakness in the method except at temperatures well above the boiling point. It was minimized by making the ampoules as small as possible. It was also important that from one experiment to the next the neck diameter should not vary. They were therefore pre-drawn to nearly the same dimensions and the ampoule then sealed to the filling system by the large end, that is, with the thin neck pointing downwards.

(*g*) *Recent Improvements*

Vibration caused by manual rotation of the break-seal shaft was eliminated by attaching the latter through a system of two universal joints that transmitted rotation, but not vibration, to a pulley rotated by dropping a weight attached to the pulley belt.

To hasten the discharge of vapour, an ampoule was devised from which the vapour issued through a wide aperture instead of a narrow neck. It consisted of a short stem carrying a thin bulb 1 cm in diameter, whose end had been drawn inwards. It was broken by a sharp tungsten carbide needle, which was driven vertically downwards into the concave end of the ampoule by a stainless steel screw (Fig. 4). If the ampoule was made with glass about 0·1 mm thick in the centre of the concave portion, and much thinner at the rim, the whole of the

bulb was shattered by the impact of the needle, permitting rapid exit of the gas.

With the new type of ampoule a sorption rate experiment can be carried out with the solid phase instead of the vapour within the ampoule. The sorption rates can then be measured less than a millisecond after the break occurs (Fig. 3). Desorption rates can also be determined. Additional advantages are that measurements can be made at low temperatures if required, while the adsorbent can be degassed at temperatures up to 600 °C.

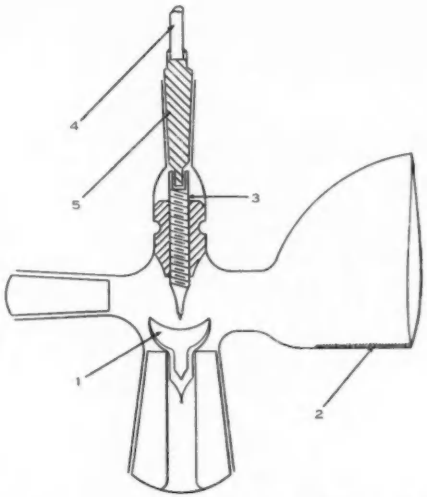

Fig. 4.—Improved ampoule and break-seal.
1, adsorbate contained in glass ampoule with a concave end and very thin rim; 2, adsorbent; 3, stainless steel screw, terminating in a tungsten carbide needle; 4, shaft connecting through universal joints to drive mechanism; 5, invar cone with tongue engaging in (3).

The pressure gauge shown in Figure 2 incorporates a number of improvements in stability, and ease of assembly. It has a sensitivity of better than 0·001 mm Hg in spite of its small size. The absolute error in pressure measurement is approximately 8 times this figure, mostly due to drift in the discriminator and the amplifier. Experiments conducted with the new apparatus are those relevant to Figure 3, the last set of results in Table 1, and the figures in Part III.

For use at 200–350 °C a modified apparatus has been designed and part constructed, in which the conventional stopcock for isolating the adsorption cell from the pumps is replaced by a vacuum-jacketed stopcock, whose plug is lubricated with a trace of graphite. The plug is rotated by a shaft, which comes down within the jacket from a ground joint, situated outside the furnace

and lubricated with silicone grease. There is negligible gas leak across the graphited plug, because the pressure gradient is small and the time short.

III. Experimental Results

(*a*) *Dependence of Rate on Amount of Adsorbent*

For the three gas-solid systems in Table 1, it was shown that the rate of gas uptake was proportional not to the first power of the mass of adsorbent, as

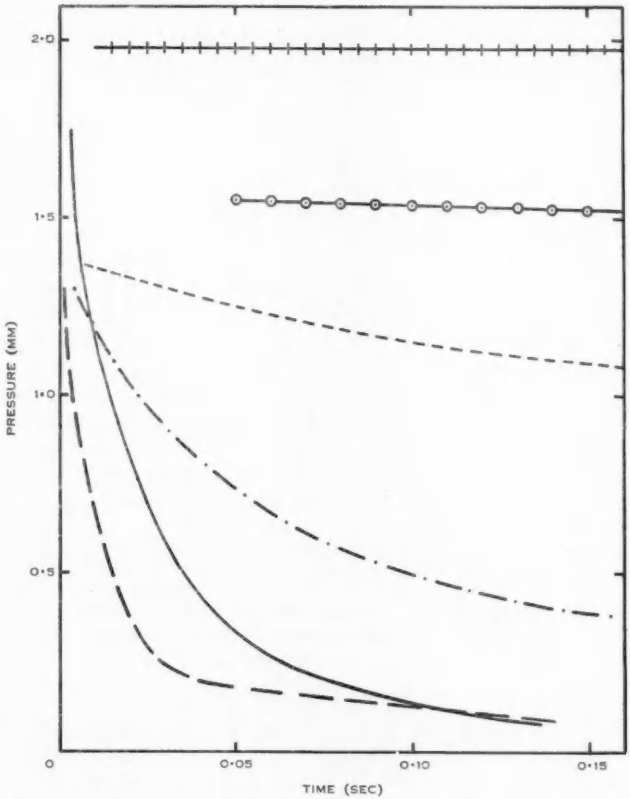

Fig. 5.—Influence of amount of adsorbent on the rate of gas uptake. Temperatures and initial pressures are given in Table 1.

- — — — *iso*Propanol on 0·3 g alumina monohydrate.
- — — — „ „ 0·1 g alumina monohydrate.
- — — Ethanol on 3·0 g thoria.
- |—|—| „ „ 0·3 g thoria.
- ——— Water on 3·0 g thoria.
- -⊙—⊙- „ „ 0·3 g thoria.

expected, but to the power two or higher. A discussion of this apparent contradiction of the law of Guldberg and Waage is given in Part III. It will be referred to, for convenience, as the dependence of rate on S^2, since the total surface area of the bed of adsorbent is proportional to the mass.

In Figure 5 the rates of *iso*propanol uptake can be compared for 0·3 and 0·1 g of alumina monohydrate, other conditions being identical. At times up to 0·14 sec the rate of pressure decrease at any instant was nine times as great for the larger amount of alumina. A lower ratio was not obtained if the rates were compared at a given pressure, or when equal amounts had been adsorbed per gram of alumina. In some experiments with thoria the mass of adsorbent was varied by a factor of 10, making the rates so different that comparison cannot be made accurately. However, it is certain that the ratio of initial rates is

TABLE 1

EFFECT OF MASS OF ADSORBENT ON RATE OF GAS UPTAKE

Adsorbent	Weight (g)	Adsorbate	Initial Pressure (mm)	Temperature (°C)	Relative Rates During the Half-Life	Half-Life (sec)
Alumina	0·1	*iso*Propanol	1·5	180	1/9	0·54
,,	0·3	,,	,,	,,		0·048
Thoria	0·3	Ethanol	2·0	,,	1/200	70
,,	3·0	,,	,,	,,		0·004
,,	0·3	Water	4·0	160	1/100	2·1
,,	3·0	,,	,,	,,		0·002
,,	0·15	,,	1·5	140	1/4	—
,,	0·3	,,	,,	,,		—

greater than 10^2. The half-life period, that is, the time for half of the adsorption to be completed, is given in Table 1 as well as the relative rates which prevailed in the first few milliseconds.

Later it was found that when water vapour was taken up by shallow beds of alumina monohydrate, the rates were proportional to S. They were independent of S when water was adsorbed on deep beds of γ-alumina contained in ampoules. When the amount of adsorbent was varied between 0·1 and 0·3 g, while the packing density and the bed diameter were held constant, the measured rates remained identical with that shown in the upper curve in Figure 3.

We have therefore encountered three types of adsorbing system, characterized by dependence of the rate on (i) S^2, (ii) S, and (iii) S^0.

(*b*) *Dependence on Temperature*

When the mass of adsorbent and the initial pressure were kept constant, while the temperature was increased, the rate of *iso*propanol uptake by alumina

monohydrate declined as shown in Figure 6. The curves are representative of 25 experiments necessitated by poor reproducibility when hydrated alumina was used as adsorbent. By plotting the initial rates in Figure 6 according to the Arrhenius equation, a straight line was obtained whose slope led to the value—12,000 cal/mol for the apparent activation energy of the process of gas uptake.

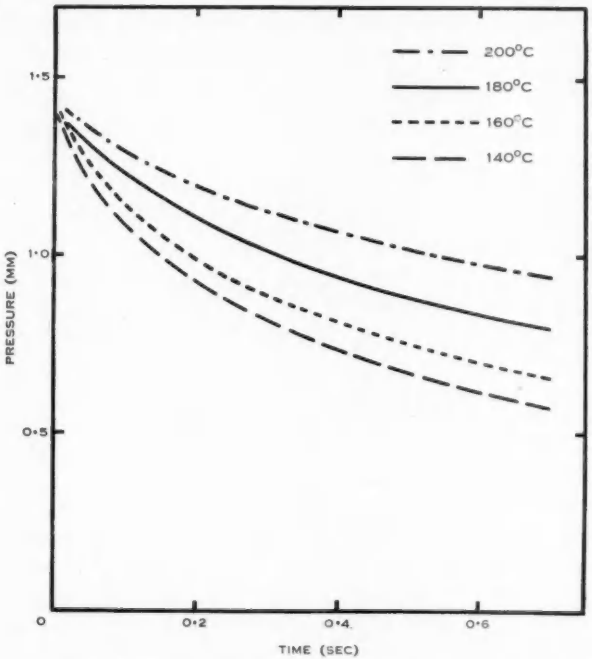

Fig. 6.—Temperature dependence of *iso*propanol sorption by alumina monohydrate.
Weight of adsorbent 0·1 g.
Initial pressure 1·5 mm Hg.

It is shown in Part III that the dependence of the rate on S^2 implies that chemisorption is the controlling step, and that a negative temperature coefficient does not argue against this conclusion. The negative coefficient which can occur whether the limiting step is Knudsen flow, chemisorption, or surface migration* is due to the dominating influence of the equilibrium adsorption constant, or adsorption isotherm.

* Whereas the rate of surface migration per molecule has a positive temperature coefficient, the total amount migrating per second is dependent on the amount that is adsorbed, and therefore on the heat of adsorption. The latter may be greater than the activation energy for migration from one site to the next, and confers a negative sign.

By passing the *iso*propanol through a bed of alumina monohydrate heated to 200 °C, it was demonstrated that at least part of the alcohol taken up was held by chemisorption. When the temperature was gradually lowered, propylene

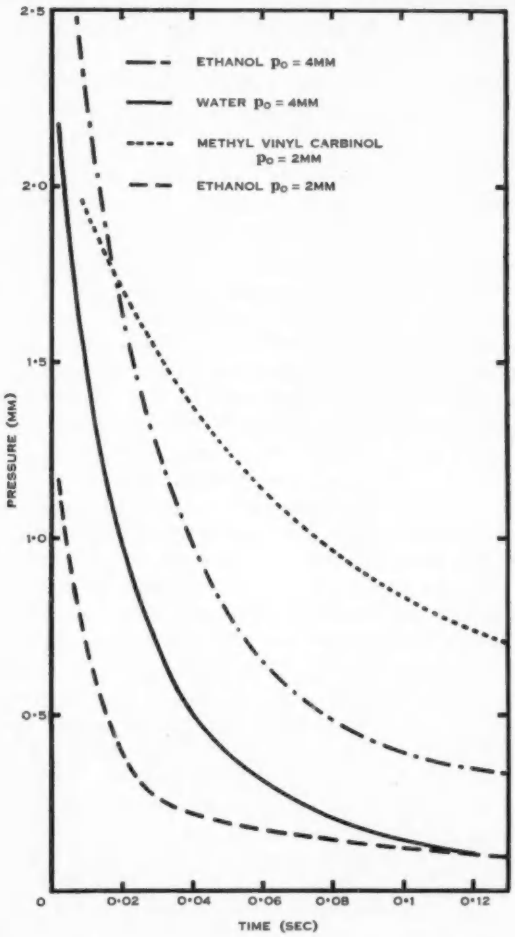

Fig. 7.—Vapour uptake at 180 °C by 3·0 g of thoria, showing dependence of rate on adsorbate and on initial pressure.

formation became slower and finally ceased just below 180° C. That is, at temperatures above 180 °C the catalytic dehydration was definitely proceeding, and it could be assumed that *iso*propanol was being chemisorbed.

In all other experiments reported in this paper the temperature coefficient of the initial rate can also be taken to be negative.

(*c*) *Dependence on Initial Pressure* (p_0)

In the two ethanol curves in Figure 7 the rate of gas uptake by thoria was first order with respect to p_0. In other less reliable experiments the rate of water uptake by thoria appeared to be proportional to $(p_0)^{1\cdot2}$.

(*d*) *Dependence on the Nature of the Adsorbate*

There was no simple relation between the rates with different adsorbate species (Fig. 7), since the rate depended upon the rate constants for adsorption and desorption as well as upon molecular size. It will be noticed in the curve for methyl vinyl carbinol that the initial pressure was higher than calculated, due to formation of some butadiene, possibly before the ampoule was broken.

(*e*) *Dependence on Geometry of Bed*

Rates for the system water-thorium oxide were independent of whether the bed was compact and uniform in depth as produced by evaporation of an alcoholic suspension, or lightly packed and irregular in contour, with approximately 10 times as much freely available surface. Since the rates were dependent on total surface area, this result indicated that the rate-determining step was either chemisorption or transport into aggregates or particles whose diameter was less than the depth of the compact bed (0·55 mm).

IV. Discussion

The process by which a gas phase is depleted by an adsorbent is made up of a number of individual steps, both consecutive and simultaneous. Where there are two parallel mechanisms, it is the faster of the two which has the greater influence, and both contribute. Thus it is not necessarily the slowest step in the process which is rate-controlling. The mechanisms that may be concerned in gas uptake are as follows :

(i) *Gas Phase Transport to Bed of Adsorbent.*—This was estimated to be faster than the observed rate of pressure decrease. The first molecules of water vapour, for example, passing from ampoule to bed, travelled at approximately 10^5 cm/sec. The rate for subsequent molecules declined presumably to the speed of sound, but the rate of gas uptake was likewise declining. As experimental evidence, the strong dependence of the observed sorption rate on total surface area argued against transport to the bed being the rate-controlling step. Also, in experiments with adsorbent absent it was found that there was no limitation of the measured pressure by the rate of transport of gas from the ampoule to the manometer.

(ii) *Adsorption.*—Methods which rely upon measuring the pressure decrease above a bed of adsorbent give a direct measure of the intrinsic rate of chemisorption only when the activation energy for adsorption is more than about 5000 cal/mol (depending upon the pore structure and the rate of desorption). However, the intrinsic rate can be calculated by fitting an experimental curve to the appropriate rate equation when the activation energy is as little as a few hundred cal/mol. These matters are discussed in Part III.

At low temperatures the rate of chemisorption may be conveniently small, but it is accompanied by considerable van der Waals's adsorption, and may become apparent only in the latter part of an experiment.

It can be claimed that the rate of gas uptake which is observed is equal to the permitted net rate of sorption by the bed (including chemisorption, occlusion, and physical adsorption), because the amount of gas-phase vapour in the bed at any instant is negligible. The observable rates are therefore relevant to the kinetics of catalysis, at the same temperature, irrespective of whether it is the chemisorption rate that is being measured.

(iii) *Poiseuille Flow within the Bed.*—For the conditions of pressure and particle size that were employed, it was calculated that streamline flow was negligible compared with molecular flow (see Part III).

(iv) *Knudsen Flow.*—While the possibility of surface migration contributing to the transport rate in the bed cannot be denied, it is shown in Part III that Knudsen flow is sufficient to account for the rates observed. In general, it can be assumed that the measured rates of gas uptake corresponded either to Knudsen flow accompanied by adsorption, or to unrestricted chemisorption.

In the kinetics of a first order heterogeneous reaction, it has been customary to assume that the equilibrium amount that can be adsorbed is an adequate measure of the surface concentration of reactant, under conditions of " steady-state " catalysis (Winfield 1950). To some extent this is justified by our experience that the equilibrium adsorption constant has a profound influence on the rate at which gas passes into a bed of adsorbent. However, even when the reaction rate is quite unrestricted by the intrinsic rate of chemisorption, the whole of E (the heat of adsorption) cannot be used in the expression to describe the experimental activation energy for the catalysis (see, also, Wheeler 1951). It will be apparent in Part II that when Knudsen flow, but not chemisorption, restricts the rate of reaction, $E/2$ must be used in place of E.

V. Acknowledgments

Thanks are due to Mr. A. E. Ferguson, Engineering School, University of Melbourne, and Messrs. G. Jones, F. Box, M. Borrell, and J. Bayston, Division of Industrial Chemistry, C.S.I.R.O., for assistance with the construction of apparatus.

VI. References

Garner, W. E., Gray, T. J., and Stone, F. S. (1949).—*Proc. Roy. Soc.* A **197**: 314.
Muncey, R. W. (1948).—*J. Coun. Sci. Industr. Res. Aust.* **21**: 141-7.
Wheeler, A. (1951).—" Advances in Catalysis." Vol. 3. (Academic Press: New York.)
Wicke, E. (1939).—*Kolloidzschr.* **86**: 167-86.
Winfield, M. E. (1945).—*J. Coun. Sci. Industr. Res. Aust.* **18**: 412-23.
Winfield, M. E. (1950).—*Aust. J. Sci. Res.* A **3**: 290-305.

TRANSIENT RATES OF GAS SORPTION

II. RATE EQUATIONS FOR TRANSPORT AND ADSORPTION IN POROUS ADSORBENTS

By K. L. Sutherland* and M. E. Winfield*

[*Manuscript received March* 16, 1953]

Summary

Equations are derived to describe the rate at which gas passes into a bed of adsorbent under conditions of constant volume and diminishing pressure. Of the processes which may be responsible for the observed rate of gas uptake, the following three are considered: (i) Knudsen flow within the bed, or within the granules of which it is composed, with simultaneous adsorption that is too fast to be a limiting factor; (ii) chemisorption which is controlled by the rate of Knudsen flow; (iii) unrestricted chemisorption.

It is shown how the rate constants used in the equations are related to the overall reaction rate constant in a catalyst pore.

I. Introduction

The present paper is concerned with the rate equations which result from considerations of the several kinds of transport and adsorption processes which may be significant under the experimental conditions described in Part I of this Series (Winfield 1953). The use of the equations to describe the experimental results will be dealt with in Part III.

Of the three known transport processes in porous adsorbents, Knudsen flow, surface migration, and Poiseuille flow, the first is the most important in industrial catalysis (see, for example, Wheeler 1951). Under our experimental conditions the pressures and pore diameters are sufficiently small that Poiseuille flow need not be considered (see Part III). Surface migration generally becomes appreciable only when surface area and surface concentration are high (Carman and Malherbe 1950). It has not been possible to obtain a workable rate equation for surface migration in a constant volume system, and this mode of transport will not be considered in the present paper. We shall therefore treat the rate of gas uptake when it is governed by the following circumstances:

(i) Transient Knudsen flow into the pores of the adsorbent, accompanied by adsorption on and desorption from the walls of the pore (Section II).

(ii) The special case of the above when adsorption and desorption are so rapid that adsorption equilibrium can be assumed. The formulae of Section II are then slowly convergent. More convenient expressions that are valid in the early stages of the process are therefore derived (Section III).

* Division of Industrial Chemistry, C.S.I.R.O., Melbourne.

(iii) Adsorption which is so slow that transport processes cannot influence the rate at which gas is taken up by a bed of adsorbent. The rates of adsorption and desorption then entirely determine the rate of gas uptake. We solve the rate equations which apply when there are two kinds of adsorption site, each with its own rate constant (Section IV).

(iv) Steady-state catalysis for a first-order reaction, with transport of reactant by Knudsen flow (Section V).

Symbols used in Parts II and III are listed at the end of this paper.

II. Adsorption and Knudsen Flow are of Comparable Speed

Imagine that the catalyst bed contains b cylindrical pores of length l and radius r. These pores are closed at one end. The catalyst is in a chamber of volume V. At a given instant the space above the adsorbent is filled with gas at a pressure p_0. We shall assume that:

(i) a distribution in pore size and length can be sufficiently described by mean values;

(ii) a constant f can be found such that the rate of flow of gas along a pore is f times the local pressure gradient;

(iii) the rate of adsorption of gas molecules on the pore wall in their vicinity is given by the local pressure, multiplied by a rate constant k_a;

(iv) the rate of desorption is k_d times the amount adsorbed per unit area, k_d being constant.

The following set of equations must be satisfied:

$$f\frac{\partial^2 p}{\partial x^2}=\frac{\pi r^2}{RT}\cdot\frac{\partial p}{\partial t}+2\pi r\cdot\frac{\partial a}{\partial t},\quad 0<x<l,\ t>0, \qquad \text{..... (1)}$$

$$\frac{\partial a}{\partial t}=k_a p-k_d a,\quad 0<x<l,\ t>0, \qquad \text{..... (2)}$$

$$p=0,\quad 0<x<l,\ t=0, \qquad \text{..... (3)}$$

$$p=p_0,\quad x=0,\ t=0, \qquad \text{..... (4)}$$

$$\frac{\partial p}{\partial x}=0,\quad x=l,\ t\geqslant 0, \qquad \text{..... (5)}$$

$$f\frac{\partial p}{\partial x}=\frac{V}{bRT}\cdot\frac{\partial p}{\partial t},\quad x=0,\ t>0, \qquad \text{..... (6)}$$

$$a=0,\quad 0<x<l,\ t=0, \qquad \text{..... (7)}$$

where a = the amount adsorbed per unit area of pore surface,
x = distance into the pore from its mouth,
p = pressure at time t,
$f=\frac{\pi r^2}{RT}\cdot D_k$.

Usually the Knudsen flow coefficient D_k is taken to be $1\cdot 33r(2RT/\pi M)^{\frac{1}{2}}$ (see, Section III (c)). The speed factor f then becomes $1\cdot 33r^3(2\pi/MRT)^{\frac{1}{2}}$.

Regarding the origin of these equations:

(1) describes the change of pressure at any plane in the pores (all considered to be in parallel) as a function of t. The amount of gas passing x is equal to the change in the amount present

in the gas phase in the element between x and $x+dx$, plus the change in the amount adsorbed in this element, plus the amount which passes the plane at $x+dx$.

(2) states that the net rate of adsorption is equal to the difference between the rate of condensation and the rate of evaporation.

(3), (7), and (4) state that the pore and its surface are free of gas at the beginning of the experiment, at which time the pressure in the vessel is p_0.

(5) gives the condition that the pore is closed.

(6) states that the amount of gas which leaves the space above the bed of adsorbent is equal to the amount which passes into the pores.

The solution of the equations may be obtained directly using the Laplace transform method (Carslaw and Jaeger 1947) and the solution is

$$\frac{p}{p_0}=\frac{1}{1+\frac{\pi r^2 lb}{V}\left(1+\frac{2k_aRT}{rk_d}\right)}+\sum_{n=1}^{\infty}\frac{\exp\left(-\beta_n\cdot t\right)}{1+\frac{\pi rbRTl}{V}\left[\frac{r}{2RT}+\frac{k_ak_d}{(k_d-\beta_n)^2}\right]\left[1-\frac{\beta_nV}{ibfRT\alpha_n^2}+\left(\frac{\beta_nV}{bfRT\alpha_n}\right)^2\right]}\times\frac{\cos\alpha_n(l-x)}{\cos\alpha_nl}, \quad \ldots\ldots\ldots\ldots\ldots\ldots (8)$$

where β_n are the roots of the equation

$$\frac{V\beta}{bfRT}+\left[\frac{\pi r\beta}{f}\left(\frac{r}{RT}+\frac{2k_a}{k_d-\beta}\right)\right]^{\frac{1}{2}}\cdot\tan l\left[\frac{\pi r\beta}{f}\left(\frac{r}{RT}+\frac{2k_a}{k_d-\beta}\right)\right]^{\frac{1}{2}}=0, \quad \ldots\ldots\ldots\ldots\ldots\ldots (9)$$

and the α_n and β_n are related by

$$\alpha^2=\frac{\pi r\beta}{f}\left(\frac{r}{RT}+\frac{2k_a}{k_d-\beta}\right). \quad \ldots\ldots\ldots\ldots\ldots\ldots (10)$$

Equation (9) gives a double infinite set of roots and one imaginary root. The behaviour of equation (9) has been discussed by Crank (1952) who independently derived a similar equation to (8).

It is important to note that the radius r can refer either to the spaces between the granules in a deep bed, or to the pores which lead from the surface to the centre of each granule, or possibly to the pores within each particle of which the granule is composed. Thus the surface area contained on the pores of radius r, and given by

$$S_p=2\pi rlb,$$

may be less than the total surface area S. It is then necessary to replace k_a and k_d in equations (8)–(10) by K_a and K_d where

$$K_a=\frac{k_aS}{S_p},$$

and

$$K_d=\frac{k_dS}{S_p}.$$

III. Adsorption Equilibrium Prevails at all Times

(a) *Equation for Knudsen Flow Accompanied by Rapid Adsorption*

The solution when adsorption is so fast that adsorption equilibrium, between gas and pore wall, is virtually attained at any instant was first given by Wilson (1948). It may also be obtained directly from equation (**8**) giving

$$\frac{p}{p_0}=\frac{1}{1+\frac{\pi r^2 lb}{V}\left(1+\frac{2k_eRT}{r}\right)}+\sum_{n=1}^{\infty}\frac{2\exp\left(-D\gamma_n^2 t\right)}{1+\frac{blfRT}{VD}+\frac{VDl}{bfRT}\cdot\gamma_n^2}\cdot\frac{\cos\gamma_n(l-x)}{\cos\gamma_n l}, \quad \ldots\ (11)$$

where the γ_n are the roots of the equation

$$\gamma l\cot\gamma l+blfRT/VD=0, \quad \ldots\ (12)$$

and

$$D=\frac{fRT}{\pi r^2+2\pi r\,k_eRT}, \quad \ldots\ (13)$$

while k_e is the intrinsic equilibrium constant, which is equal to k_a/k_d when Henry's law applies.

For the experimental data presented in Part I and Part III it was found that equation (**11**) was unsatisfactory for numerical calculations because of the slow convergence of the series.

An approximate solution of the problem for sufficiently small times is readily obtained.

The differential equations governing this case are given by (**3**), (**4**), (**5**), (**6**), and (**7**) and equation (**1**) is replaced by

$$f\cdot\frac{\partial^2 p}{\partial x^2}=\frac{\pi r^2}{RT}\cdot\frac{\partial p}{\partial t}+2\pi r k_e\cdot\frac{\partial p}{\partial t}. \quad \ldots\ (14)$$

The amount adsorbed, a, is everywhere replaced by $k_e p$ and we assume, as previously, that k_e is not a function of pressure.

The subsidiary equations obtained by the Laplace transform are

$$\frac{\mathrm{d}^2\bar{p}}{\mathrm{d}x^2}-\frac{\lambda}{D}\cdot\bar{p}=0, \qquad 0<x<l, \quad \ldots\ (15)$$

$$\frac{\mathrm{d}\bar{p}}{\mathrm{d}x}=0, \qquad x=l, \quad \ldots\ (16)$$

$$\frac{fbRT}{V}\cdot\frac{\mathrm{d}\bar{p}}{\mathrm{d}x}=\lambda\bar{p}-p_0, \qquad x=0. \quad \ldots\ (17)$$

Here λ is a number whose real part is positive and large enough to make the following integral convergent

$$\bar{p}=\int_0^{\infty} p\ \mathrm{e}^{-\lambda t}\,\mathrm{d}t.$$

The solution to (**15**)–(**17**) is

$$\bar{p}=p_0 H\ \frac{\cosh q(l-x)}{q\sinh ql+H\lambda\cosh ql}, \quad \ldots\ (18)$$

where $q^2=\lambda/D$ and $H=V/fbRT$.

Write equation (**18**) as

$$\frac{\bar{p}}{p_0 H} = \frac{e^{-qx} + e^{qx-2ql}}{(q+H\lambda)\left[1+\frac{H\lambda-q}{H\lambda+q}\cdot e^{-2ql}\right]}, \quad \ldots\ldots\ldots (19)$$

and expand the second factor in the denominator by the binomial theorem, retaining only the first two terms of the expansion. We find a sum of terms for which the transforms may be written directly.

For the solution at $x=0$, which gives the pressure in the space above the bed of adsorbent, we find

$$\left(\frac{p}{p_0}\right)_{x=0} = e^{Y^2}\,\mathrm{erfc}\; Y + 4Y\pi^{-\frac{1}{2}}(e^{-Z^2}+e^{-4Z^2}) - 4Y(Y+Z)e^{-Z^2}e^{(Y+Z)^2}\,\mathrm{erfc}\;(Y+Z)$$
$$-(1+8YZ+4Y^2)e^{-4Z^2}e^{(Y+2Z)^2}\mathrm{erfc}\;(Y+2Z)+\ldots, \quad \ldots\ldots (20)$$

where

$$Y = U\sqrt{Dt} = \frac{b}{V}[\pi rtfRT(r+2RTk_e)]^{\frac{1}{2}},$$

$$Z = l/\sqrt{Dt} = l\left[\frac{\pi r(r+2RTk_e)}{tfRT}\right]^{\frac{1}{2}}.$$

As in equation (**8**), k_e must usually be replaced by K_e, where

$$K_e = \frac{k_e S}{S_p}.$$

(*b*) *Application of Equation* (**20**)

For the adsorbing systems described in Part III it was found that up to the half-life, or even further, all except the first term in equation (**20**) could be neglected. That is, the simple expression

$$\frac{p}{p_0} = e^{Y^2}\,\mathrm{erfc}\; Y \quad \ldots\ldots\ldots\ldots\ldots (21)$$

was adequate for most purposes, since the rate at large values of time was of little interest.

The initial rate can be shown to be

$$-\frac{dp}{dt} = \frac{p_0 Y}{(\pi)^{\frac{1}{2}}t}, \qquad \frac{p}{p_0} > 0{\cdot}8. \quad \ldots\ldots\ldots\ldots (22)$$

By fitting equation (**21**) to an experimental rate curve Y can be determined. It is then a simple matter to calculate the rate of gas uptake at those very small times at which the rate cannot be measured experimentally.

Equation (**20**) can be applied when the adsorption is van der Waals, or a chemisorption in which the activation energy is small. How small this energy must be depends upon the pore dimensions. It will be indicated in Part III that for gas uptake by shallow beds of thoria the activation energy for adsorption must be no more than a few hundred cal/mol for equations (**20**) or (**21**) to apply. If it is less than 4000 cal, equation (**8**) may be used, while beyond that the chemisorption equation of the next section might be applicable.

Since r is usually negligible compared with $2RTk_e$, Y can be written

$$Y=\frac{\check{D}_k b\pi r^2 t^{\frac{1}{2}}}{V\sqrt{D}},$$

where

$$\frac{D_k}{\sqrt{D}}=1\cdot 94k_e^{\frac{1}{2}}(RT)^{\frac{1}{4}}(M\pi)^{-\frac{1}{4}}.$$

By substituting in equation (**22**) it is seen that the rate of gas uptake is at first proportional to

$$\frac{p_0 b r^2 k_e^{\frac{1}{2}}(RT)^{\frac{1}{2}}}{V M^{\frac{1}{2}} t^{\frac{1}{2}}}. \quad \ldots\ldots\ldots\ldots\ldots\ldots \quad (23)$$

The rate is proportional to the number of pores, b, which conduct the gas, and therefore to the cross-sectional area of the bed, if it is deep, or to the surface area S if it is shallow.

The temperature dependence of the rate is given by

$$k_e^{\frac{1}{2}}T^{\frac{1}{2}}=\text{constant}\times e^{E/2RT}\,.\,T^{\frac{1}{2}}, \quad \ldots\ldots\ldots\ldots \quad (24)$$

where E is the heat of adsorption. Generally $T^{\frac{1}{2}}$ is negligible compared with the exponential factor. Thus the process of gas uptake by Knudsen flow accompanied by rapid adsorption has initially a negative temperature coefficient, and appears to have a negative activation energy of magnitude $0\cdot 5E$.

(c) Applicability of the Knudsen Expression for Molecular Flow

When gas is first admitted to the vicinity of a bed of adsorbent, the length of pore being utilized for transport and adsorption of gas is less than the pore radius. It might be expected that at very small times the " short-tube " formula (Kennard 1938, p. 307) for the molecular diffusion coefficient should be used instead of the " long-tube " formula (Kennard 1938, p. 305) assumed in our rate equations. This would reduce the calculated rate by a factor of 4 when $l=r$. However, in our rate experiments most of the gas that enters a pore is removed from the gas phase, and the situation then resembles that for effusion through an orifice. A compromise between the " short-tube " and the " orifice " formula seems to be desirable. Although the " long-tube " formula is too fast at small values of l/r to provide this compromise, it is the only sufficiently simple expression available which can be used over a wide range of pore lengths. It must be expected that rates which it predicts will be somewhat greater than those found experimentally, particularly in the early part of the curve. It is estimated that the rates of gas uptake calculated in Part III are in error by a factor of 2 at worst, as a result of adopting the " long-tube " expression. Under transient conditions however the molecular streaming is faster than under steady-state conditions of flow, and this would reduce the error.

(d) Errors Introduced by Assuming Henry's Law

Without assuming a direct proportionality between the gas pressure and the equilibrium amount adsorbed, we cannot solve the rate equations for a constant volume system, except when transport rates can be neglected. Even

at low pressures the experimentally determined adsorption isotherms are far from linear. However, the calculated rates of gas uptake are proportional to only the square root of the Henry's law constant, and so the error may be no more than a few per cent., as shown in Part III.

IV. Uniform Pressure Throughout the Pore Space at all Instants

When the intrinsic rate of adsorption is small, transport processes cannot influence the rate of gas uptake by the bed of adsorbent. The observable rate becomes equal to the net rate at which gas can be adsorbed when it has free access to the total surface area S.

An equation can be derived to describe the chemisorption on an array of sites of n different energies, but the result for a variable pressure system is too cumbersome to be useful. We shall give the solution for $n=2$.

Let the activation energies for adsorption and desorption be E_{a1} and E_{d1} on surface S_1, and E_{a2} and E_{d2} on surface S_2. Then if a_1 and a_2 are the amounts per unit area adsorbed at time t on S_1 and S_2 respectively,

$$\frac{da_1}{dt}=u_1p-v_1a_1, \qquad t>0, \quad \ldots\ldots\ldots\ldots\ldots\ldots \quad (25)$$

$$\frac{da_2}{dt}=u_2p-v_2a_2, \qquad t>0, \quad \ldots\ldots\ldots\ldots\ldots\ldots \quad (26)$$

where

$$u_1=P_a e^{-E_{a1}/RT}; \qquad u_2=P_a e^{-E_{a2}/RT};$$
$$v_1=P_d e^{-E_{d1}/RT}; \qquad v_2=P_d e^{-E_{d2}/RT};$$

and P_a, P_d are the frequency factors for adsorption and desorption respectively.

It is assumed that the different behaviour of the two kinds of site is entirely due to the different energy requirements, and that the activation energies are independent of surface coverage.

From the conservation of mass we can also write

$$\left.\begin{aligned} p&=p_0-Fa_1-Ga_2, \qquad t>0, \\ \text{and} \qquad a_1&=a_2=0, \qquad t=0, \end{aligned}\right\} \quad \ldots\ldots\ldots\ldots \quad (27)$$

where

$$F=RTS_1/V \text{ and } G=RTS_2/V.$$

Using the Laplace transform, equations (25), (26), and (27) become

$$\lambda\bar{a}_1=u_1\bar{p}-v_1\bar{a}_1,$$
$$\lambda\bar{a}_2=u_2\bar{p}-v_2\bar{a}_2,$$
$$\bar{p}=p_0/\lambda-F\bar{a}_1-G\bar{a}_2.$$

Solving these three equations for $\bar{p}$ gives

$$\frac{\bar{p}}{p_0}=\frac{1}{\lambda[1+Fu_1/(\lambda+v_1)+Gu_2/(\lambda+v_2)]}.$$

The inversion of this Laplace transform is straightforward and leads to the result

$$\frac{p}{p_0}=A+Be^{-Q_1t}+Ce^{-Q_2t}, \quad \ldots\ldots\ldots\ldots\ldots\ldots \quad (28)$$

where

$$A=\frac{v_1v_2}{Q_1Q_2},$$

$$B=\frac{(v_1-Q_1)(v_2-Q_1)}{Q_1(Q_1-Q_2)},$$

$$C=\frac{(v_1-Q_2)(v_2-Q_2)}{Q_2(Q_2-Q_1)},$$

while $-Q_1$ and $-Q_2$ are the two roots of the quadratic equation

$$\lambda^2+(v_1+v_2+Fu_1+Gu_2)\lambda+(Fu_1v_2+Gu_2v_1+v_1v_2)=0.$$

V. Adsorption and Reaction Within a Single Pore of a Catalyst Pellet

(*a*) *Distribution of Adsorbed Gas in a Pore During Catalysis*

The distribution of adsorbed reactant in a pore during "steady-state" catalysis can be determined simply, for a first order reaction, when the fraction of potentially active sites covered by reactant is not large. If the pore is less than 1000 Å in diameter, and the pressure less than 2 atm, it can be assumed that transport of reactant into the pore, and of product outwards, is achieved by Knudsen flow (Wheeler 1951) with no interference between the two species of gas molecule.

Following the methods and nomenclature of Section II we have

$$2\pi r\left(\frac{\partial a}{\partial t}\right)\cdot \mathrm{d}x=2\pi r(K_a\cdot p-K_d\cdot a)\mathrm{d}x-2\pi r(K_r\cdot a)\mathrm{d}x, \quad \ldots\ (29)$$

assuming the activation energies for adsorption, desorption, and reaction to be constant. Here K_r is the reaction rate constant per unit area of pore wall for the surface conversion of adsorbed reactant, and a is the surface concentration of adsorbed reactant at time t on any element of length $\mathrm{d}x$ (radius r) situated x cm from the pore mouth.

We may also write

$$f\left(\frac{\partial^2 p}{\partial x^2}\right)\cdot \mathrm{d}x=\frac{\pi r^2}{RT}\cdot\left(\frac{\partial p}{\partial t}\right)\cdot \mathrm{d}x+2\pi r(K_a\cdot p-K_d\cdot a)\cdot \mathrm{d}x. \ldots\ (30)$$

When a steady-state pressure p_S is reached at the pore mouth, $\partial p/\partial t$ and $\partial a/\partial t$ become zero. Then from equation (29)

$$K_r\cdot a=K_a\cdot p-K_d\cdot a,$$

that is

$$a=p\left(\frac{K_a}{K_d+K_r}\right). \quad \ldots\ (31)$$

From equation (30)

$$\frac{\partial^2 p}{\partial x^2}=\frac{2\pi rp}{f}\cdot\left(\frac{K_aK_r}{K_d+K_r}\right).$$

Put $K_a K_r/(K_d+K_r)=K$ and $f/2\pi rK=D_r$, then

$$D_r\left(\frac{\partial^2 p}{\partial x^2}\right)=p.$$

This can be solved to give

$$p=p_S \cdot \frac{\cosh D_r^{-\frac{1}{2}}(l-x)}{\cosh D_r^{-\frac{1}{2}} l}, \quad \ldots\ldots\ldots\ldots (32)$$

where $x\sqrt{2}$ is the straight-line distance from the surface of a spherical pellet of diameter $2l/\sqrt{2}$ (assuming the usual deviousness factor of $\sqrt{2}$).

Equation (**32**) gives the pressure distribution, and with equation (**31**) the adsorbate distribution, within a catalyst pellet operating under steady-state conditions. The complex rate constant $K_a K_r/(K_d+K_r)$ is equivalent to k/RT, where k is the constant employed by Wheeler (1951) to represent the overall reaction rate constant for gas immediately adjacent to the adsorbing surface. Wheeler shows how k can be determined from a single catalytic experiment.

(*b*) *Adsorption Rate per Pore*

The rate of adsorption and reaction per pore when p_S is constant, and under the conditions described in Section V (*a*), is given by Thiele's equation (see Wheeler 1951) or may be obtained directly from equation (**32**) in the form

$$-f\left(\frac{\partial p}{\partial x}\right)_{x=0}=p_S \cdot f \cdot D_r^{-\frac{1}{2}} \tanh D_r^{-\frac{1}{2}} l,$$

or

$$\text{rate}=\frac{h}{l} \cdot f p_S \tanh h,$$

where $h=l(2KRT/rD_k)^{\frac{1}{2}}$ and has the same numerical value as Wheeler's h.

VI. Symbols Used

a = moles of gas adsorbed per cm^2 of pore wall,
a_1 and a_2 = values of a for surfaces S_1 and S_2 respectively,
A, B, and C = constants in the chemisorption equation (**28**), dimensionless,
b = number of pores in a bed of adsorbent, dimensionless,
$D=fRT/(\pi r^2+2\pi r k_e RT)$, cm^2 sec^{-1},
D_k = Knudsen diffusion coefficient, cm^2 sec^{-1},
$D_r=f/2\pi rK$, cm^2,
e = base of Napieran logarithms,
E = heat of adsorption, cal mol^{-1},
E_{a1} and E_{a2} = activation energy for adsorption on S_1 and S_2 sites respectively, cal mol^{-1},
E_{d1} and E_{d2} = corresponding activation energies for desorption, cal mol^{-1},
f = speed factor $=D_k\pi r^2/RT$, mol cm^3 dyn^{-1} sec^{-1},
$F=RTS_1/V$, dyn mol^{-1},
$G=RTS_2/V$, dyn mol^{-1},
$h=l(2KRT/rD_k)^{\frac{1}{2}}$, dimensionless,
$H=V/fbRT$, sec cm^{-1},
k_a = intrinsic adsorption velocity constant, mol dyn^{-1} sec^{-1},

k_d=intrinsic desorption velocity constant, sec^{-1},
k_e=intrinsic equilibrium constant for adsorption, mol dyn^{-1},
$K=K_aK_r/(K_d+K_r)$, mol dyn^{-1} sec^{-1},
$K_a=k_a.S/S_p$, mol dyn^{-1} sec^{-1},
$K_d=k_d.S/S_p$, sec^{-1},
$K_e=k_e.S/S_p$, mol dyn^{-1},
K_r=reaction rate constant for surface conversion, sec^{-1},
l=mean pore length, cm,
M=molecular weight, dimensionless,
p=pressure at time t, dyn cm^{-2},
p_0=pressure at $t=0$, dyn cm^{-2},
P_a and P_d=frequency factors for adsorption and desorption respectively, same units as k_a and k_d,
$q=(\lambda/D)^{\frac{1}{2}}$, cm^{-1},
Q_1 and Q_2=constants in chemisorption equation (**28**), sec^{-1},
r=mean pore radius, cm,
R=gas constant, dyn cm deg^{-1} mol^{-1}, or cal deg^{-1} mol^{-1},
S=total surface area of bed of adsorbent, cm^2,
S_1 and S_2=surface areas of type 1 and type 2 surfaces respectively, cm^2,
S_p=pore surface$=2\pi rlb$, cm^2,
t=time, sec,
T=temperature, °K,
u_1 and u_2=adsorption rate constants on S_1 and S_2 sites respectively, mol dyn^{-1} sec^{-1},
v_1 and v_2=corresponding desorption rate constants, sec^{-1},
$U=1/DH$, cm^{-1},
V=volume of adsorption cell, cm^3,
x=distance from pore mouth, cm,
$Y=U(Dt)^{\frac{1}{2}}$, dimensionless,
$Z=l/(Dt)^{\frac{1}{2}}$, dimensionless,
α_n=quantity defined by equation (**10**), cm^{-1},
β_n=roots of equation (**9**), sec^{-1},
γ_n=roots of equation (**12**),
λ=Laplace transform variable, sec^{-1}.

VII. Acknowledgment

We are indebted to Mr. J. A. Barker of the Division of Industrial Chemistry, C.S.I.R.O., for helpful suggestions.

VIII. References

Carman, P. C., and Malherbe, P. le R. (1950).—*Proc. Roy. Soc.* A **203**: 165-78.
Carslaw, H. S., and Jaeger, J. C. (1947).—"Conduction of Heat in Solids." (Oxford Univ. Press.)
Crank, J. (1952).—*Phil. Mag.* (7) **43**: 811-26.
Kennard, E. H. (1938).—"Kinetic Theory of Gases." (McGraw-Hill Book Co.: New York.)
Wheeler, A. (1951).—"Advances in Catalysis." Vol. 3. (Academic Press: New York.)
Wilson, A. H. (1948).—*Phil. Mag.* **39**: 48-58.
Winfield, M. E. (1953).—*Aust. J. Chem.* **6**: 221.

TRANSIENT RATES OF GAS SORPTION

III. PORE STRUCTURE, ADSORPTION ISOTHERMS, AND CALCULATED RATES AT CONSTANT VOLUME

By K. L. SUTHERLAND* and M. E. WINFIELD*

[*Manuscript received March* 16, 1953]

Summary

The pore structure has been determined for the thoria, alumina monohydrate, and γ-alumina adsorbents of Part I of this Series; also the Henry's law constants when the adsorbate is water vapour at 140 °C. Using these quantities in the equations given in Part II it is shown how the calculated rate of Knudsen flow, accompanied by rapid adsorption on the pore walls, can account for the experimental rates of gas uptake by the two aluminas. None of the equations can account for the dependence of the rate of uptake by thoria on the square (or higher power) of the mass of the bed. It is suggested that a poisoning phenomenon may be responsible.

In deciding the nature of the limiting step in gas uptake by an adsorbent, the dependence of the rate on the mass of the bed is a useful criterion. The temperature coefficient is not informative unless it is positive.

The methods and results described in Parts I, II, and III can be applied in the study of gas adsorption and flow in the catalyst pellets of a fixed-bed industrial reactor. They should also be capable of predicting the unsteady reaction rates within a granule in a fluidized bed.

I. INTRODUCTION

The rate equations derived in Part II of this Series (Sutherland and Winfield 1953) are now applied to the calculation of certain of the sorption rates, the experimental measurement of which was described in Part I (Winfield 1953). To obtain the constants required by the rate equations we have determined the pore dimensions for the thoria, alumina monohydrate, and γ-alumina adsorbents, and the adsorption isotherms for one of the adsorbates—water vapour. The present calculations are confined to water vapour at 140 °C and an initial pressure of 1·5 mm Hg, so that ready comparison can be made of results obtained with different pore systems.

Equation (**22**) of Part II, which is concerned with Knudsen flow unimpeded by the speed of adsorption, is referred to here as the flow equation and used only in its approximate form

$$\frac{p}{p_0} = e^{Y^2} \operatorname{erfc} Y, \quad \ldots\ldots\ldots\ldots\ldots\ldots \quad (1)$$

where p and p_0 are the pressures at times t and zero respectively in a vessel of constant volume V, containing a bed of adsorbent at temperature T. The

* Division of Industrial Chemistry, C.S.I.R.O., Melbourne.

pores which limit the flow have a mean radius r, mean length l, and are b in number. If R is the gas constant and M the molecular weight,

$$Y=\frac{1\cdot 9\, br^2t^{\frac{1}{2}}K_e^{\frac{1}{2}}(\pi RT)^{\frac{1}{2}}}{VM^{\frac{1}{2}}}, \qquad r\ll 2K_eRT, \quad \ldots\ldots \quad (2)$$

where $K_e=k_eS/2\pi rlb$, k_e is the Henry's law constant, and S is the total surface area of adsorbent. All other pores are assumed to be in adsorption equilibrium with those of radius r.

The terms chemisorption equation and chemisorption-flow equation refer respectively to equations (**28**) (gas uptake controlled entirely by adsorption) and (**8**) (Knudsen flow restricted by slow adsorption) of Part II.

We are concerned with transient phenomena in a constant-volume system, in which the pressure is a function of time. Although not as important in chemical industry as the " steady-state ", transient conditions prevail in the following: reactions in " static " systems, for example, laboratory hydrogenations; explosive reactions; oxidation of coal and coke, and reactions in fluidized catalyst beds; adsorbent protective devices such as gas masks; the study of induction periods and initial rates of reaction in biological systems.

The results obtained with a constant-volume apparatus may be used to calculate rates at constant pressure. The constants determined by fitting the appropriate equations for constant volume to the experimental results, are inserted into the analogous expressions for constant pressure conditions (for the latter equations see, for example, Barrer (1941), Wheeler (1951), and Wicke (1939)).

II. Pore Structure of Adsorbents

In the terminology which we shall use, a catalyst " bed " consists of a large number of either granules or agglomerates packed into a reaction vessel. A " granule " is a hard composite of " particles." An " agglomerate " is analogous to a granule, but is readily broken and re-formed by gentle shaking. The spaces between granules are " intergranular voids ", while those between particles are " interparticle voids ". The term " pore " embraces any type of void within the bed.

The pores which can limit the rate at which gas is taken up by the bed are either the intergranular voids or the interparticle voids. Only rarely need smaller pores be considered. Details of the methods of determining pore structure may be found in the work of Carman (1938 and later), Dallavalle (1943), Wheeler (1951), etc.

Diminishing degrees of agglomeration are indicated by progressively smaller subscripts to the symbols d, r, and ε. Whereas r_3, r_2, etc. refer to the dimensions of agglomerates, granules, or particles, the symbol r is reserved for the mean radius of the pores that limit the rate of gas uptake.

(*a*) *Shallow Beds of Alumina Monohydrate*

(i) *Intergranular Voids.*—Each bed consisted of alumina granules, spread in a thin layer not more than three granules deep, on the bottom of the adsorption cell of volume $V=232$ c.c. described in Part I (Winfield 1953).

The apparent density of the bed, $d_3=1\cdot16$ g/c.c., was determined by weighing a small glass vessel of known volume which was packed with the granules by a standard procedure with reproducibility of 1 per cent. To obtain d_2, the apparent density of an average granule, a sample of the alumina was contained in an evacuated bulb of known volume. Mercury was admitted at a pressure just sufficient to force it between the granules, and the volume of mercury determined. The correct pressure, 300 mm Hg, was found by plotting the result of several measurements at different pressures (see Anderson *et al.* 1947).

From the result $d_2=1\cdot72$, and the relation

$$d_2(1-\varepsilon_3)=d_3,$$

we obtained

$$\varepsilon_3=0\cdot33,$$

where ε_3 is the porosity between the granules.

To determine r_2, the radius of an average granule, the flow rate was measured at a known small pressure differential when dry nitrogen was passed through a deep bed of the alumina, packed as in the determination of d_3. Then from Carman's (1950) modification of the Kozeny equation, and using $\varepsilon_3=0\cdot33$, r_2 was found to be $3\cdot3\times10^{-3}$ cm.

Let the irregularly shaped channels through which the gas passed in the determination of r_2 be replaced by uniform-bore cylinders, each of the same radius r. Then it can be shown that

$$r=r_2\left[\frac{4\varepsilon_3{}^{3/2}}{3\pi^{\frac{1}{2}}(1-\varepsilon_3)}\right]^{1/3}. \quad \ldots\ldots\ldots\ldots\ldots \quad (3)$$

This led to $r=1\cdot9\times10^{-3}$ cm.

(ii) *Interparticle Voids.*—Let each granule be composed of particles of mean radius r_1 and apparent density d_1, with a porosity between the particles of ε_2. By measuring the volume change when a weighed amount of adsorbent was immersed in diethyl ether, d_1 was estimated to be $2\cdot8$.

Since

$$d_1(1-\varepsilon_2)=d_2,$$

therefore

$$\varepsilon_2=0\cdot39.$$

From the B.E.T. surface area of $51\cdot1$ m^2g^{-1} (Part I),

$$r_1=\frac{3}{51\cdot1d_1}$$

$$=2\cdot1\times10^{-6} \text{ cm}.$$

Then from a relation of the same form as equation (3)

$$r=1\cdot4\times10^{-6} \text{ cm},$$

where the mean pore radius r now refers to the interparticle voids.

Let l be the average pore length within the granules (approximately spherical). Following Wheeler (1951, p. 259)

$$l=\frac{r_2\sqrt{2}}{3}$$

$$=1\cdot53\times10^{-3}\text{ cm.}$$

If there were b pores of mean length l in a bed containing 0·1 g of alumina monohydrate, then from Wheeler (1951, p. 258)

$$b=\text{number of granules}\times4\pi r_2^2\left(\frac{\varepsilon_2}{\pi r^2\sqrt{2}}\right)$$

$$=2\cdot4\times10^{12}.$$

Finally

$$S=0\cdot1\times51\cdot1\times10^4=5\cdot1\times10^4\text{ cm}^2/0\cdot1\text{ g.}$$

(*b*) *Deep Beds of γ-Alumina*

The granules of adsorbent were contained in ampoules as described in Part I, in the form of beds of diameter 0·40 cm, and depth up to 2 cm. The degree of packing was the same as for the flow experiment to determine r_2, in Section II (*a*). Since the γ-alumina was formed from the alumina monohydrate (by heating at 300 °C at $<1\mu$ pressure) the granule size was assumed to be the same. Thus if the intergranular voids were represented by b pores of mean radius r and length l running from the top to the bottom of a bed containing 0·3 g of γ-alumina, then

$$r=1\cdot9\times10^{-3}\text{ cm, (see Section II (}a\text{))}$$

and

$$l=3\cdot42\text{ cm,}$$

from direct measurement of the bed depth, assuming a deviousness factor of $\sqrt{2}$.

The number of pores is given by

$$b=\frac{\pi\text{ (radius of bed)}^2}{\pi r^2+\pi r_2^2}$$

$$=2\cdot8\times10^3,$$

while

$$S=0\cdot3\times201\times10^4=6\cdot0\times10^5\text{ cm}^2/0\cdot3\text{ g.}$$

(*c*) *Shallow Beds of Thoria*

The structure of the thoria particles has been described in detail by Beckett and Winfield (1951). Agglomerates formed from the 1μ particles commonly reached a diameter of 1 mm. A bed consisted of a layer, up to three deep and 7 cm in diameter, of these " large agglomerates ".* They were so easily damaged that the usual methods for determining porosity failed to give reliable values. The following procedure was therefore adopted :

From 134 measurements with a projection microscope the mean radius of the large agglomerates was estimated to be

$$r_3=1\cdot0\times10^{-2}\text{ cm}\quad\text{(standard deviation }0\cdot5\times10^{-2}\text{).}$$

* Since the density of the large agglomerates was about one-ninth of the true density of thoria, they must have been formed by a long succession of agglomerations (see Wilson 1953).

By squeezing or dissecting under a microscope it was found that each large agglomerate was made up of " small agglomerates ", of mean radius r_2. By measuring the projections of 51 of these, r_2 was estimated to be $1{\cdot}0\times10^{-3}$ cm (standard deviation $0{\cdot}6\times10^{-3}$).

Since the small agglomerates consisted of some thousands of very small particles, it was reasonable to expect that they tended to assume a spherical shape. The porosity between the small agglomerates was therefore taken to be the same as for perfect spheres, that is, $\varepsilon_3=0{\cdot}37$ (Carman 1938). Then from equation (3)

$$r=6{\cdot}4\times10^{-4}\text{ cm},$$

where r is now the mean radius of the voids, between the small agglomerates, by which gas would be transported from the surface to the centre of the large agglomerates. If the number of these pores in a $0{\cdot}15$ g bed is b and their mean length l, then by the methods of Section II (a)

$$b=3{\cdot}6\times10^{6}$$

$$=5{\cdot}0\times10^{-3}\text{ cm},$$

$$S=0{\cdot}15\times24{\cdot}3\times10^{4}=3{\cdot}6\times10^{4}\text{ cm}^2.$$

III. Adsorption Equilibria and Henry's Law Constants

(*a*) *Method*

The adsorption-rate cell described in Part I was modified to permit measurement of adsorption isotherms. A small bulb containing the adsorbate liquid was cooled by a film of water freshly formed from ice melting in the upper part of a Dewar vessel. After flowing over the bulb, the water was removed continuously by a suction line. The temperature of the liquid in the bulb remained at $0{\cdot}07$ to $0{\cdot}08$ °C for long periods, corresponding to a vapour pressure variation of about 1 part in 1000. Each addition of vapour to the adsorbent was made by first filling a 246 c.c. bulb (maintained at 18 °C with sufficient accuracy by tap water in a Dewar vessel) with vapour at the saturation pressure corresponding to $0{\cdot}07$ °C ($4{\cdot}60$ mm Hg in the case of water vapour). This was then admitted to the adsorbent within the cell, of volume $233{\cdot}5$ c.c., after isolating the small bulb. When equilibrium was established, the residual pressure in the cell was measured with the glass diaphragm manometer.

The isotherms were confirmed by repeating the measurements using twice the weight of adsorbent. This gave an isotherm with twice as many experimental points in a given pressure range, and thus a measure of the cumulative errors (about $0{\cdot}3$ per cent. at the end of an isotherm).

(*b*) *Isotherms*

Figures 1, 2, and 3 give the low pressure isotherms for adsorption of water at 140 °C on thoria, alumina monohydrate, and γ-alumina. Isotherms for water on the same thoria at higher pressures have been given by Winfield (1950).

(c) *Henry's Law Constants*

As shown in Part II we are obliged to use a linear isotherm in the rate calculations based on the flow equation (**1**). The error, however, is not serious, since the rate is proportional to the square root of k_e.

In Figures 1, 2, and 3, straight lines from the origin have been drawn through the experimental isotherms at 0·75 mm Hg (which is the half-life pressure when $p_0 = 1{\cdot}5 \times 1333$ dyn cm^{-2}). These were found to give satisfactory linear representation of the experimental isotherms for use in the flow equation, over the period of the half-life of a sorption rate experiment. The error introduced in calculating p, using the linear isotherms in place of the experimental, was usually less than 5 per cent. of p_0.

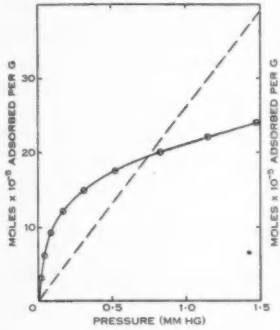

Fig. 1

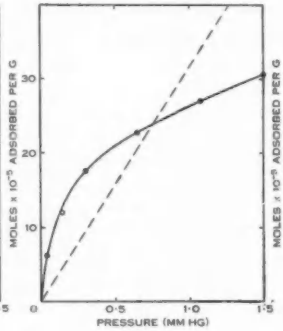

Fig. 2

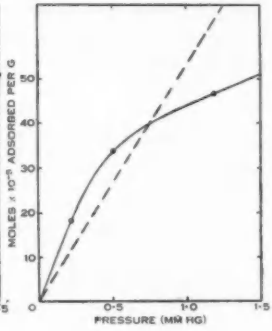

Fig. 3

Fig. 1.—Low pressure isotherm for water adsorption on thoria at 140 °C. The full line is the experimental isotherm, while the broken line is the linear isotherm from which the Henry's law constant is taken.

Fig. 2.—Isotherm for adsorption of water on alumina monohydrate at 140 °C.

Fig. 3.—Water adsorption isotherm on γ-alumina at 140 °C.

Table 1 gives the Henry's law constants which are used later in this paper, and correspond to the linear isotherms in Figures 1, 2, and 3.

TABLE 1

ADSORPTION OF WATER VAPOUR AT 140 °C, AND PRESSURES UP TO $1{\cdot}5 \times 1333$ DYN CM^{-2}

Adsorbent	k_e (mol dyn^{-1} cm^{-2})	K_e (mol dyn^{-1} cm^{-2})		
		$r = 6{\cdot}4 \times 10^{-4}$ (cm)	$r = 1{\cdot}4 \times 10^{-6}$ (cm)	$r = 1{\cdot}9 \times 10^{-3}$ (cm)
Thoria	$3{\cdot}5 \times 10^{-13}$	$4{\cdot}1 \times 10^{-10}$		
Alumina monohydrate	$4{\cdot}6 \times 10^{-13}$		$7{\cdot}3 \times 10^{-13}$	
γ-Alumina	$2{\cdot}0 \times 10^{-13}$			$1{\cdot}4 \times 10^{-9}$

IV. Application of the Flow Equation

Equation (1) is used to calculate the rate of gas uptake when it is controlled by Knudsen flow accompanied by relatively fast adsorption, so that adsorption equilibrium can be assumed between the flowing gas and the neighbouring pore wall. For water vapour at 140 °C, $M=18$ and $T=413\cdot3$. Values for all other constants required have been given in the preceding sections.

(*a*) *Deep Beds of γ-Alumina*

For flow through the intergranular voids of the 0·3 g bed described in Section II (*b*)

$$Y=0\cdot30\times t^{\frac{1}{2}}.$$

From equation (1) and a table of error functions the values of p/p_0 for a series of values of t can then be obtained directly, with the result shown by the broken line in Figure 4.

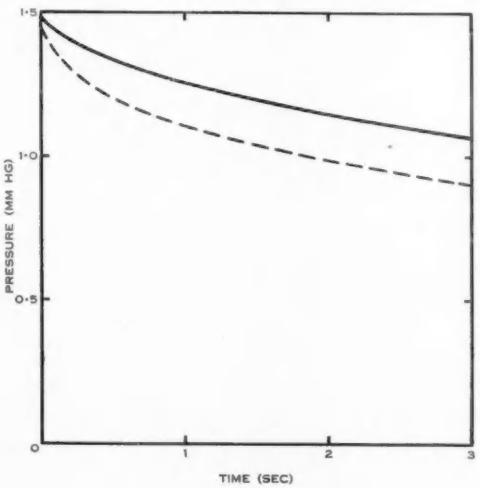

Fig. 4.—Comparison of experimental rate of uptake of water by a deep bed of γ-alumina (full line) with the rate calculated from the flow-equation (broken line). Temperature 140 °C, mass of adsorbent 0·3 g.

Better agreement between experiment and theory cannot be expected, because the "long-tube" formula for the Knudsen coefficient can lead to calculated rates which are too high at small values of t (see Part II). The disparity in Figure 4 is not sufficient to suggest that our assumption of adsorption equilibrium between gas and pore wall is invalid. If the Poiseuille flow contribution to transport were taken into account, it would increase the calculated rate by about 7 per cent.

If the limiting process were Knudsen flow into interparticle voids, instead of intergranular voids, we find.

$$Y = 13 \cdot 3 \times t^{\frac{1}{2}}.$$

Equation (**1**) then predicts an initial rate that is more than 40 times the experimental rate. Also, if interparticle flow were limiting, the rate of gas uptake according to the flow equation would be proportional to the amount of adsorbent present, whereas experimentally it was independent.

Transport into the particles within each granule was calculated to be much faster than interparticle flow.

(*b*) *Shallow Beds of Alumina Monohydrate*

The beds were too shallow for intergranular flow to be limiting. For Knudsen flow of water vapour into the granules of the 0·1 g bed of alumina monohydrate described in Section II (*a*),

$$Y = 2 \cdot 8 \times t^{\frac{1}{2}}.$$

Equation (**1**) then leads to the broken line in Figure 5. Poiseuille flow within the granules was negligible. As in the previous section the agreement between experiment and theory is as good as can be expected.

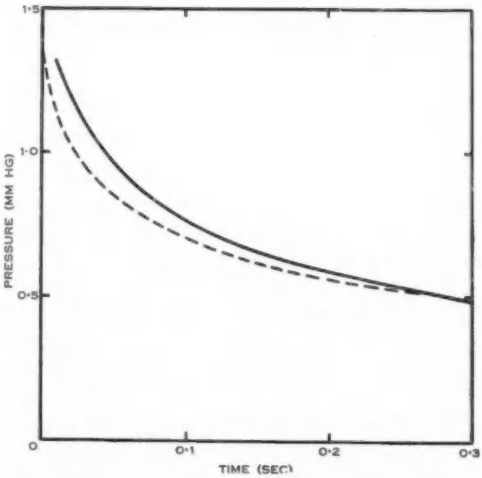

Fig. 5.—Experimental rate (full line) and rate calculated from the flow-equation (broken line) for water uptake by a shallow bed of alumina monohydrate. Temperature 140 °C, mass 0·1 g.

The flow equation predicts that for the shallow beds the initial rate will be proportional to the first power of the amount of adsorbent used (or S), while for the deep beds in Section IV (*a*) the rate should be independent of S. Both have been confirmed by experiments with water vapour as adsorbate (Part I).

(*c*) *Shallow Beds of Thoria*

Flow between the large agglomerates could not be limiting because they were packed only two deep.

If the slow step were Knudsen flow into the large agglomerates, accompanied by rapid adsorption, then using the pore dimensions given in Section II (*c*)

$$Y = 23 \times t^{\frac{1}{2}}.$$

A plot of equation (**1**) for this value of Y is shown in Figure 6 by a broken line. It will be seen that the experimental curve (full line) represents a rate of gas uptake many times less than calculated on the assumption of adsorption equilibrium.

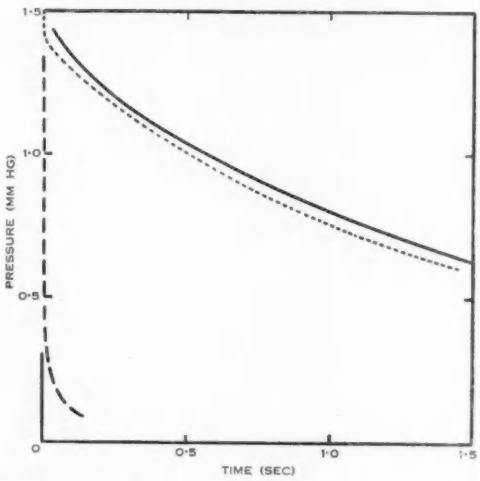

Fig. 6.—Calculated and experimental rates of water sorption by a shallow bed of thoria. Temperature 140 °C, mass 0·15 g. Experimental (full line); flow equation (broken line); chemisorption equation (dotted line), assuming an activation energy of 6500 cal mol^{-1} on 98 per cent. of the sites utilized and zero on the remainder.

When the flow equation is used to calculate the rate of gas uptake if flow into the small agglomerates were limiting, or into even smaller assemblages of particles, the rate obtained is very much greater than that shown for the large agglomerates.

Two alternatives remain : either the slow step is chemisorption, or Knudsen flow accompanied by relatively slow adsorption on the pore walls.

V. Application of the Chemisorption-Flow Equation

From the adsorption isotherms given by Winfield (1950) and from the curvature of the isotherm in Figure 1 it may be calculated that the heat of adsorption of water on thoria at 140 °C, when the surface coverage approaches

zero, is 21,000 cal/mol. We therefore take E_d, the activation energy for desorption, to be $21{,}000+E_a$, where E_a is the activation energy for adsorption. Different values of E_a may then be tested in the equation (**8**) of Part II, or in an approximation for small values of t which may readily be derived using methods described by Carslaw and Jaeger (1947). For each value of E_a, k_d (the intrinsic rate constant for desorption) is calculated using the desorption rate equation given by Glasstone, Laidler, and Eyring (1941, p. 354). The corresponding values of k_a can then be obtained from

$$k_e=\frac{k_a}{k_d}.$$

Using the above procedure we found that under our conditions the chemisorption-flow equation need be employed only in a narrow range of E_a values. If E_a is greater than 4000 there is little error in neglecting Knudsen flow. That is, the rate of adsorption can be assumed to account for the experimental rate of gas uptake. When E_a is less than a few hundred calories, the flow equation (**1**) may be used without much loss of accuracy in place of the inconvenient chemisorption-flow expression. Comparison of calculated and experimental rates showed that E_a was approximately 6000 cal. We therefore attempted to describe the experimental results for the thoria-water system by means of the chemisorption equation (see Section VI).

In the estimation of k_a and k_d it was noticed that k_a contains an entropy factor of 3×10^{-4}, or even smaller. This suggests that the act of adsorption of the water vapour which is taken up at 140 °C and about 1 mm pressure occurs only on a very small proportion of the sites and is followed by migration to other sites.

VI. Application of the Chemisorption Equation

Various values of the activation energies, and the proportion of the surface to which they refer, were tested in the 2-site equation (**28**) of Part II. By comparing the results with the experimental rate for a 0·15 g bed of thoria at 140 °C and $p_0=1\cdot5\times1333$ (see Section II (*e*) and Fig. 6), it was found that the average site utilized in an experiment under these conditions of mass, pressure, and temperature required an activation energy of 6400 cal/mol. In other words the chemisorption equation does not demand unreasonable values of any of the constants.

The equation is incapable, however, of describing the experimental results when the amount of adsorbent is altered. Whatever the values assigned to the activation energies and the fraction of the surface on which they apply, the chemisorption equation cannot predict adsorption rates which are proportional to more than the first power of S (see Part II). Indeed we are unable to conceive any reasonable physical picture of the adsorption process which could form the basis of a rate equation that shows the dependence on S^2.

An analysis of the experimental curves for different values of S leads to the conclusion that either :

(i) the rate of desorption is proportional to p while that of adsorption is independent of p ; or

(ii) the rate of desorption is independent of p as generally believed, while the rate of adsorption is inversely proportional to p^2.

Adsorption and desorption are both functions of surface coverage.

While it is conceivable that the desorption process could depend on pressure, a poisoning effect is a more ovbious explanation for the anomalous dependence on S. For a fixed volume of adsorbate the poison would inhibit a greater proportion of sites in the smaller sample of adsorbent. However, we can see no fault in the experimental technique which could adequately account for such an effect. The anomaly has proved to be reproducible in three different combinations of adsorbent and adsorbate (Part I, Table 1) in spite of changes in design of all parts of the apparatus. We believe that the effect is confined to adsorbing systems in which chemisorption limits the rate of gas uptake.

An explanation for the rate dependence on S^2, or higher power of S, cannot be provided on the basis of the curvature of the adsorption isotherm. For water on thoria the non-linearity of the isotherm accounts for a dependence of only $S^{1\cdot2}$.

It is customary to think that the rate of chemisorption has a positive temperature coefficient. However, the measured rate is the net rate after deducting the rate of desorption. It can be shown that the net rate may have a negative temperature coefficient, due to desorption increasing more than gross adsorption when the temperature is raised. We have found the temperature coefficient to be an insensitive test for discriminating between the various kinds of process which may limit the rate of gas uptake by a bed of adsorbent. Where negative coefficients are mentioned in Part I they do not eliminate the possibility that chemisorption is rate-controlling.

VII. Conclusions

For many purposes the rate of gas uptake by a catalyst bed in which adsorption is rapid can be calculated accurately enough by means of equation (**1**), after first determining the pore dimensions and an adsorption isotherm. Before greater accuracy can be achieved it may be necessary to study the Knudsen diffusion coefficient under transient conditions, and also its dependence upon l/r.

When adsorption is not fast compared with flow, it is necessary to employ one or other of the less convenient expressions (**28**) and (**8**) of Part II. Of these the latter appears to be needed only in a very narrow range of adsorption velocities. The importance of the equations is that once their validity has been established by experiment, they permit the measurement of the intrinsic rate constants for adsorption and desorption, k_a and k_d. These quantities have seldom been determined, in spite of their great significance in heterogeneous kinetics.

The chemisorption equation for two or three kinds of adsorption sites should be capable of describing most of the features of gas uptake by a catalyst bed when it is limited by the rate of adsorption. There would be advantages in using instead an equation in which the activation energies change smoothly

with surface coverage. We have not yet been able to solve this problem for a variable pressure system.

Dependence of the observed rate on bed geometry is a useful criterion of the nature of the limiting step in the process of gas uptake, but independence tells little. Likewise, the temperature coefficient is informative only when positive. All of the possible limiting processes (including surface migration) appear to be capable of exhibiting a negative coefficient in the measured rate.

The most significant test that we have found is the dependence on amount of adsorbent (or total surface area S). To the best of our knowledge the criteria at small values of t will prove to be as shown in Table 2, when the bed cross section is kept constant. The pressure dependence needs further investigation.

TABLE 2

CRITERIA OF LIMITING STEP IN GAS UPTAKE

Power of S	Slow Step Indicated
0	Gas flow through depth of bed
<1	Probably surface migration
1	Gas flow into granules
>1	Chemisorption

It may be thought that our experimental conditions, in which the pressures are about 10^{-3} atm, are remote from those in industrial reactors. We have employed low pressures with the object of keeping the fraction of surface covered by adsorbate small. Since molecular flow depends not on the pressure but on the pressure gradient, results obtained at low pressures can be applied to high pressure conditions provided Knudsen flow is still predominant. In a considerable number of industrial catalyses at moderate pressures, Knudsen flow is the principal mode of transport within the catalyst pellets, as pointed out by Wheeler (1951).

Within the pellets, and during a catalytic conversion, the steady-state conditions of Knudsen flow that have been almost exclusively dealt with by other investigators (for example, Carman 1950) are not attained. The conditions resemble those which would prevail if one of our sorption rate experiments could be "frozen", at the instant when the fraction of the pore length being utilized for adsorption equalled that during the catalytic conversion (see Part II, Section V (a)). Thus we may hope that a study of transient sorption will lead to a better understanding of reaction rates in pores. This is particularly true for fluidized systems, since in these the partial pressure of reactant, at the pore mouth, is subject to continual change as the granule circulates within the reactor.

VIII. ACKNOWLEDGMENTS

Messrs. J. Bayston, B. Wilson, and R. Carter, of the Division of Industrial Chemistry, C.S.I.R.O., are thanked for advice and assistance with apparatus.

IX. References

Anderson, R. B., McCartney, J. T., Hall, W. K., and Hofer, L. J. E. (1947).—*Industr. Engng. Chem.* **39**: 1618-28.

Barrer, R. M. (1941).—"Diffusion in and Through Solids." (Cambridge Univ. Press.)

Beckett, R., and Winfield, M. E. (1951).—*Aust. J. Sci. Res.* A **4**: 644-50.

Carman, P. C. (1950).—*Proc. Roy. Soc.* A **203**: 55-74.

Carman, P. C. (1938).—*J. Soc. Chem. Ind.* **57**: 225-34.

Carslaw, H. S., and Jaeger, J. C. (1947).—"Conduction of Heat in Solids." (Oxford Univ. Press.)

Dallavalle, J. M. (1943).—"Micromeritics." (Pitman: New York.)

Glasstone, S., Laidler, K. J., and Eyring, H. (1941).—"The Theory of Rate Processes." (McGraw-Hill Book Co.: New York.)

Sutherland, K. L., and Winfield, M. E. (1953).—*Aust. J. Chem.* **6**: 234.

Wheeler, A. (1951).—"Advances in Catalysis." Vol. 3. (Academic Press: New York.)

Wicke, E. (1939).—*Kolloidzschr.* **86**: 167-86.

Wilson, B. W. (1953).—*Aust. J. Appl. Sci.* **4**: 300-15.

Winfield, M. E. (1950).—*Aust. J. Sci. Res.* A **3**: 290-305.

Winfield, M. E. (1953).—*Aust. J. Chem.* **6**: 221.

SOLVENT EFFECTS IN THE SPECTRA OF BENZENE, TOLUENE, AND CHLOROBENZENE AT 2600 AND 2000 Å

By N. S. Bayliss* and Lois Hulme†

[*Manuscript received February* 27, 1953]

Summary

The ultraviolet spectra of benzene, toluene, and chlorobenzene at 2600 and 2000 Å have been measured in carbon tetrachloride, chloroform, *cyclo*hexane, *n*-hexane, ethanol, and water. Compared with the gases the solution spectra are all displaced to the red by amounts that agree qualitatively with the predicted effect of the solvent refractive index and the transition intensity according to the theory of Bayliss (1950). Quantitative agreement with this theory can be obtained only by assuming the effective cavity occupied by the solute molecule to be considerably smaller than the actual molecular size. The significance of this effect is discussed. The intensities of the solution spectra vary with the solvent refractive index, but in a way that is incompatible with the classical theory of Chako (1934). A marked increase in the intensity (particularly in toluene) is found where the solute absorption is close to an absorption band of the solvent, that is, for the 2600 Å transitions in carbon tetrachloride and to a less extent in chloroform. In the 2600 Å transition of benzene, a band appears in water, chloroform, and carbon tetrachloride that is very close to the position of the (0,0) band that is forbidden in the gas spectrum. The nature of this band is discussed.

I. Introduction

The present paper is the first of several in which it is proposed to make a careful study of solvent effects on the absorption spectra of organic molecules. In spite of the extensive literature on the subject, which we will not attempt to review at this stage, solvent effects on spectra are far from being well understood, a situation which is perhaps only to be expected in view of the difficulty of precisely describing the interaction forces between molecules in the liquid state. We shall sometimes find it desirable to repeat previous work, for several reasons. The fact that solvent effects are often slight changes of a second order suggests the need for the greatest possible precision in the measurements; in this respect much of the earlier work needs revision in the light of modern spectrophotometric technique. Furthermore a great amount of published work that gives solution data has been done with other objectives in mind and is not reported in a form that is suitable for our present purpose. The effect of solvents on spectral intensities, for example, has not in the past been given the attention it deserves.

* Department of Chemistry, University of Western Australia, Nedlands, W.A.

† This paper is adapted from the thesis presented by Miss L. Hulme in partial fulfilment of the requirements for the degree of B.Sc. with Honours, University of Western Australia; present address: Chemical Physics Section, Division of Industrial Chemistry, C.S.I.R.O., Melbourne.

Amongst the various ways in which solvents may affect solute spectra, the following effects always seem to be present.

(*a*) *Displacement of Solution Spectrum*

The frequency of the solution spectrum is displaced relative to that of the gas. The displacement is usually to the red, and one of us (Bayliss 1950) has shown on general theoretical grounds that there should be a red shift in solution depending on the solvent refractive index, the size of the solute molecule, and the intensity of the transition. This result, at least as far as the refractive index is concerned, has been confirmed in several cases (Badger and Pearce 1951; Coggeshall and Pozefsky 1951), while Sheppard (1942) in an earlier review stated that the refractive index is the dominating influence in all non-polar solvents. On the other hand there are examples where the solvent refractive index is not the dominating factor (Maddams and Schnurmann 1949), and also somewhere the solvent shift is to the blue and not to the red, as in the brown solutions of iodine and in the " blue-shift " spectra of some nitrogen-containing organic compounds (McConnell 1952). In certain merocyanine dye spectra studied by Brooker, Keyes, and Heseltine (1951), where the gas spectra are unknown, there are large blue shifts relative to normal solvents that seem to be correlated not with the refractive index but with the hydrogen bonding power of the solvent (Bayliss and McRae 1952). The theory of a red shift depending on the solvent refractive index, though approximate, is quite general, and the existence of exceptions shows that the electrostatic polarization forces considered by this theory are not the only ones that operate between solute and solvent, and that the total solvent shift may be the resultant of several types of solute-solvent interaction (Bayliss 1950; Herington and Kynaston 1952). It is one of the objectives of a study such as this to determine the type of interaction which is dominant in any given case.

(*b*) *Blurring of Vibrational Structure*

Vibrational structure, when present in the gas spectrum, is blurred and sometimes completely obliterated in solution. Some degree of blurring is to be expected; but the reason for complete obliteration in some cases is not fully understood. Substantial blurring has been correlated with hydroxylic solvents (Brode 1943); Kasha (1950), in discussing the spectra of aromatic compounds containing hetero-atoms, has shown that $\pi^* \leftarrow n$ transitions are greatly blurred in solution compared with $\pi^* \leftarrow \pi$.

(*c*) *Modification of Absorption Intensity*

The absorption intensity may be modified in solution. Experimental data on this effect are not as abundant as those on frequency displacements, partly because true intensities are difficult to measure in gas spectra with well-marked vibrational structure. Some authors have used ε_m, the maximum extinction coefficient, as a measure of intensity; but this is theoretically unsound. The true measure of the intensity of an electronic transition is the integrated intensity over the whole band system as expressed for example by the oscillator strength f (Mulliken and Rieke 1941). There seem to be no quantum-theoretical

studies of spectral intensities in solution ; the treatments by Chako (1934) and by Kuhn (1935) are based on classical theory and predict that f increases in solution according to a function of the solvent refractive index. Chako's prediction of increased intensity in solution is realized qualitatively, if not quantitatively, in some cases such as the visible absorption of bromine (Bayliss, Cole, and Green 1948) ; in other cases such as that of isoprene (Jacobs and Platt 1948) the intensity in solution seems to be unchanged.

In this paper we deal with the spectra of benzene and two simple derivatives, toluene and chlorobenzene. The gas spectrum of benzene in the ultraviolet consists of three electronic band systems ; a weak system ($f\sim0\cdot002$) near 2600 Å with well-resolved vibrational structure, a moderately intense system ($f\sim0\cdot07$) near 2000 Å with diffuse vibrational structure, and an intense system ($f\sim0\cdot7$) with practically no vibrational structure and with its maximum near 1800 Å.

The gas spectra of toluene and chlorobenzene are similar in general to that of benzene, with three band systems in each case occurring at approximately the same wavelengths and with roughly the same intensities. The intense transitions near 1800–1900 Å require vacuum technique and can be observed in only a very limited range of solvents ; they will not be considered here. Our work is concerned with the 2000 and 2600 Å transitions which are within the range of spectrophotometers of the Beckman type.

The solvents were chosen with reference to availability, simplicity of chemical structure, and variety of properties such as refractive index, dipole moment, and hydrogen-bonding power. The solution spectra were measured with a Beckman spectrophotometer, and since special attention was being given to the intensities, due regard was paid to the characteristics of this type of instrument. In spectra such as those of benzene, toluene, and chlorobenzene, where there are narrow vibrational bands at least in the 2600 Å transition, changes in the instrument slit width have a marked effect on the apparent values of the extinction coefficients, and to a less extent on the observed positions of intensity maxima (see Section II). For this reason, all spectra that have to be compared with one another have been measured at *constant slit width* to avoid the difficulties arising from this instrumental source.

II. Experimental

All materials were carefully purified by methods derived mainly from Weissberger and Proskauer (1935). The criteria of purity such as refractive index (n), freezing point (f.p.), density (d), and boiling point (b.p.) are quoted below and are compared with those of Timmermans (1950), the latter being denoted by T. and given in parentheses.

Benzene.—B.D.H. AnalaR benzene was shaken with sulphuric acid until the acid was colourless and the isatin test for thiophene was negative. It was dried, further purified by four fractional freezings, and finally distilled over sodium, $n_{\mathrm{D}}^{22\cdot5}$ 1·4998 (T. = 1·4995 by interpolation) ; f.p. 5·50 °C (T. = 5·496 °C).

Toluene.—B.D.H. laboratory reagent was shaken with mercury and then with sulphuric acid to remove sulphur compounds and until the isatin test was

negative. It was dried successively over calcium chloride and sodium, and finally fractionated over sodium, n_D^{15} 1·4980 (T.=1·49985); d^{25} 0·8603 (T.=0·8622). It seems that likely impurities such as higher alkyl benzenes, which have lower values than toluene for n and d, were not completely removed by our procedure.

Chlorobenzene.—B.D.H. laboratory reagent was dried with calcium chloride and fractionated, n_D^{20} 1·5240 (T.=1·52460).

Ethanol.—Commercial "absolute" ethanol *ex*-fermentation was distilled with 12N sulphuric acid to remove amine bases, and was then fractionated with 30 c.c. distilled water per litre to remove benzene. The product was tested in the Beckman spectrophotometer and shown to be free of benzene. Its water content was determined from measurements of n and d.

Ethanol (Absolute).—Ethanol (96 per cent.) was refluxed twice with freshly calcined lime and distilled, n_D^{25} 1·3594 (T.=1·3595). Timmermans (1950) states that this treatment forms traces of aldehyde which absorbs at 2100 Å. Our sample absorbed appreciably at this wavelength (transmission of 1 cm layer at 2100 Å=10 per cent.); but it was transparent at longer wavelengths.

n-*Hexane.*—B.D.H. laboratory reagent "specially pure for spectroscopy" was purified by Castille and Henri's method (Weissberger and Proskauer 1935). The product had the high refractive index of n_D^{26} 1·3770 (T.=1·3717) and the low transmission of 46 per cent. (1 cm layer) at 2100 Å, indicating that it probably still contained traces of unsaturated compounds.

cyclo*Hexane.*—B.D.H. laboratory reagent "special for spectroscopy" was shaken first with alkaline, and then with acid, potassium permanganate. After washing with dilute sodium carbonate solution it was dried over calcium chloride and distilled. To remove traces of benzene it was then fractionally frozen five times, dried over sodium, and fractionated, n_D^{16} 1·4282 (T.=1·42834 by interpolation); f.p. 5·6 °C (T.=6·48 °C). The transmission curve showed that all absorbing impurities had been removed except one causing very slight absorption near 2550 Å; this might be either benzene or perhaps 1,3-*cyclo*hexadiene. The freezing point is low; however, Thompson and Ubbelohde (1950) have referred to the difficulty of obtaining "convergence" in the freezing point of this compound.

Chloroform.—B.D.H. AnalaR chloroform, which had been stored in the dark over calcium chloride, was fractionated over fresh calcium chloride immediately before use, n_D^{20} 1·4453 (T.=1·4455); b.p. 60·8–61·0 °C (T.=61·2 °C).

Carbon Tetrachloride.—The B.D.H. material (technical) was shaken three times with alcoholic sodium hydroxide at 50–60 °C to remove carbon disulphide, washed with water until the iodoform test indicated that all alcohol had been removed, dried over calcium chloride, and fractionated, n_D^{21} 1·4590 (T.=1·4597 by interpolation); b.p. 76·7–76·8 °C (T.=76·75 °C). The transmission (1 cm layer) was 25 per cent at 2650 Å.

Water.—Laboratory distilled water was redistilled twice from glass.

(*a*) *Procedure*

Extinction coefficients were measured with a Beckman quartz spectrophotometer, model DU. The path lengths were 1 cm and 1 mm (both nominal*), the latter path being obtained by inserting 0·9 cm silica spacers in the 1 cm cells. One cell was always reserved for the pure solvent, the other for the solution being investigated. Cell matching factors were determined over the complete range of wavelengths so that the appropriate correction could be applied where necessary to the extinction measurements. In practice, the correction was needed only when using cells plus spacers in the shortest wavelength range. When working with a 1 mm path length near a solvent absorption band, that is, in a region where the solvent absorbs appreciably, it was also necessary to correct the extinctions for the slight difference in path length between the solvent and solution cells.

When an absorption spectrum has well-resolved vibrational structure, as in all the cases studied in this paper, the measured extinction coefficients are quite sensitive to the slit width in an instrument of the Beckman type when the wavelength band transmitted by the slit is comparable in width with the vibrational bandwidths in the spectrum. We therefore kept the slit as narrow as possible, and more important we *kept the slit width constant* in each series of measurements of one solute in a series of solvents. In some of the later measurements the instrument sensitivity was increased, and the required slit width reduced correspondingly, by substituting a 10,000 MΩ resistor for the standard 2000 MΩ phototube load resistor in the Beckman instrument. The nominal bandwidths in each case are shown in the usual way in Figures 1–9.

Depending on the intensity of the spectrum, the solutions ranged in concentration between 0·005 and 0·0001M. Standard stock solutions were made up by adding solute to previously weighed standard flasks partly filled with solvent, and finding the weight of the added solute by difference. The stock solutions were then made up to volume by adding pure solvent. Stock solutions were diluted, by a factor never exceeding 1 : 100, to obtain the solutions for measurement. The standard flasks, the pipettes, and the microburette were all calibrated for both water and benzene.

(*b*) *Results*

The results have been expressed as molar extinction coefficients ε defined by the usual formula

$$\log_{10}(I_0/I) = \varepsilon c l,$$

where I_0 and I are respectively the incident and transmitted intensities, c is the concentration (mol l^{-1}), and l is the path length (cm). They are plotted in Figures 1–9 as curves of ε against the wave number ν. These curves were drawn from readings at intervals of 2·5, 5, or 10 Å, depending on the degree of fine structure. The solvents are identified by the following number code: 2, carbon tetrachloride ; 3, chloroform ; 4, *cyclo*hexane ; 5, *n*-hexane ; 6, ethanol (absolute) ; 6′, ethanol (95 per cent.) ; 6″, ethanol (91 per cent.) ; 7, water.

* In the calculations we used the actual lengths as given by the manufacturers.

The main peaks have been designated arbitrarily by the letters *a*, *b*, ...; the values of ε and ν at these peaks are recorded and compared with the gas values where known, in Tables 1–6. The peak frequencies were obtained from the plotted curves by two observers whose estimates generally agreed within 10 or 15 cm^{-1}. The intensity of each transition can be expressed by the oscillator strength *f*, defined by

$$f = 4 \cdot 313 \times 10^{-9} \int \varepsilon d\nu.$$

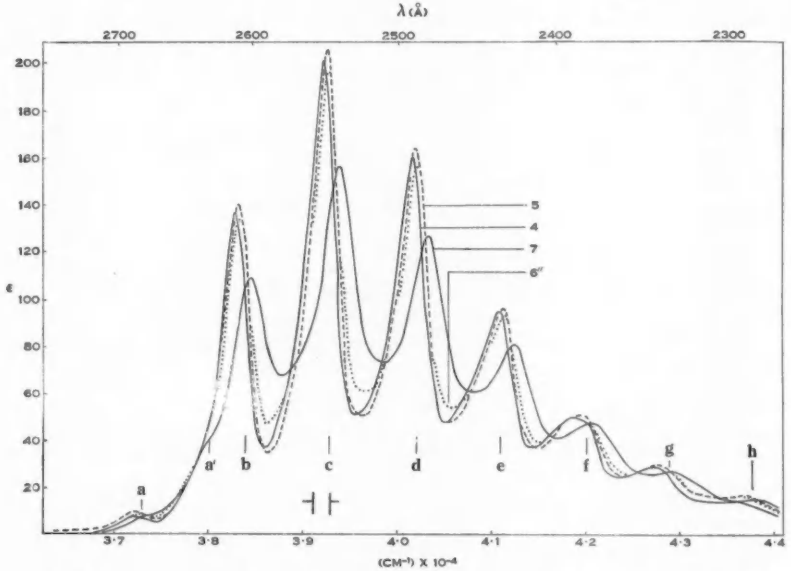

Fig. 1.—Benzene (2600 Å) in *cyclo*hexane (4), *n*-hexane (5), ethanol (6), and water (7).

The *f* values were calculated from the ε-ν curves by graphical integration; in the case of the 2600 Å transition from the long wavelength onset of the absorption to the minimum between the 2600 and 2000 Å transitions, for the 2000 Å transitions between this minimum and 2000 Å. Absorption by the solvent in some cases made it impossible to obtain the complete *f* for the 2600 Å transition; in these we have computed *f* to arbitrary cut-offs designated in each case. Values of *f*, together with gas values where known, are given in Table 7.

(*c*) *Experimental Errors*

Experimental errors are difficult to assess, since some of them depend on instrumental factors that are not readily controlled. Concentrations of solutions were known to within better than 1 per cent. Cell lengths were given by the manufacturers to 0·001 cm. In the 2600 Å region, repetition of readings using new solutions checked with original readings to within 1 per cent. We estimate

the probable error in this region as about 2 per cent. subject to the effect of slit width, which we kept narrow, particularly in the toluene and chlorobenzene spectra. Absolute frequencies depend on the manufacturer's calibration of the spectrophotometer, this was checked at the line Hα in the hydrogen source. Relative frequencies between different spectra are probably good at least to within 20 cm^{-1}.

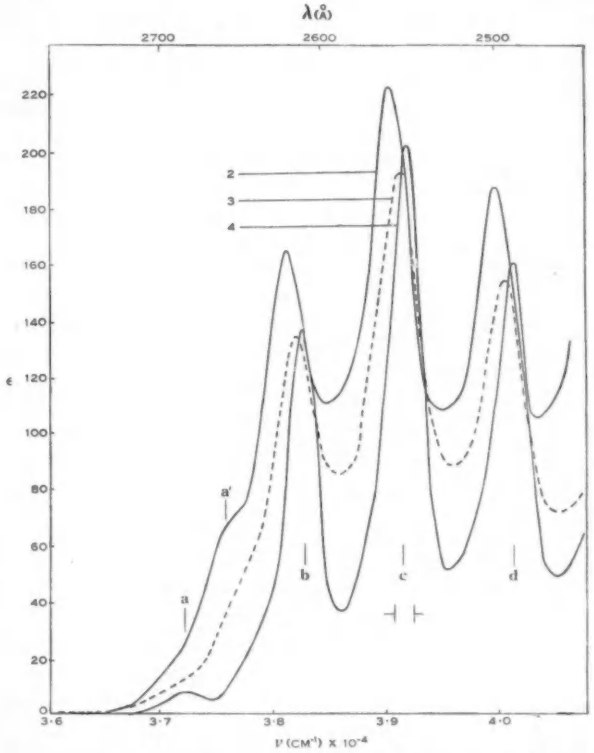

Fig. 2.—Benzene (2600 Å) in carbon tetrachloride (2), chloroform (3), and *cyclohexane* (4).

In the 2000 Å region, errors are greater owing to the increasing effect of stray light and the wider slits that had to be employed. Corrections for cell matching factors amounted to as much as 7 per cent. when the 0·1 cm cells were used in this region. All the pure solvents absorb appreciably in this region, and corrections had to be applied since the path lengths in the pure solvent and solution cells were not equal. Duplicate measurements differed by as much as 4 per cent. It is possible that results in this region are subject to errors of up to 10 per cent. in ε.

III. Discussion

(*a*) *Frequency Displacements*

The magnitude of the red shift due to the solvent refractive index was derived by one of us (Bayliss 1950) on the basis of a simplified model in which the solute transition was regarded as the creation of a point dipole at the centre of a spherical cavity in a continuous dielectric solvent medium. The resulting expression was

$$\Delta\nu = C\left(\frac{f}{\nu a^3}\right)\left(\frac{n^2-1}{2n^2+1}\right), \quad \ldots\ldots\ldots\ldots\ldots\ldots \quad (1)$$

where f is the oscillator strength of the transition, ν is the frequency in cm^{-1}, a is the cavity radius, and n is the refractive index of the solvent at the frequency ν. The numerical factor C was found to be between 7×10^9 and 10^{10}.

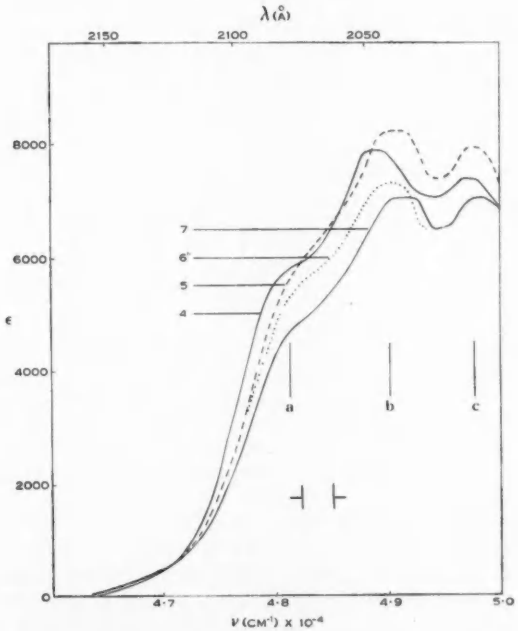

Fig. 3.—Benzene (2000 Å) in *cyclo*hexane (4), *n*-hexane (5), ethanol (6), and water (7).

In applying equation (1) to the results of Tables 1-6, it is seen that all the solution spectra are displaced to the red as compared with the gas state. In any one spectrum the different vibrational bands are displaced by approximately equal but not identical amounts, showing that there are small changes in the vibrational frequencies superimposed on the shift of each electronic transition as a whole. Our results do not confirm the statement quoted by Sheppard

(1942) that, in the 2600 Å transition of benzene, the low frequency bands are displaced to the red and the high frequency bands to the violet. Displacements of selected vibrational bands are summarized in Table 7, together with values of f, n, and the appropriate functions of n. In the 2600 Å transitions the shifts are between 100 and 500 cm^{-1} and show an obvious qualitative correlation with the solvent refractive index. The 2000 Å transition of benzene is displaced by about four times the amount of that at 2600 Å; the 2000 Å transition of toluene is too diffuse to measure the shifts accurately; gas data are lacking for the

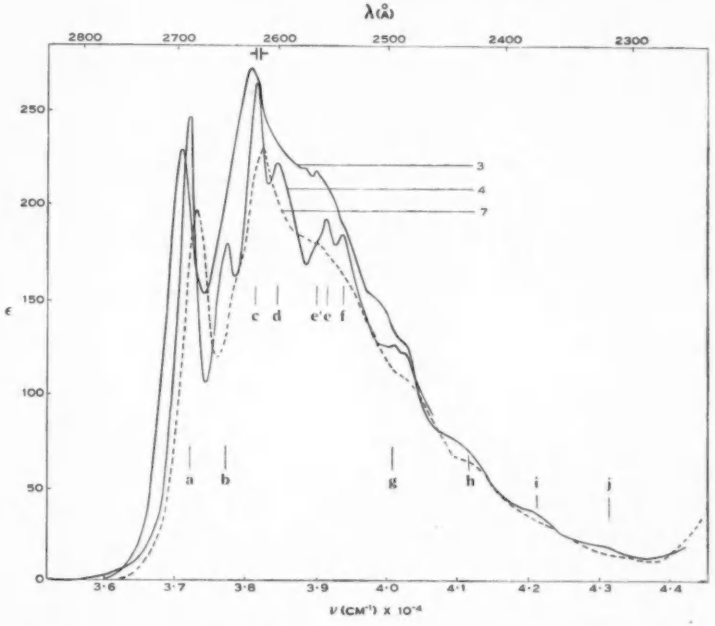

Fig. 4.—Toluene (2600 Å) in chloroform (3), *cyclo*hexane (4), and water (7).

2000 Å transition of chlorobenzene, whose displacements are therefore referred in Table 7 to the solution in water. These shifts also correlate with the appropriate value of n in each case, and it appears that equation (**1**) is at least qualitatively valid for all the spectra in Table 7, suggesting that the refractive index effect is *dominant* in all the cases considered in this paper.

The quantitative application of equation (**1**) can be tested in several ways. Firstly, it is predicted that $\Delta\nu$ should be a linear function of either $(n^2-1)/(2n^2+1)$ or $f(n^2-1)/(2n^2+1)$, and both of these refractive index functions have been included in Table 7. Since f varies from solvent to solvent, it seems rational to choose the latter function for test, and Figure 10 shows $\Delta\nu$ plotted against $f(n^2-1)/(2n^2+1)$. In order to obtain comparable results over the whole range

of solvents, it has been necessary to use the values of f computed to the arbitrary cut-offs designated in Table 7. The predicted linear relation is satisfactory for the 2600 Å transitions of benzene and toluene, except for anomalous points in water. The 2600 Å transition of chlorobenzene also gives a straight line,

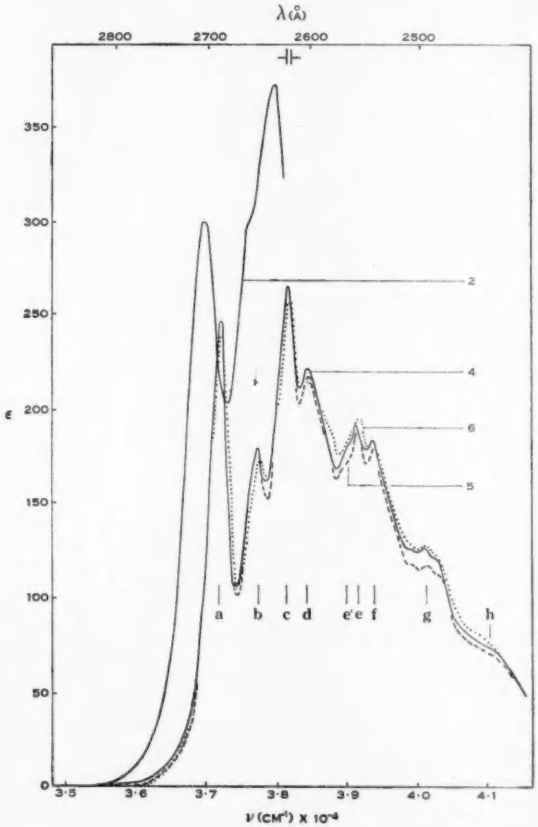

Fig. 5.—Toluene (2600 Å) in carbon tetrachloride (2), *cyclo*hexane (4), *n*-hexane (5), and ethanol (6).

which, however, does not pass through the origin. In the 2000 Å transitions, the points for benzene depart considerably from the predicted linearity, while the chlorobenzene points are satisfactorily linear, but owing to the absence of gas data it is not known whether the line would pass through the origin if the displacements had been reckoned from the gas spectrum instead of from the solution in water.

Equation (1) furthermore predicts that for the different transitions of any one solute, $\Delta\nu$ should be proportional to the oscillator strength f. Table 7 shows that this is true in a qualitative sense, since the shifts observed in the moderately strong 2000 Å transitions of benzene and chlorobenzene are between two and four times those of the weaker 2600 Å transitions. Quantitatively it seems that other factors are involved. Taking the one example of benzene in

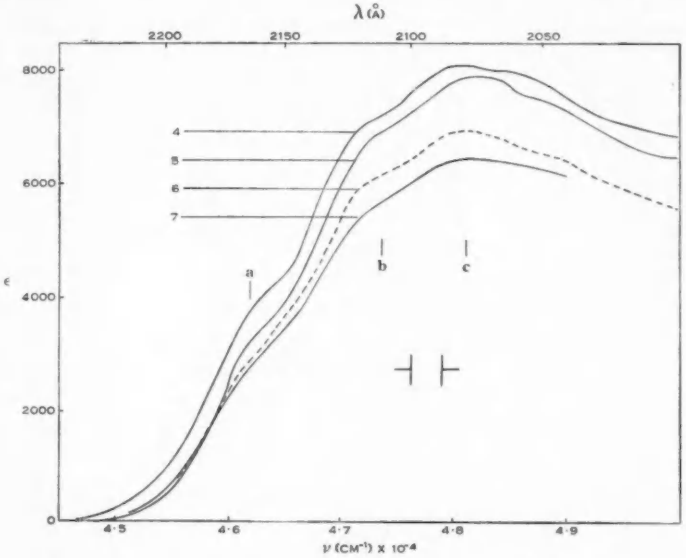

Fig. 6.—Toluene (2000 Å) in *cyclo*hexane (4), *n*-hexane (5), ethanol (6), and water (7).

*cyclo*hexane, the red shift of the 2000 Å transition is about 3·5 times that of the transition at 2600 Å; the oscillator strengths, however, are in the ratio of about 45 : 1.

This quantitative discrepancy leads to the discussion of the absolute magnitude of the red shift as predicted by the complete application of equation (1). The only uncertain and not directly measurable quantity in this equation is a, the cavity radius. In the case of the intense (V, N) transition of benzene at 1800 Å, Bayliss (1950) showed that the red shift in *n*-heptane could be accounted for by equation (1) by assuming a to be between 2·6 and 3·0 Å, values which are close to the known dimensions of the benzene molecule. If we use the case of benzene in *cyclo*hexane as representative of the data in this paper, equation (1) accounts for the red shift of the 2000 Å transition if $a = 1{\cdot}5$ Å, and of the 2600 Å transition if $a = 0{\cdot}7$ Å. Thus the required value of a becomes progressively less than the actual solute molecular radius the weaker the

transition. It is also worth noting that Bayliss (1950) also found that the red shifts in the weak visible transitions of bromine and iodine required a to be near 0·7 Å, a value considerably less than the actual molecular radii.

The results of the preceding paragraph seem to have a significance whose theoretical nature is not quite clear. An alternative way of expressing them is to say that weak (forbidden) transitions have much greater red shifts than are predicted by equation (**1**). The model employed in this equation of a point dipole in a spherical cavity is an obviously artificial one, and it is known for example from the work of Scholte (1949) that the value of the constant C of

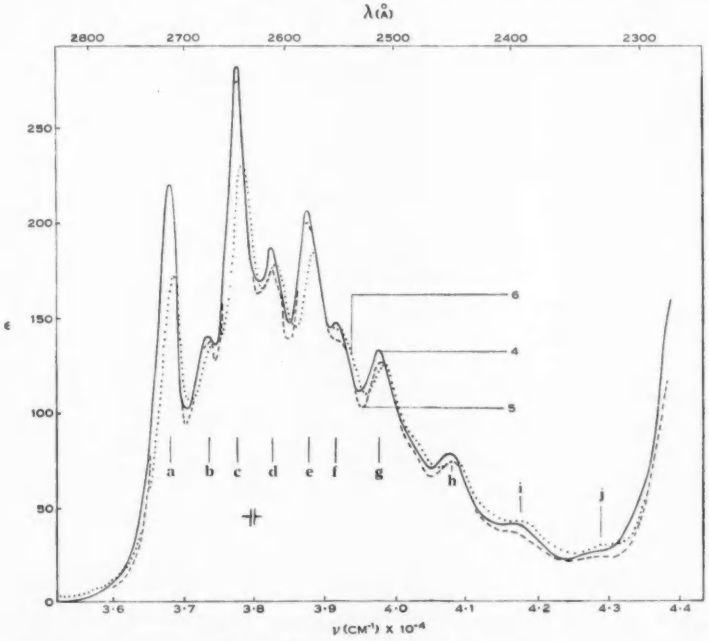

Fig. 7.—Chlorobenzene (2600 Å) in *cyclo*hexane (4), *n*-hexane (5), and ethanol (6).

equation (**1**) is changed if the cavity is not spherical. This, however, cannot explain the results, since even if our value of C is incorrect because the solute molecule is not spherical, this is no reason why C should have different values for different transitions in the same solute. On the other hand the transition dipole is not strictly in an empty cavity in the solvent, since actually it is embedded in the solute molecule whose " electronic atmosphere " is not very different from that of the solvent molecules. If the transition dipole is small and is located well " inside " the solute molecule, the " outer " part of the solute molecule might legitimately be regarded as forming part of the solvent so far as electrostatic polarization forces are concerned. This may well be the reason

why the effective cavity radius a is smaller for the weaker transitions with smaller transition dipoles ; unfortunately the complete discussion of this question seems to be beyond the resources of current theory.

(*b*) *Intensities*

According to the theory of Chako (1934), oscillator strengths in solution should be increased relative to the gas state by the factor $(n^2+2)^2/9n$, where n is the solvent refractive index (Mulliken and Rieke 1941). For values of

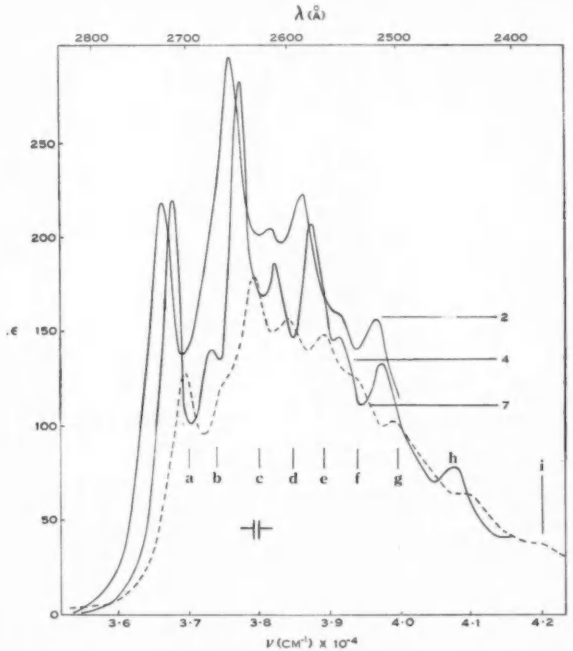

Fig. 8.—Chlorobenzene (2600 Å) in carbon tetrachloride (2), *cyclo*-hexane (4), and water (7).

$n=1{\cdot}37$, $1{\cdot}47$, and $1{\cdot}54$ (covering roughly the range of n in Table 7), the respective values of the Chako factor are $1{\cdot}22$, $1{\cdot}31$, and $1{\cdot}38$. Unfortunately, gas intensity data seem to be available only for benzene (2600 and 2000 Å) and for toluene (2000 Å). In each of these cases the intensities in the solvents of lower refractive index, such as water and ethanol, are *less* than in the gas, instead of 20 to 30 per cent. greater as predicted. Almasy and Laemmel's (1951) value of $0{\cdot}0020$ for the gaseous f in benzene (2600 Å) is probably uncertain owing to the difficulty of measuring the intensity of a band system with sharply resolved fine structure. (Their value of $f=0{\cdot}0016$ for this system in hexane is very close to ours.) On the other hand, the gaseous f's for the more diffuse

systems at 2000 Å in benzene and toluene should be reliable. It seems that Chako's classical theory is not adequate for these spectra, in keeping with the conclusion reached by Jacobs and Platt (1948).

Comparing the solution spectra amongst themselves, and using the f's taken to the arbitrary cut-offs (Table 7), it is seen that the 2600 Å transitions of all three compounds have practically identical intensities in water, ethanol, *n*-hexane, and *cyclo*hexane, and that the intensity shows a sharp rise in each case in chloroform and carbon tetrachloride. The rise is particularly marked in the case of toluene in carbon tetrachloride, where f is nearly double that in

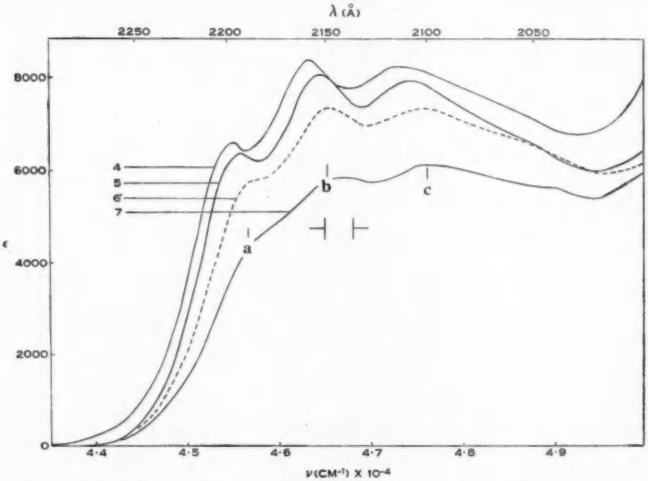

Fig. 9.—Chlorobenzene (2000 Å) in *cyclo*hexane (4), *n*-hexane (5), ethanol (6), and water (7).

n-hexane, and in all cases it is much greater than would be expected if the Chako factor governed the intensity ratios between solvents. We believe it to be significant that this sharp increase in f occurs when the solvent has an absorption band close to that of the solute ; in both chloroform and carbon tetrachloride absorption by the solvent confines measurements to the low frequency edge of the solute transition. Unpublished work by one of us (N.S.B.) shows that the perturbing influence of the solvent on the solute should be particularly strong when solvent and solute have excited states that are close together in energy. The 2000 Å transitions (see Table 7) all show a steady increase in f as the solvent n increases ; here too the increases are always greater than would be predicted by the Chako factor.

(*c*) *The* a′ *Band in Benzene* (2600 Å)

An interesting feature of the benzene spectra in Figures 1 and 2 (see also Table 1) is the appearance of a new band or shoulder, which we have designated

a', occurring between the *a* and *b* bands in water, chloroform, and carbon tetrachloride, but not in the gas or in the other solvents. While our work was in progress, we learned that this band had already been reported in carbon tetrachloride solution by Ham, Platt, and McConnell (1951), and that Ham (1953)* has shown it to be present as the first member of a progression in a glassy hydrocarbon solvent at liquid nitrogen temperatures, and considerably enhanced when the glassy solvent contains carbon tetrachloride.

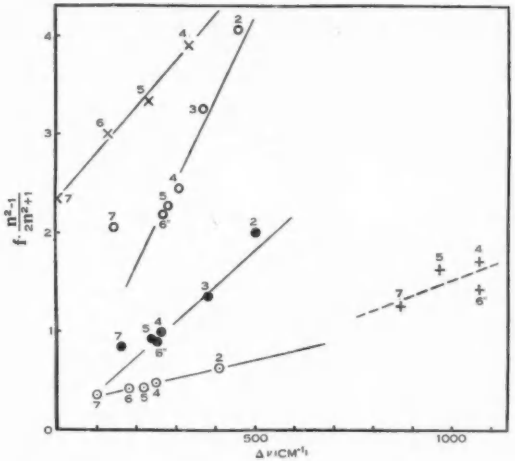

Fig. 10.—Plots of frequency displacements against function of solvent refractive index and transition intensity. ○ Benzene (2600 Å); ● Toluene (2600 Å); ⊙ Chlorobenzene (2600 Å); + Benzene (2000 Å); × Chlorobenzene (2000 Å) (shift referred to chlorobenzene in water). The vertical scale gives $f.(n^2-1)/(2n^2+1)\times10^4$ for benzene at 2600 Å; $f.(n^2-1)/(2n^2+1)\times10^3$ for toluene and chlorobenzene at 2600 Å; $f.(n^2-1)/(2n^2+1)\times10^2$ for chlorobenzene and benzene at 2000 Å.

The 2600 Å transition ($^1B_{2u}\leftarrow{}^1A_{1g}$) in benzene gas is forbidden, and the (0, 0) band does not appear in the gas or in most solvents. Band *b* is a (1←0) transition involving the excited state e^+_g vibration whose frequency in the gas is 520 cm^{-1} and which makes the transition allowed. Band *a* is the (0←1) transition involving the corresponding e^+_g ground-state frequency of 606 cm^{-1} (Sponer *et al.* 1939). Thus the *a* and *b* bands are separated by 1128 cm^{-1} (520+606) in the gas state and by 1145 cm^{-1}, for example, in *n*-hexane. The bands *b*, *c*, *d*, . . . are the (1←0) progression involving the totally symmetrical frequency whose value for the gas in the excited state is 923 cm^{-1}. In solution (Table 1), the intervals between these bands are somewhat variable since the observed peak maxima are necessarily averaged over groups of bands which are resolved

* We are indebted to Mr. J. S. Ham for the privilege of seeing his paper in manuscript.

TABLE 1

BENZENE, 2600 Å TRANSITION

Values of ν (cm^{-1}) and ε (in italics); slit width = 0·50 mm

Band	Gas*	Water (7)	Ethanol (91%) (6″)	*n*-Hexane (5)	*cyclo*-Hexane (4)	Chloroform (3)	Carbon Tetrachloride (2)
a	37482	~37230	~37230	~37175	~37175	Band too diffuse	
		8	*9*	*10*	*8*		
b	38610	38460	38340	38320	38280	38223	38150
		109	*134*	*140*	*137*	*134*	*164*
c	39533	39390	39265	39255	39225	39165	39075
		177	*196*	*206*	*201*	*192*	*222*
d	40455	40320	40200	40180	40150	40080	40000
		127	*157*	*164*	*161*	*153*	*187*
e	41377	41220	41120	41120	41070	—	—
		81	*94*	*97*	*95*		
f	42298	~42090	41880	41930	41850	—	—
		47	*51*	*51*	*50*		
g	43022†	~42910	42750	42750	42700	—	—
		28	*30*	*30*	*29*		
h	43952†	~43750	43670	43670	43670	—	—
		16	*17*	*18*	*15*		
a′	—	New shoulder appears at 37950 cm^{-1} $\varepsilon = 38$				Shoulder at 37750 cm^{-1} $\varepsilon = 40$–50	Shoulder (more resolved) at 37600 cm^{-1} $\varepsilon = 66$

* Gas data from Sponer (1947), except those marked † which are from Lauer and Oda (1936).

TABLE 2

BENZENE, 2000 Å TRANSITION

Values of ν (cm^{-1}) and ε (in italics); slit width = 1·0 mm

Band	Gas*	Water (7)	Ethanol (6″)	*n*-Hexane (5)	*cyclo*Hexane (4)
b	49970	49100	48900	49000	48900
	~*6600*	*7000*	*7300*	*8100*	*7880*
c	50900	49900	49700	49800	49700
	~*6300*	*6700*	~*7000*	*7800*	*7360*

* Gas data from Pickett, Muntz, and McPherson (1951).

TABLE 3

TOLUENE, 2600 Å TRANSITION

Values of ν (cm^{-1}) and ε (in italics); slit width = 0·15 mm

Band	Gas*	Water (7)	Ethanol (94%) (6′)	*n*-Hexane (5)	*cyclo*-Hexane (4)	Chloroform (3)	Carbon Tetrachloride (2)
a	37473	37310	37220	37230	37210	37090	36970
		197	*239*	*247*	*247*	*229*	*~300*
b	37938 }	—	37760	37725	37725	—	—
	37999 }		*173*	*177*	*180*		
c	38401	38240	38170	38180	38150	38060	37980
		229	*260*	*264*	*266*	*273*	*~372*
d	38665	Structure indistinct	38440	38460	38440		
			215	*217*	*222*		
e	39365	,,	39160	39120	39120	38980	
			196	*189*	*193*	*219*	
f	39593 }	,,	39370	39370	39370		
	39628 }		*183*	*180*	*185*		
g†	Structure too complex	,,	~40080	40160	40080		
			129	*118*	*127*		
h	,,	,,	Shoulder	Shoulder	Shoulder		
i	,,	,,	,,	,,	,,		
j	,,	,,	,,	,,	,,		
e′	39191	,,	V. slight shoulder	V. slight shoulder	V. slight shoulder	38840	
						220	

* Gas data from Sponer (1942).

† Band *g* is one of three diffuse bands.

TABLE 4

TOLUENE, 2000 Å TRANSITION

Values of ε (in italics)

Band*	Water (7)	Ethanol (6)	*n*-Hexane (5)	*cyclo*Hexane (4)
c†	*6400*	*6950*	*7800*	*8100*

* Bands are extremely diffuse, but appear to be coincident except for the intensity factor.

† Band *c* has its maximum at ~48100 cm^{-1} in each solvent.

in the gas spectrum. However, we found the average spacing in our six solvents to be 930 cm^{-1}.

The missing (0, 0) band in the gas should occur at a frequency 520 cm^{-1} lower than that of band *b*. Now the interval between *b* and *a'* in water is 510 cm^{-1}, in chloroform 470 cm^{-1}, and in carbon tetrachloride 550 cm^{-1}. Bearing in mind the limited accuracy of our measurements, especially where shoulders such as *a'* are concerned, these values suggest strongly that *a'* is in fact the (0, 0) band which has become allowed as the result of solvent-solute interaction. The (0, 0) band, and the progression based on it (*I* series) appear in solid benzene owing to the effect of crystal forces in breaking down the D_{6h} symmetry of the isolated benzene molecule (Sponer *et al.* 1939). When one considers a solute molecule surrounded by a solvent cage, one might similarly expect the symmetry of the solute molecule to be modified, especially when the solvent exerts a strong perturbation, as carbon tetrachloride undoubtedly does on benzene (see intensity results above). Such an effect might depend, not on the symmetry of the individual solvent molecule, but *on the geometry of the way in which the solvent molecules can pack around the solute.*

On the other hand Ham (1953), after carefully reviewing the data in solid benzene and in the glassy solvents, concludes that the *a'* band and its accompanying progression are more likely to be due to a separate electronic transition involving an upper state of symmetry $^3E_{1u}$. The enhancement in glassy solvents containing carbon tetrachloride is regarded by him as the result of the effect of the heavy chlorine atoms of the solvent in increasing spin-orbit coupling and thus relaxing the prohibition of the singlet-triplet transition. This effect does not account for our observation that the *a'* band appears in water, a solvent that does not possess heavy atoms. It is also a remarkable coincidence that the *a'* band appears so close to the predicted (0, 0) position. Ham (1953) has pointed out that there are small frequency discrepancies in the crystal and glassy solvent data that are not easy to account for if the *I* series is a (0, 0) progression involving the $^1B_{2u}$ state, so that it seems that the final decision must await further data.

(*d*) *Fine Structure*

The compounds studied in this paper add little to our understanding of the blurring of fine structure in solution. In benzene (2600 Å), blurring is more prominent in those solvents where the *a'* band appears (water, chloroform, carbon tetrachloride); in toluene (2600 Å) it is most marked in water and chloroform; in chlorobenzene (2600 Å) it is evident in water. In the diffuse 2000 Å transitions it is slightly more pronounced in water than in the other solvents (Figs. 4–9). There is no marked correlation with the hydroxylic nature of the solvent, since the spectra in ethanol are, in general, almost as well resolved as those in *n*-hexane.

IV. Acknowledgment

The authors gladly acknowledge the financial assistance of the University Research Fund.

TABLE 5

CHLOROBENZENE, 2600 Å TRANSITION

Values of ν (cm^{-1}) and ε^*(in italics); slit width = 0·15 mm

Band	Gas*	Water (7)	Ethanol (100%) (6)	*n*-Hexane (5)	*cyclo*-Hexane (4)	Chloroform (3)	Carbon Tetrachloride (2)
a	37052	36950	36870	36830	36800	36730	36640
		128	*172*	*215*	*221*		*219*
b	37577	Shoulder ~37520	37420	37380	37340	Shoulder	
		~127	*137*	*137*	*141*		
c	38018	37920	37840	37790	37770	37720	37630
		185	*231*	*277*	*283*		*296*
d	38504	38400	38300	38240	38240	38220	38180
		157	*179*	*175*	*187*		*205*
e	38981	38910	38840	38760	38760	38700	38650
		149	*184*	*200*	*207*		*223*
f	Structure	Shoulder	Shoulder	Shoulder		Shoulder	Shoulder
	too	~39290	~39200	~39200	39140		~39120
	complex	*~126*	*~144*	*~138*	*147*		*~161*
g	,,	39920	39840	39780	39740	39740	39680
		103	*125*	*126*	*133*		*157*
h	,,	~40790	~40860	~40820	40720		
		~65	*74*	*74*	*78*		
i, j	,,	Shoulder	Shoulder	Shoulder	Shoulder		

* Gas data from Sponer and Wollman (1941).

TABLE 6

CHLOROBENZENE, 2000 Å TRANSITION

Values of ν (cm^{-1}) and ε (in italics); slit width = 1·0 mm

Band	Gas	Water (7)	Ethanol (6′)	*n*-Hexane (5)	*cyclo*Hexane (4)
a	Data not		~45720	45600	45500
	available		*5800*	*6360*	*6580*
b	,,	46670	46540	46440	46340
		5800	*7360*	*8080*	*8380*
c	,,	~47620	~47620	47440	47300
		6100	*7320*	*7900*	*8240*

TABLE 7

COMPARISON OF BENZENE, TOLUENE, AND CHLOROBENZENE, 2600 AND 2000 Å TRANSITIONS

Transitions	Solvent	f (total)	f (to cut-off)	$\Delta\nu$ (cm^{-1})	n (solvent)	$\frac{n^2-1}{2n^2+1}$	$f\left(\frac{n^2-1}{2n^2+1}\right)$
Benzene 2600 Å	Gas	0·0020[a]		0			
	Water (7)	0·0015	0·0011[b]	143[c]	1·375[d]	0·186	0·000205
	Ethanol (6′)	0·0017	0·0011	268	1·408	0·198	0·000218
	n-Hexane (5)	0·0017	0·0011	278	1·428	0·205	0·000226
	*cyclo*Hexane (4)	0·0016	0·0011	308	1·482	0·222	0·000244
	Chloroform (3)		0·0014	368	1·516	0·232	0·000325
	Carbon tetrachloride (2)		0·0017	458	1·540	0·239	0·000406
Benzene 2000 Å	Gas	0·12[r]	0·065[e, f]	0[g]			
	Water (7)		0·063	870	1·42[h]	0·202	0·0127
	Ethanol (6′)		0·067	1070	1·46	0·215	0·0144
	n-Hexane (5)	(0·12)[s]	0·073	970	1·49	0·224	0·0164
	*cyclo*Hexane (4)		0·072	1070	1·54	0·240	0·0173
Toluene 2600 Å	Gas			0			
	Water (7)	0·0030	0·00045[t]	163[j]	1·369[k]	0·184	0·000828
	Ethanol (6′)	0·0033	0·00045	253	1·404	0·196	0·000882
	n-Hexane (5)	0·0033	0·00045	243	1·420	0·202	0·000909
	*cyclo*Hexane (4)	0·0033	0·00045	263	1·474	0·219	0·000986
	Chloroform (3)		0·00059	383	1·505	0·229	0·001351
	Carbon tetrachloride (2)		0·00085	503	1·525	0·235	0·001998
Toluene 2000 Å	Gas		0·12[q]	Bands too diffuse to observe displacements			
	Water (7)		0·098[e]				
	Ethanol (6)		0·102				
	n-Hexane (5)		0·115				
	*cyclo*Hexane (4)		0·123				
Chlorobenzene 2600 Å	Gas			0			
	Water (7)	0·0028	0·0019[l]	102[m]	1·369[n]	0·184	0·000350
	Ethanol (6)	0·0029	0·0021	182	1·402	0·196	0·000412
	n-Hexane (5)	0·0028	0·0021	222	1·420	0·202	0·000424
	*cyclo*Hexane (4)	0·0030	0·0022	252	1·473	0·219	0·000482
	Chloroform (3)			322	1·505	0·229	
	Carbon tetrachloride (2)		0·0027	412	1·523	0·234	0·000632
Chlorobenzene 2000 Å	Water (7)		0·116[e]	0[o]	1·42[p]	0·202	0·0234
	Ethanol (6′)		0·140	130	1·46	0·215	0·0301
	n-Hexane (5)		0·149	230	1·49	0·224	0·0334
	*cyclo*Hexane (4)		0·163	330	1·54	0·240	0·0391

[a] Value from Almasy and Laemmel (1951). [b] Cut-off for benzene (2600 Å) taken between bands *d* and *e*. [c] $\Delta\nu$ for benzene (2600 Å) taken for band *c*. [d] Refractive index data from Landolt-Börnstein (1936) for 2540 Å and 20 °C; interpolation used where necessary. [e] Cut-off taken as 2000 Å. [f] Gas intensity estimated from Pickett, Muntz, and McPherson (1951). [g] $\Delta\nu$ for benzene (2000 Å) taken for band *b*. [h] Data from Landolt-Börnstein (1936) extrapolated to 2000 Å. [i] Cut-off for toluene (2600 Å) taken to minimum after band *a*. [j] Data for band *a*. [k] Refractive index data for 2690 Å. [l] Cut-off between bands *f* and *g*. [m] Data for band *a*. [n] Refractive index data for 2720 Å. [o] $\Delta\nu$ values relative to value in water, and taken for band *b*. [p] Refractive index data for 2000 Å. [q] Intensity from Platt and Klevens (1947). [r] Pickett, Muntz, and McPherson (1951). [s] *f* in *n*-heptane to cut-off at 2000 Å by Platt and Klevens (1947). This is considerably greater than our value to the same cut-off in *n*-hexane.

V. References

Almasy, F., and Laemmel, H. (1951).—*Helv. Chim. Acta.* **34** : 462.

Badger, G. M., and Pearce, R. S. (1951).—*Spectrochim. Acta.* **4** : 280.

Bayliss, N. S. (1950).—*J. Chem. Phys.* **18** : 292.

Bayliss, N. S., Cole, A. R. H., and Green, B. G. (1948).—*Aust. J. Sci. Res.* A **1** : 472.

Bayliss, N. S., and McRae, E. G. (1952).—*J. Amer. Chem. Soc.* **74** : 5803.

Brode, W. R. (1943).—"Chemical Spectroscopy." 2nd Ed. p. 205. (John Wiley and Sons : New York.)

Brooker, L. G. S., Keyes, G. H., and Heseltine, D. W. (1951).—*J. Amer. Chem. Soc.* **73** : 5350.

Chako, N. Q. (1934).—*J. Chem. Phys.* **2** : 644.

Coggeshall, N. D., and Pozefsky, A. (1951).—*J. Chem. Phys.* **19** : 980.

Ham, J. S. (1953).—*J. Chem. Phys.* (in press).

Ham, J. S., Platt, J. R., and McConnell, H. (1951).—*J. Chem. Phys.* **19** : 1301.

Herington, E. F. G., and Kynaston, W. (1952).—*J. Chem. Soc.* **1952** : 3143.

Jacobs, L. E., and Platt, J. R. (1948).—*J. Chem. Phys.* **16** : 1137.

Kasha, M. (1950).—*Disc. Faraday Soc.* **9** : 14.

Kuhn, W. (1935).—*Z. phys. Chem.* B **30** : 356.

Landolt-Börnstein (1936).—"Physikalisch-Chemische Tabellen." 5th Ed. (J. Springer : Berlin.)

Lauer, K., and Oda, R. (1936).—*Ber. dtsch. chem. Ges.* **69** : 851.

McConnell, H. (1952).—*J. Chem. Phys.* **20** : 700.

Maddams, W. F., and Schnurmann, R. (1949).—*J. Chem. Phys.* **17** : 108.

Mulliken, R. S., and Rieke, C. A. (1941).—*Rep. Progr. Phys.* **8** : 231.

Pickett, L. W., Muntz, M., and McPherson, E. M. (1951).—*J. Amer. Chem. Soc.* **73** : 4862.

Platt, J. R., and Klevens, H. B. (1947).—*Chem. Revs.* **41** : 301.

Scholte, T. G. (1949).—*Physica, 's Grav.* **15** : 437.

Sheppard, S. E. (1942).—*Rev. Mod. Phys.* **14** : 303.

Sponer, H. (1942).—*J. Chem. Phys.* **10** : 672.

Sponer, H. (1947).—*Chem. Revs.* **41** : 281.

Sponer, H., Nordheim, G., Sklar, A. L., and Teller, E. (1939).—*J. Chem. Phys.* **7** : 207.

Sponer, H., and Wollman, S. H. (1941).—*J. Chem. Phys.* **9** : 816.

Thompson, F. W., and Ubbelohde, A. R. (1950).—*Trans. Faraday Soc.* **46** : 349.

Timmermans, J. (1950).—"Physico-chemical Constants of Pure Organic Compounds." (Elsevier Book Co. : New York.)

Weissberger, A., and Proskauer, E. (1935).—"Physical Constants of Organic Solvents." (Oxford Univ. Press.)

ELECTROKINETIC PROPERTIES OF CASSITERITE

By D. J. O'Connor* and A. S. Buchanan*

[*Manuscript received February* 4, 1953]

Summary

Simultaneous ζ-potential and surface conductivity measurements have been made on three samples of cassiterite (SnO_2) in water, in solutions of HCl, alkalis, inorganic salts, and the flotation collector reagent sodium cetyl sulphate. It is probable that the intrinsic surface charge of cassiterite in water is negative and that it is due to surface ionization as a very weak acid. Two of the solids possessed a negative surface whilst the positive charge of the third seemed to be due to ionization of a strongly basic impurity. Those samples having a negative charge showed little reaction with sodium cetyl sulphate alone, but appreciable adsorption of cetyl sulphate ion took place in acid solution. On the other hand, the sample with the positive surface reacted with cetyl sulphate ion even in the absence of acid. In all cases adsorption of cetyl sulphate was completely reversible.

I. Introduction

Because cassiterite (SnO_2) is the major source of tin, its surface chemistry has been the subject of several investigations, particularly with regard to the selective separation of the mineral from its ores by collectors. Hergt, Rogers, and Sutherland (1947) investigated the collecting action of sodium cetyl sulphate ($NaC\overline{S}$) on cassiterite using both captive bubble and cylinder flotation tests. More recently Edwards and Ewers (1951) studied in detail the adsorption of sodium cetyl sulphate on natural and synthetic samples of cassiterite and found that significant adsorption occurred only at pH <5, and further, that flotation of cassiterite by cetyl sulphate was efficient only under such conditions of pH.

Cassiterite is a suitable material for electrokinetic studies, since it occurs as massive crystals which may readily be ground to a size suitable for preparing porous packings for the streaming potential cell. In addition it is virtually insoluble (hence giving the requisite high resistances for observing streaming potentials), and yet there is reason to believe that there are groups on its surface capable of ionization, and thus producing an electrical double layer, namely,

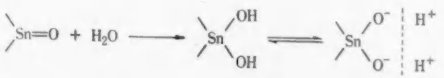

Cassiterite has the 6,3 coordination rutile structure (Wells 1950) with oxide anions, arranged in octahedra, coordinating the stannic ions, and it is reasonable

* Chemistry Department, University of Melbourne.

to suppose that a part of the crystal surface will consist of oxide ions, able to take part in the above reaction. Edwards and Ewers (1951) have shown that the surface groups are amphoteric in nature.

Cassiterite resembles silica in the properties of surface hydration and ionization. Wood (1946) suggests that the negative charge possessed by silica when in contact with water may arise either by adsorption of hydroxyl ions or by formation of a surface layer of partly ionized silicic acid gel. He considers that no distinction can be drawn between these two processes.

Jacobs (1952) has similarly attributed the negative potential of an arsenious sulphide sol to dissociation of the pseudo sol acid formed by reaction of As_2S_3 with water. In addition Ghosh, Chakravarty, and Kundu (1951) found that the charge of a MnO_2 sol was negative, and our interpretation of their results is that this is due to surface dissociation similar to the above.

Gaudin and Sun (1946) investigated the electrokinetic potential of cassiterite in relation to its flotation properties. Electrophoretic measurements on one sample showed that the solid was negatively charged with a ζ-potential of 23 mV. Increase of hydrogen ion concentration made the potential less negative, whilst increase of hydroxyl ion concentration made it more negative. The double layer was therefore supposed to arise from adsorption of hydrogen and hydroxyl ions by the solid ; in water alone an excess adsorption of the latter would account for the negative surface. As the subsequent discussion will show, this explanation is inadequate, particularly in view of the ion exchange properties of cassiterite.

During the present investigation the ζ-potential and surface conductivity of cassiterite have been studied in water and in solutions of alkalis, an acid, inorganic salts, and the flotation collector reagent sodium cetyl sulphate.

II. Electrokinetic Calculations

The ζ-potential was calculated from streaming potential measurements using the Helmholtz-Smoluchowski equation modified to take account of surface conductance, namely,

$$\zeta = \frac{4\pi\eta E\kappa'}{DP},$$

where η is the viscosity, D the dielectric constant of the liquid within the double layer, E the streaming potential, and P the pressure under which liquid is forced through the plug. κ' is the conductivity of the liquid within the pores of the plug, and was determined experimentally from the measured resistance R of the plug, and its " cell constant " C, thus

$$\kappa' = \frac{C}{R}.$$

C was determined by measuring the resistance of the plug filled with 0·1N KCl of known conductivity.

Surface conductivity (κ_s) is due to the excess of ions in the double layer as compared with the bulk of the solution and κ' is therefore the sum of the surface

conductivity and the bulk conductivity of the streaming liquid. Specific surface conductivity defined in this way has the dimensions of ohm^{-1} cm^{-1}, and for comparative purposes is a more convenient quantity to use than the quantity defined by Bikerman (1940) which has the dimensions ohm^{-1}.

There has been much speculation in the literature as to the appropriate values of dielectric constant within the double layer (for example, Grahame 1950 ; Conway, Bockris, and Ammar 1951). However, correct values are as yet uncertain, and hence ζ-potentials have been calculated using values of D for the solvent in bulk at each experimental temperature. Whilst values of ζ so obtained are not absolute, they are useful for comparative purposes.

As in previous publications (Buchanan and Heymann 1948, 1949), the convention is adopted of giving to the ζ-potential the same sign as that of the charge on the solid surface. This procedure is convenient when interpreting the effects of electrolytes on the ζ-potential, since such effects have usually been explained in terms of preferential ion adsorption by the solid, for example, preferential adsorption of a positive ion by a solid with a negative ζ-potential reduces the absolute magnitude of this potential. Over small concentration ranges the change in ζ has been taken as giving an approximate indication of the change in surface charge density on the solid (that is, of ion adsorption). However, over larger concentration ranges a complete treatment must also include the effects of variation in double layer thickness. Such a treatment will be presented in a subsequent paper.

III. Experimental Method and Materials

The streaming cell was similar in design to that used by Buchanan and Heymann (1948) for the investigation of sparingly soluble sulphates. The crystals were packed in an 11 mm diameter glass tube between two perforated bright platinum electrodes, about 4 cm apart. To prevent crystals of cassiterite escaping through the holes of the electrodes, a layer of large crystals (-22 $+30$ B.S.S. mesh) was packed next to each electrode and the bulk of the packing (-52 $+72$ B.S.S. mesh) was held tightly in place between these layers. The rate of streaming of liquid through the plugs was about 7 ml/min/cm Hg.

The streaming potentials were measured with a Cambridge valve potentiometer, values from a few millivolts up to 2 or 3 V being recorded. An A.C. bridge (Philips type T.A. 160) was used for measuring streaming cell resistances, values of which were as high as 3 to 4 MΩ.

To avoid contamination of the cassiterite with surface active impurities, all solutions were prepared using distilled water from which organic matter had been removed by a second distillation from alkaline permanganate in an all-glass still. This water had a specific conductivity of $<1{\cdot}0\times10^{-6}$ ohm^{-1} cm^{-1}. Electrolyte solutions were prepared from A.R. chemicals, recrystallized from conductivity water when necessary.*

* The authors are indebted to Mr. W. E. Ewers, Division of Industrial Chemistry, C.S.I.R.O., for provision of the pure sodium cetyl sulphate used in this investigation.

Three samples (*A*, *B*, and *C*) of cassiterite of Australian origin were investigated. Sample *A* was air ground in a glass mortar and the fines (−100 B.S.S. mesh) eliminated by decantation of a water slurry. The crystals were then repeatedly washed with warm conductivity water and dried in an electric oven at 110 °C. Both samples *B* and *C* were air ground in an iron mortar, then fractionated and thoroughly washed as above. Sample *A* contained 74·6 per cent., *B* 75·4 per cent., and *C* 75·8 per cent. tin, as compared with 78·77 per cent. required for pure cassiterite.*

After fusion with Na_2O_2 and extraction with HCl, qualitative tests confirmed the presence of iron in all samples ; that in sample *B*, however, was greatly in excess of the amounts present in *A* and *C*. Qualitative spectrographic analysis also recorded the following elements (amongst others) as impurities : Na (except in sample *B*), Ca, Mg, Al, Si, Cr, Cu, and Mn.

Samples of cassiterite (0·5 g, ground to less than 200 mesh in an iron mortar) were shaken with 10 ml of conductivity water, and the pH changes of the suspensions noted (Table 1). These measurements indicate that small amounts of alkaline impurity are present in samples *B* and *C*, that in sample *B* being appreciable.

TABLE 1

PH MEASUREMENTS OF CASSITERITE SUSPENSIONS

Sample	Initial pH (dist. H_2O)	Final pH
A	6·0	6·0
B	6·1	7·4
C	6·0	6·5

In the subsequent discussion, samples *A* and *C* are bracketed together, a procedure warranted by their similar electrokinetic behaviour. Sample *B*, on the other hand, was characteristically different in its properties and therefore is considered separately.

IV. RESULTS AND DISCUSSION : SAMPLES *A* AND *C*

(*a*) *The ζ-Potential in Water*

The charge on both samples *A* and *C* in conductivity water was negative. On the basis of this observation and in accord with the interpretation of Edwards and Ewers (1951) it is suggested that the electric double layer at the cassiterite-

* We are indebted to Mr. T. F. Wallace, Ore Dressing Section, C.S.I.R.O., for performing these analyses.

water interface is produced by surface ionization, the reaction in neutral or slightly acid solution being

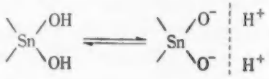

The highly mobile hydrogen ions reside in the outer part of the double layer and the surface is left with a negative charge. This representation is schematic only and is not intended to indicate that each surface Sn^{++++} has 2 dissociable groups attached to it.

Some typical values of ζ for samples *A* and *C* in conductivity water are given in Table 2. When dissolved CO_2 was removed from the streaming water, the negative potential increased from 288 to 380 mV, suggesting that dissociation of the cassiterite is very sensitive to hydrogen ion concentration, an observation confirmed when using HCl solutions as streaming liquids (Section IV (*b*)). The variation in potentials in Table 2 is probably due mainly to variation in the pH of the water, since normally CO_2 was not excluded from the system.

TABLE 2

MEAN VALUES OF ζ-POTENTIAL OF CASSITERITE IN CONDUCTIVITY WATER

Sample	Treatment	ζ-Potential (mV)
A	Initial value	—288
	CO_2-free conductivity water	—380
	After treatment with HCl	—241
	After treatment with NaOH	—246
	After treatment with $Ba(NO_3)_2$	—249
	After treatment with $K_4Fe(CN)_6$ ..	—209
	After treatment with NaCS	—216
	After treatment with NaCS and 1×10^{-4}N HCl	—248
C	Initial value	—103
	After treatment with HCl	—170
	After treatment with NaCS	—128
	After treatment with NaCS and 1×10^{-4}N HCl	—130

The surface conductivity (κ_s) of samples *A* and *C* in water was $7\cdot0$ and $6\cdot8\times10^{-6}$ ohm^{-1} cm^{-1} respectively, as compared with the bulk specific conductivity of redistilled water of $1\cdot0\times10^{-6}$ ohm^{-1} cm^{-1}. Other sparingly soluble solids such as $BaSO_4$, $PbCrO_4$, ZnS, etc. previously investigated (Buchanan and Heymann 1948; O'Connor and Buchanan, unpublished data) have negligible surface conductivity. The high value for cassiterite is in part to be explained

by the comparatively large ζ-potential (high surface charge density) and also by the high mobility of the hydrogen ions in the diffuse layer. It appears that in this case diffuse layer ions provide surface conductance; ions in the inner layer may also contribute although their mobilities are probably much reduced.

(b) The ζ-Potential in Acid Solution

Even in very low concentrations of HCl (1×10^{-5}N) the potential of the cassiterite was reduced to zero (Fig. 1); this could be due to repression of dissociation of the surface groups, and/or to preferential adsorption of hydrogen ons by the solid, namely,

The first process seems most important since the dissociation is very sensitive to hydrogen ion; no other electrolyte was found capable of reversing the sign of the charge. The merits of the second mechanism are more doubtful: some adsorption of HCl into the double layer must occur since the surface conductivity for sample *A* increases from 7×10^{-6} to 12×10^{-6} ohm^{-1} cm^{-1} in 1×10^{-5}N HCl, but this may be due to preferential adsorption of chloride by the solid, the hydrogen ion remaining in the diffuse layer. It is necessary to postulate this process in explanation of the curve in higher concentrations.

The solids develop positive potentials in concentrations greater than 1×10^{-5}N, and above 1×10^{-4}N the values decrease slightly with increasing concentration (Fig. 1). It is probable that the amphoteric stannic oxide reacts in acid solution as follows:

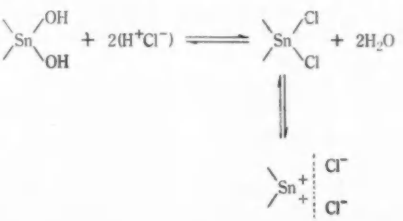

Evidence for its occurrence is provided by the ease of adsorption of cetyl sulphate ion on cassiterite in acid solution (*vide* Section IV (*f*)). It is probable that ionization of the surface chloride takes place to some extent (thus giving a positive surface), although little is known of the ionization of the normally covalent stannic chloride in aqueous solution because of hydrolysis reactions. Ionization of $SnCl_4$ certainly occurs in liquid SO_2 (Ephraim 1948). Furthermore, the postulated mechanism of the hydrolysis reaction (Emeléus and Anderson 1945) involves elimination of HCl, namely,

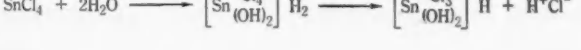

This reaction must involve ionization of the Sn-Cl bond.

In addition to the above mechanism which increases the positive charge on the solid, preferential adsorption of chloride ion, tending to decrease this charge, probably also takes place. The two processes balance one another since the potential remains constant or may even diminish slightly over a range of concentration. Adsorption of chloride is supported by the large increase in surface conductivity (Fig. 1) probably resulting from accumulation of mobile hydrogen counter ions in the diffuse layer.

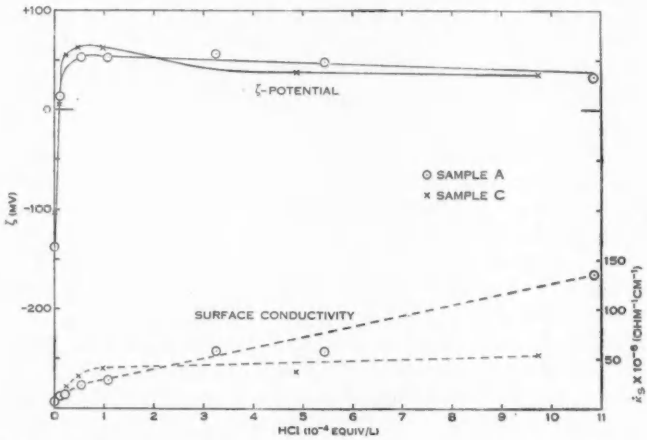

Fig. 1.—Variation of the ζ-potential and surface conductivity ($\varkappa_s$) of cassiterite (samples *A* and *C*) with the concentration of HCl.

With HCl and with all other electrolytes, ion exchange and adsorption equilibrium for both samples *A* and *C* were established immediately and were found to be reversible on washing the plug with water.

(c) *The ζ-Potential in Alkaline Solutions*

The effects of NaOH, KOH, and $NaHCO_3$ solutions on the ζ-potential and surface conductivity of sample *A* are of the same order of magnitude (Fig. 2). Ion exchange (or neutralization), namely,

results in an initial increase in negative potential since the sodium salt is dissociated to a greater extent than the weak acid. In addition, preferential adsorption of sodium ions accounts for the subsequent decrease in negative potential and will be favoured by the comparatively high negative charge of the

surface—similar effects have been observed with $PbCrO_4$ (O'Connor and Buchanan, unpublished data). The second process will be of increasing importance as the concentration of the solution increases since the majority of the surface groups will have reacted with the alkali in lower concentration.

Our observations are in agreement with the findings of Gaudin and Chang (1952) and Gaudin, Spedden, and Laxen (1952) who studied, with the use of radioactive tracers, the adsorption of both sodium and barium ions on quartz. They found that adsorption increased with both concentration and the pH of the solution, and it is probable that their results can be interpreted in terms of an ion exchange and adsorption mechanism similar to the above.

The surface conductivity (Fig. 2) shows little change until the concentration corresponding to the minimum in the potential curve is exceeded; thereafter

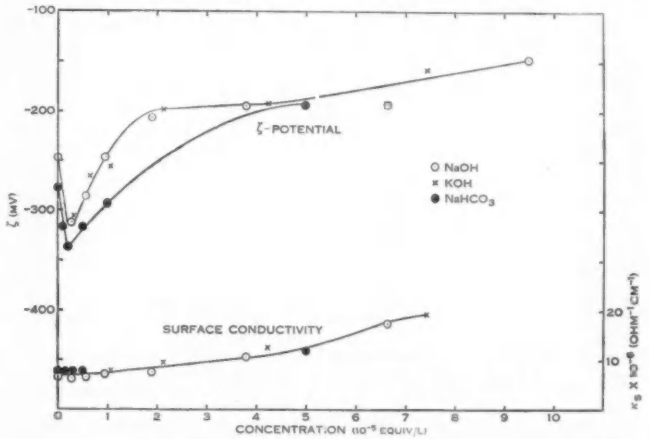

Fig. 2.—Variation of the ζ-potential and surface conductivity (κ_s) of cassiterite (sample *A*) with the concentration of NaOH, KOH, and $NaHCO_3$.

it increases steadily. Initially, highly mobile hydrogen ions are being replaced in the double layer by less mobile sodium ions; the deficiency is, however, partly overcome by entry of mobile hydroxyl ions into the diffuse layer and the effects appear to cancel. In higher concentrations where the second potential-determining process is more important, there is a steady rise in surface conductivity. The surface conductivity effects are small in comparison with those in acid solution, and this may be due to the fact that a proportion of the ions entering the diffuse layer are bicarbonate and carbonate rather than hydroxyl. Conductimetric titration indicated that the NaOH and KOH solutions of low concentration ($<10^{-4}$N) contained appreciable proportions of bicarbonate and carbonate. Moreover, $NaHCO_3$ solutions (Fig. 2) showed effects similar to the hydroxides thus lending support to this interpretation.

Barium hydroxide caused the potential to become less negative, without an intervening minimum (Fig. 3). As with the other alkalis, the two mechanisms of ion exchange and ion adsorption are envisaged. The absence of the minimum suggests that the barium ions are bound more strongly to the surface groups than are sodium or potassium, a statement in agreement with findings on weak acid exchange resins (Nachod 1949). Consequently adsorption of barium ions by the solid will be the major potential-determining step and it will lead to a reduction in the negative charge on the solid. The increase in surface conductivity with $Ba(OH)_2$ is of the same order of magnitude as with NaOH and KOH.

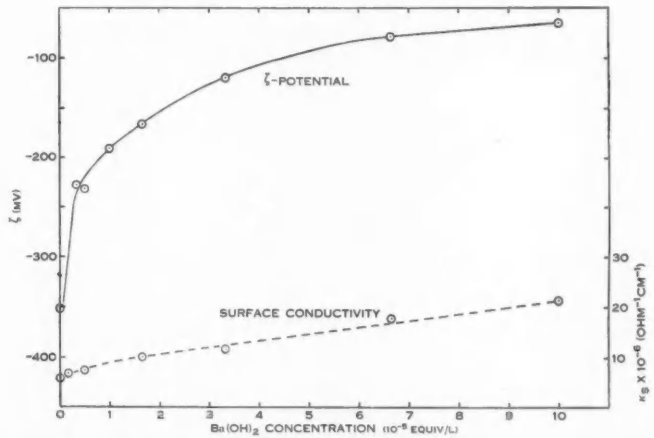

Fig. 3.—Variation of the ζ-potential and surface conductivity (κ_s) of cassiterite (sample *A*) with the concentration of $Ba(OH)_2$.

(*d*) *The ζ-Potential in Solutions of* $NaNO_3$, KNO_3, $Ca(NO_3)_2$, $Ba(NO_3)_2$, *KCl, and* K_2SO_4

The results for sample *A* are shown in Figure 4. They are essentially similar for all salts when allowance is made for differences in initial ζ-potentials which are probably due to slight variations in pH of the streaming liquids (see Section IV (*a*)). In all cases, the potential is made less negative and the surface conductivity increased to a small extent. As before, the mechanisms of cation exchange and cation adsorption may be postulated to account for the results. Cation exchange seems to occur, since Edwards and Ewers (1951) observed a decrease of pH on treating pure synthetic SnO_2 with solutions of neutral salts. The extent of this reaction is probably less than that of the corresponding reaction with the alkalis which is thought to cause the initial minimum in the alkali curves (Section IV (*c*) and Fig. 2), since a similar minimum does not appear in the salt curves. Preferential adsorption of positive ions must take place, since the potential becomes less negative, and such adsorption will be favoured by the high initial negative charge on the surface. The small increase

in surface conductivity is probably due to the increased population of ions, resulting from adsorption, in the double layer. The magnitudes of the effects on ζ-potential and surface conductivity vary slightly with the properties of the ions involved.

(*e*) *The ζ-Potential in $K_3Fe(CN)_6$ and $K_4Fe(CN)_6$ Solutions*

The effect of ferricyanide (Fig. 5) is quite similar to that of the salts of the preceding section and an analogous explanation is suggested. Ferrocyanide, however, displays significant differences: the negative potential increases in low concentration, reaches a minimum at 1×10^{-6} equiv/l, and then decreases

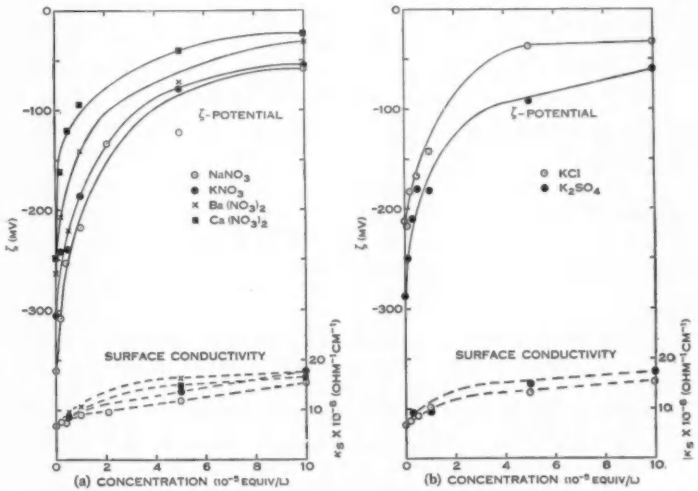

Fig. 4.—Variation of the ζ-potential and surface conductivity (κ_s) of cassiterite (sample *A*) with the concentration of: (*a*) $NaNO_3$, KNO_3, $Ca(NO_3)_2$, $Ba(NO_3)_2$, and (*b*) KCl, K_2SO_4.

with increasing concentration. In low concentration, in addition to exchange of H^+ by K^+, there seems to be marked preferential adsorption of $Fe(CN)_6^{----}$ by the solid. However, high negative potentials (−355 mV) are thus produced and consequently adsorption of potassium ions is stimulated to an extent sufficient to control the potential, which then becomes less negative. It is not unlikely that the quadrivalent ferrocyanide should be adsorbed since multivalent ions generally show increased adsorption on solids. Undoubtedly, some adsorption of tervalent ferricyanide occurs with $K_3Fe(CN)_6$, but not in sufficient amount to control the course of the potential curve.

Surface conductivity is appreciable in both solutions, the magnitude in ferrocyanide somewhat exceeding that in ferricyanide. This may be due to the greater mobility of ferrocyanide ion.

(f) The ζ-Potential in Sodium Cetyl Sulphate Solutions

With sodium cetyl sulphate in water, as Edwards and Ewers (1951) have shown, cation exchange occurs, sodium replacing hydrogen. This results in a

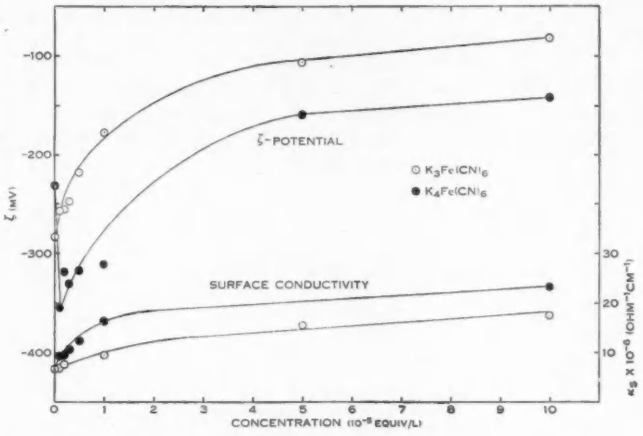

Fig. 5.—Variation of the ζ-potential and surface conductivity (κ_s) of cassiterite (sample *A*) with the concentration of $K_3Fe(CN)_6$, and $K_4Fe(CN)_6$.

more negative potential (Fig. 6 (*a*)). Subsequently, as in the alkali and salt solutions, preferential adsorption of sodium ion onto the solid tends to make the potential less negative. There is probably little reaction of cetyl sulphate ion

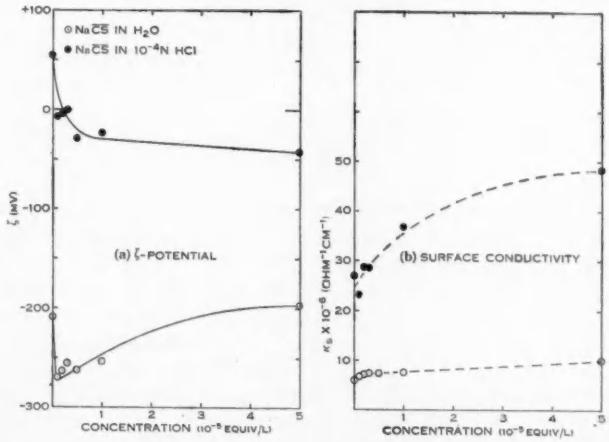

Fig. 6.—Variation of (*a*) the ζ-potential and (*b*) the surface conductivity (κ_s) of cassiterite (sample *A*) with the concentration of sodium cetyl sulphate in water and in 10^{-4}N HCl.

with the surface since its adsorption will be inhibited by the high negative charge of the solid. Surface conductivity effects are small (Fig. 6 (*b*)) : hydrogen ions of the diffuse layer are replaced by greater numbers of less mobile sodium and cetyl sulphate ions.

Cetyl sulphate reacts with cassiterite in solutions of pH 4 (Edwards and Ewers 1951). The initial potential of sample *A* at such a pH is positive (+55 mV in 10^{-4}N HCl) which, as shown in Section IV (*b*), is probably due to substitution of hydroxyl ions on the surface by chloride and dissociation of the Sn–Cl bond. The cetyl sulphate ion may now replace the chloride and is probably more firmly bound than the latter. In addition, the potential becomes negative, which can only be due to adsorption of cetyl sulphate ions by the surface, electrostatic repulsion no longer hindering this process. The appreciable surface conductivity shown in the acid solutions of cetyl sulphate (Fig. 6 (*b*)) is no doubt due to adsorption of cetyl sulphate ion, a proportion of the positive counter ions in the diffuse layer being mobile hydrogen ions.

After the cassiterite had been treated with the acid solution of cetyl sulphate, the original negative potential was quickly re-established on streaming with water, indicating that the Sn–CS bond is easily hydrolysed.

As the surface charge of samples *A* and *C* is negative, it is to be expected that cationic surface active agents (of the type cetyl trimethyl ammonium bromide) would function as collectors for these materials, and in fact the above reagent is a collector for SnO_2 in alkaline medium, but it is not selective.

V. Results and Discussion : Sample *B*

(*a*) *The ζ-Potential in Water*

This sample was found to have a positive and somewhat variable potential in water (Table 3).

Table 3

Mean values of ζ-potential of sample *B* in conductivity water

Treatment	ζ-Potential (mV)
After 2 days' streaming with water	+197
After treatment with HCl	+167
„ „ „ NaCS	+120
„ „ „ „ and 1×10^{-4}N HCl	+130

In general, the positive potential diminished over a period of time, suggesting that leaching of impurity from the surface was responsible for the change. Furthermore, it was noted that, if the plug was allowed to stand for a period in conductivity water, the potential was negative immediately after resumption of streaming. However, it quickly decreased and changed to positive on further streaming with water. This transient negative charge may be associated with

release of alkali into the solution by the solid (Table 1, Section III), since deliberate addition of NaOH to the streaming solution caused a similar reversal of sign of the charge (Section V (*c*)).

Since cassiterite itself, as demonstrated with samples *A* and *C*, appears to undergo surface ionization as a weak acid leaving the solid with a negative surface, it seems probable that *surface ionization* of a basic impurity, providing a diffuse layer of hydroxyl ions, is responsible for the positive charge of sample *B*. As indicated above, alkaline impurity *in solution* tends to make the surface negative, and is therefore unlikely to produce the observed positive potential. If the impurity is a strong base its ionization will outweigh that of the weak acid groups of the cassiterite even though the former is present in comparatively small proportion.

The nature of the basic impurity responsible for the positive surface charge on sample *B* has not become apparent during the course of this investigation. Calcium, magnesium, and iron are all present (Section III) and are possibilities,

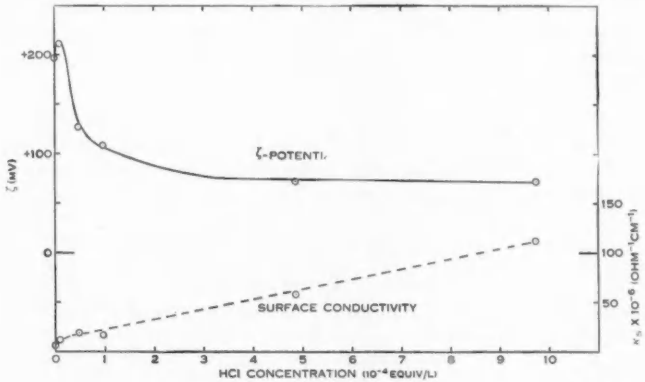

Fig. 7.—Variation of the ζ-potential and surface conductivity (κ_s) of cassiterite (sample *B*) with the concentration of HCl.

the latter if it was present in the ferrous state. In this connection the following observation may be of importance. After ignition in air to 850 °C, the potential of sample *B* was negative (−40 mV) and the crystals, originally grey and black, became ochreous in colour, suggesting that the ignition had oxidized iron to the ferric state. Of the three samples of cassiterite, only *B* contained appreciable amounts of this element (Section III); the moderately strong base, ferrous hydroxide, may therefore be responsible for the positive charge of sample *B*.

The surface conductivity of sample *B* (about 5×10^{-6} ohm^{-1} cm^{-1}) is of the same order as that for samples *A* and *C*; it is presumably due to highly mobile hydroxyl ions in the diffuse layer.

(*b*) *The ζ-Potential in Acid Solutions*

On application of increasing concentrations of HCl the potential at first becomes more positive, reaches a maximum, and then decreases to a constant

positive value of about 70 mV (Fig. 7). The acid will certainly react with the basic impurity responsible for the positive charge, resulting in replacement of hydroxyl by chloride ions in the diffuse layer and formation of water; this reaction is unlikely to change the potential greatly. In addition, by analogy with samples *A* and *C* (Section IV (*b*)), reaction of HCl with the cassiterite should occur, namely,

this reaction accounting for the increase in positive potential. The subsequent decrease in positive potential can only be due to preferential adsorption of chloride ions by the solid, the hydrogen counter ions entering the diffuse layer, where they contribute to the surface conductivity which increases appreciably (Fig. 7).

(*c*) *The ζ-Potential in Alkaline Solutions*

The positive potential decreases steadily and eventually becomes negative (Fig. 8). Both reaction with the acid groups of the cassiterite (see Section IV (*c*)) and preferential adsorption of negative hydroxyl ions account for this result.

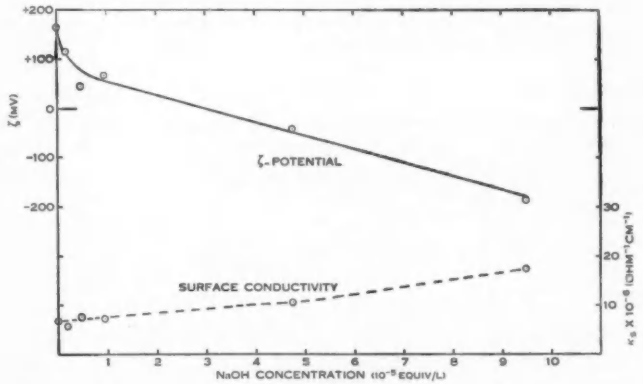

Fig. 8.—Variation of the ζ-potential and surface conductivity (κ_s) of cassiterite (sample *B*) with the concentration of NaOH.

The surface conductivity increase is small (Fig. 8) and may be associated with the increasing population of sodium ions in the diffuse layer.

(*d*) *The ζ-Potential in Sodium Cetyl Sulphate Solutions*

Since the surface ionization of sample *B* is basic in character, it is to be expected that cetyl sulphate would react with the surface without the aid of hydrogen ions; this in fact was observed. The potential curves due to cetyl

sulphate in water alone and in acid solution are very similar, the positive surface being readily changed to negative (Fig. 9). It is therefore probable that flotation of this sample of cassiterite could be achieved by cetyl sulphate in water alone.

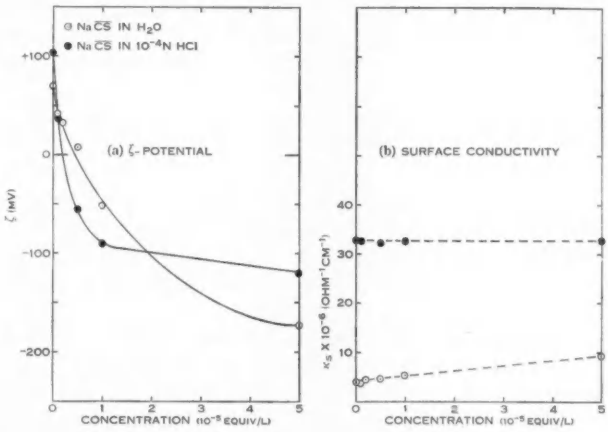

Fig. 9.—Variation of (*a*) the ζ-potential and (*b*) the surface conductivity (κ_s) of cassiterite (sample *B*) with the concentration of sodium cetyl sulphate in water and in 10^{-4}N HCl.

In the absence of acid, cetyl sulphate ions will replace hydroxyl ions in the diffuse layer, probably being more firmly bound to the surface than the latter. The negative charge which appears in the presence of the cetyl sulphate may be due to the normal dissociation of the sodium salt of cassiterite, namely,

$$\mathrm{Sn(OH)_2} \rightleftharpoons \mathrm{Sn(O^-H^+)_2} + 2(\mathrm{Na^+\overline{CS}^-}) \rightleftharpoons \mathrm{Sn(O^-Na^+)_2} + 2(\mathrm{H^+\overline{CS}^-})$$

and to preferential adsorption of the negative cetyl sulphate ions.

The surface conductivity shows a small increase which may be associated with removal of hydroxyl ions from the diffuse layer and their substitution by sodium ions. Even if cetyl sulphate ions are adsorbed by the solid, the positive counter ions in the diffuse layer will be sodium rather than hydrogen, and therefore no large increase in surface conductivity can be expected.

In the presence of HCl, in addition to the above reactions of cetyl sulphate with the surface, reaction with the cassiterite itself may be stimulated by way of the mechanism suggested for samples *A* and *C* (Section IV (*f*)). The surface conductivity shows little change from its high value associated with 10^{-4}N HCl, on increasing concentration of cetyl sulphate. This result is surprising in view of the increase observed in similar circumstances for sample *A* (Fig. 6 (*b*)); but the effect may be associated with the presence of alkaline impurity in sample *B*.

VI. Acknowledgments

The authors are grateful to Dr. J. C. Nixon, Mining Department, University of Melbourne, and Mr. W. E. Ewers, Division of Industrial Chemistry, C.S.I.R.O., Melbourne, for reading the manuscript. One of us (D.J.O'C.) wishes to acknowledge gratefully the receipt of financial support from funds which had been made available to the Mining Department, University of Melbourne, by a group of Australian metal mining companies.

VII. References

Bikerman, J. J. (1940).—*Trans. Faraday Soc.* **36**: 154.
Buchanan, A. S., and Heymann, E. (1948).—*Proc. Roy. Soc.* A **195**: 150.
Buchanan, A. S., and Heymann, E. (1949).—*J. Colloid Sci.* **4**: 137.
Conway, B. E., Bockris, J. O'M., and Ammar, I. A. (1951).—*Trans. Faraday Soc.* **47**: 756.
Edwards, G. R., and Ewers, W. E. (1951).—*Aust. J. Sci. Res.* A **4**: 627.
Emeléus, H. J., and Anderson, J. S. (1945).—"Modern Aspects of Inorganic Chemistry." (Van Nostrand Inc.: New York.)
Ephraim, F. (1948).—"Inorganic Chemistry." (Gurney and Jackson: London.)
Gaudin, A. M., and Chang, C. S. (1952).—*Min. Engng., N.Y.* **4**: 193.
Gaudin, A. M., Spedden, H. R., and Laxen, P. A. (1952).—*Min. Engng., N.Y.* **4**: 693.
Gaudin, A. M., and Sun, S. C. (1946).—Min. Tech. Amer. Inst. Min. Metall. Engrs. T.P. 2005.
Ghosh, B. N., Chakravarty, S. N., and Kundu, N. L. (1951).—*J. Indian Chem. Soc.* **28**: 319.
Grahame, D. C. (1950).—*J. Chem. Phys.* **18**: 903.
Hergt, H. F. A., Rogers, J., and Sutherland, K. L. (1947).—Min. Tech. Amer. Inst. Min. Metall. Engrs. T.P. 2081.
Jacobs, G. (1952).—*Trans. Faraday Soc.* **48**: 355.
Nachod, F. C. (1949).—"Ion Exchange." (Academic Press: New York.)
Wells, A. F. (1950).—"Structural Inorganic Chemistry." (Clarendon Press: Oxford.)
Wood, L. A. (1946).—*J. Amer. Chem. Soc.* **68**: 437.

THE STRUCTURE OF DIMEDONE AND THE EFFECT OF SOLVENTS ON KETO–ENOL TAUTOMERISM

By O. L. Angell* and R. L. Werner*

[*Manuscript received March* 19, 1953]

Summary

An infra-red spectroscopic examination of dimedone has shown that in non-polar solvents this compound exists in the diketo- rather than the mono-enol form. Such behaviour suggests that where intramolecular hydrogen bonding cannot stabilize the enolic form, as it can, for example, in acetyl acetone, there is little tendency for the 1,3-diketones to enolize. In other media, the equilibrium shifts in favour of the mono-enol, those solvents which are basic or easily form hydrogen bonds having the greatest influence. On the other hand the dielectric constant *per se* of the solvent has little effect on the equilibrium.

In contrast with diosphenol, it is shown that the hydroxyl group in the mono-enolic form of dimedone has some effect on the mesomerism of the system –C=C–C=O.

I. Introduction

From a recent paper (Le Fèvre, Maramba, and Werner 1953) it will be noted that in diosphenol mesomerism of the system –C=C–C=O is little affected by the presence of a hydroxyl group in the α-position to the carbonyl group. It seemed of interest to compare this compound with one in which the hydroxyl group was in the β-position as in the mono-enolic form of a 1,3-diketone.

Hukins and Le Fèvre (1949) have made an infra-red spectroscopic examination of dimedone (5,5-dimethyl-1,3-*cyclo*hexanedione, I) in carbon tetrachloride and have reported it to be enolic II. Rasmussen, Tunnicliff, and Brattain (1949) found that in chloroform dimedone is at least partly enolic. This compound therefore appeared to be quite suitable, particularly as intramolecular hydrogen bonding cannot occur. For our purposes it was necessary to know the frequency of the carbonyl groups and dimedone was therefore re-examined in both the 3 and 6μ regions. The results, which were somewhat unexpected, are presented below.

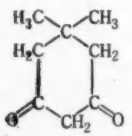

(I)

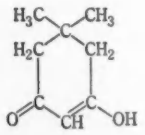

(II)

* School of Applied Chemistry, N.S.W. University of Technology, Broadway, Sydney.

II. Experimental

(i) *Materials.*—The dimedone was a laboratory sample which was twice recrystallized from water and dried over calcium chloride, m.p. 148 °C. Deutero-dimedone was prepared by recrystallizing dimedone from heavy water. The mono-ethyl ether of dimedone was prepared by the method of Crossley and Renouf (1908) with the exception that the water formed was removed as a ternary azeotrope with the aid of benzene. The product was obtained as white crystals, m.p. 60 °C. The piperitone and isophorone were laboratory samples which were freshly distilled before use.

All the solvents used were the usual laboratory standard but precautions were taken to ensure that they were quite dry.

Benzene and carbon tetrachloride were dried over phosphorus pentoxide before use and filtered; pyridine was dried over potassium hydroxide pellets; dioxane and diethyl ether were dried over sodium; the other solvents were freshly distilled.

(ii) *Apparatus.*—The spectra were obtained with a Perkin-Elmer model 12C infra-red spectrometer with sodium chloride prism, calibrated in the usual manner against published data (Oetjen, Kao, and Randall 1942). Due to the low solubility of dimedone, dilute solutions were used in most cases and because of this, solvent absorption often proved troublesome. Several spectra, each with a blank, were therefore obtained on each sample and the absorption curves drawn by careful point-by-point division. Concentrations (where these are known) and cell lengths are shown on the figures while dotted lines indicate the limits imposed by solvent absorption.

III. Discussion

Initially, dimedone was examined in dilute solution in non-polar solvents. In carbon tetrachloride (1 cm cell) a satisfactory spectrum was obtained throughout the entire region from 2500 to 3800 cm^{-1} which clearly showed the C–H stretching frequencies between 2850 and 3000 cm^{-1} (Fig. 1*A*) but only very weak absorption outside this range. Although benzene is not as favourable a solvent as carbon tetrachloride because of its lower transparency, reliable readings could be made between 3120 and 3800 cm^{-1} and within these limits with a saturated solution (*c.* 0·2 per cent., 1 mm cell), the absorption did not exceed 5 per cent. at any point.

An inspection of the absorption curves of some phenolic compounds of approximately the same molecular weight as dimedone (for example, Friedel 1951) shows that in such cases the intensity of the hydroxyl band is about the same or greater than the intensity of the nearby C–H stretching bands and a similar result would be expected for dimedone in the mono-enolic form. That very little absorption occurs in this region is therefore good evidence for the presence of the diketo-form and the absence of appreciable amounts of the enol. This is contrary to the results of a previous investigation (Hukins and Le Fèvre 1949) in which two bands whose intensity was approximately half that of the C–H bands were reported in the region normally associated with the absorption

of hydroxyl groups. It has been our experience that in the dilute solutions which must necessarily be employed because of the low solubility of dimedone, traces of water can cause discrepancies between the transmission of successive spectra in this region. It seems likely that the bands recorded by the above authors were due to this, particularly as the band at 2·70μ is not a known characteristic of hydroxyl groups (Fox and Martin 1940).

In the 6μ region dimedone has two strong bands at 1733 and 1713 cm^{-1} in carbon tetrachloride which are reproduced closely in benzene (Figs. 2*A* and 2*B*). Apart from these there are only weak absorption bands above 1580 cm^{-1}, the limit imposed by the absorption of benzene. These two bands are in a

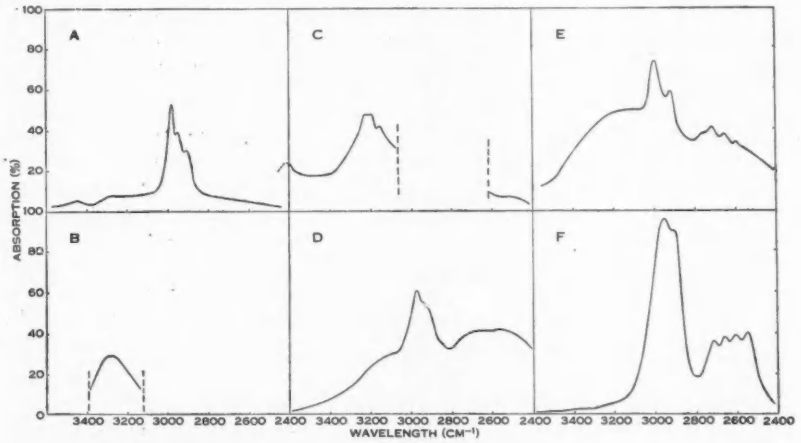

Fig. 1.—Dimedone in various solvents, 3μ region. *A*, saturated solution in carbon tetrachloride 1 cm cell; *B*, saturated solution in acetonitrile, 0·2 mm cell; *C*, *c.* 4 per cent. w/w solution in dioxane, 0·2 mm cell; *D*, *c.* 6 per cent. w/w solution in pyridine, 0·13 mm cell; *E*, 2·0 per cent. w/w solution in chloroform, 0·13 mm cell; *F*, solid "Nujol" mull.

position normally associated with the vibrations of unconjugated carbonyl groups (for example, *cyclo*hexanone, 1714 cm^{-1}, Hartwell, Richards, and Thompson (1948)) and the doubling is reminiscent of other cases in which two equivalent groups occur in close proximity in a molecule, for example, symmetrical diacyl peroxides have an average separation of 25 cm^{-1} between the two carbonyl bands (Davison 1951). Together with the absence of a hydroxyl band the above bands clearly point to the presence of the diketo-form.

If the mono-enolic form were present one would have expected bands due to the conjugated carbonyl group, somewhere in the region 1640–1670 cm^{-1} as can be seen from the values for this band given in the table for piperitone, diosphenol, and the ethyl ether of dimedone, all of which have closely similar structures to the enol. It can be seen, however, that there is comparatively little absorption in this region in the case of dimedone. It is possible to reconcile the above conclusion with the evidence of dipole moment measurements which

give a value of 3·46 D for dimedone (Hukins and Le Fèvre 1949). An examination of a model of dimedone, assuming the chain form of the molecule (Beckett, Pitzer, and Spitzer 1947) shows that the angle between the two carbonyl groups is somewhat less than 120°. A simple calculation using a value of 2·90 D for the C=O bond moment gives an angle of 106° if the resultant is 3·46 D.

The presence of the diketo-form and the absence of any possibility of stabilization of an enolic form by intramolecular hydrogen bonding makes dimedone a particularly suitable compound with which to examine the effect of solvents on keto-enol tautomerism.

In Figures 2*C*–*H*. the spectrum of dimedone is shown in the 6μ region in a variety of solvents. In acetonitrile (Fig. 2*C*) the two bands of the diketo-form are reproduced at 1728 and 1700 cm^{-1} while two new bands of comparable intensity have appeared at 1640 and 1612 cm^{-1}. Comparison with similar bands in dimedone ethyl ether leaves little doubt that these are due to the presence of the enolic form. That the C=C band (1612 cm^{-1}) is of greater intensity than the C=O (1640 cm^{-1}) is not unusual as a similar state of affairs exists with mesityl oxide (Barnes *et al.* 1944) as well as in other cases.

Complementary to this evidence is the appearance of a band due to the hydroxyl group at approximately 3280 cm^{-1}. Because of solvent absorption exact measurement of the peak of this band was difficult and there may possibly be other bands which are obscured by the solvent (Fig. 1*B*). However, there is little doubt that a band due to the hydroxyl group exists in this region. In Figures 2*D* and 2*E* the spectra in dioxane and diethyl ether are shown. In them, the features discussed above are reproduced with the exception that there is a progressive reduction in the concentration of the diketo-form. In dioxane the absorption could also be followed in the 3μ region (Fig. 1*C*) and a strong band was recorded at 3210 cm^{-1} which is close to the band observed in acetonitrile. In pyridine (Fig. 2*F*) the transition to enol is virtually complete as no trace remains of the bands around 1700 cm^{-1}. The strength of the hydrogen bonding in this case can be judged from the maximum of the broad hydroxyl band which has been lowered to 2600 cm^{-1} (Fig. 1*D*).

In Figure 2*G* the spectrum in *o*-dichlorobenzene reveals that only the diketo-form is present, as in neutral solvents, for there is no absorption near 1650 cm^{-1}. In this case the two ketone bands are merged into one at 1710 cm^{-1}.

It is interesting, when considering these results, to compare the behaviour of dimedone with acetylacetone. Both these compounds consist of the system R–CO–CH_2–CO–R, where R is an alkyl group. It would appear that in the absence of hydrogen bonding the 1,3-diketo-system is more stable than the mono-enol as is shown by dimedone in carbon tetrachloride and benzene. Where conditions favourable to intramolecular hydrogen bonding occur, however, this position may be reversed and in acetylacetone the equilibrium mixture contains some 80 per cent. of the enolic form (Meyer 1911, 1912). In a complementary fashion a change in the equilibrium in dimedone can be brought about by the action of an electron-donor solvent which stabilizes the enol by intermolecular hydrogen bonding, and this is particularly the case with the more basic solvents

such as pyridine. In this connection it may be noted that the efficiency of diethyl ether over dioxane in stabilizing the enol follows the order of electron-donor capacity given by Gordy and Stanford (1940, 1941). The conclusion above is supported by the work on ethyl acetoacetate in which the enol is

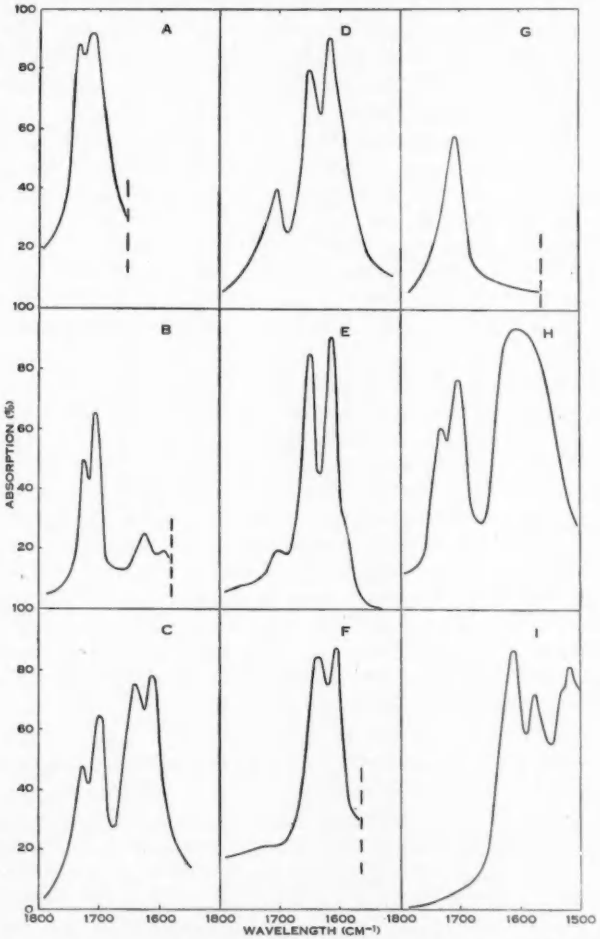

Fig. 2.—Dimedone in various solvents, 6μ region. *A*, saturated solution in carbon tetrachloride, 1 cm cell; *B*, saturated solution in benzene, 1 mm cell; *C*, saturated solution in acetonitrile, 0·2 mm cell; *D*, *c.* 4 per cent. w/w solution in dioxane, 0·2 mm cell; *E*, saturated solution in diethyl ether, 1 mm cell; *F*, *c.* 6 per cent. solution in pyridine, 0·13 mm cell; *G*, saturated solution in *o*-dichlorobenzene, 1 mm cell; *H*, 2·0 per cent. solution in chloroform, 0·13 mm cell; *I*, solid "Nujol" mull.

stabilized to the extent of some 8 per cent. in the pure liquid by intramolecular effects, but to the extent of 56 per cent. with the assistance of intermolecular hydrogen bonding which occurs in pyridine (Meyer 1911). On the other hand the spectrum in *o*-dichlorobenzene clearly shows that the dielectric constant of the solvent as such, has little influence on the stability of the enol. *o*-Dichlorobenzene has a fairly high dielectric constant ($\varepsilon = 7 \cdot 5$), but one would only expect weak hydrogen bonding effects and dimedone is apparently not enolized in this solvent.

Finally, the behaviour of dimedone in chloroform (Fig. 2*H*) deserves comment. The two bands of the diketo-form appear again at 1730 and 1705 cm^{-1} (Rasmussen, Tunnicliff, and Brattain (1949) give only one band in place of our close pair), but the bands of the enolic form are combined to form one fairly broad band centred at 1610 cm^{-1} (Rasmussen 1605 cm^{-1}). Stabilization of the enol by dimerization through two hydrogen bridges as suggested by Rasmussen, Tunnicliff, and Brattain (1949) is clearly incompatible with the stereochemistry of these compounds. Furthermore, the absence of the enol in benzene, even at a sufficiently high concentration to allow association, indicates that there is no tendency towards this dimerization. It appears that the enolic form has been stabilized by dipolar interaction between the solvent and the hydroxyl group and this is supported by the shape and position of the broad hydroxyl band in the 3μ region (Fig. 1*E*).

A comparison of the carbonyl frequencies of piperitone, dimedone ethyl ether, and diosphenol in various solvents shows that a lowering of this frequency occurs in chloroform relative to other solvents. Such a shift is also apparent in other data on the effect of solvents on the frequency of the carbonyl vibration (Hartwell, Richards, and Thompson 1948) and it would seem that this is due to the interaction between the carbonyl group and the chloroform. A similar effect occurring in dimedone would account for the coalescence of the two bands of the enolic form.

In the solid state, dimedone exhibits broad absorption in the 4μ region centred approximately at 2620 cm^{-1} (Fig. 1*F*). This is unusually low for a hydroxyl group and not what would be expected of a molecule with the mono-enolic structure (compare with diosphenol which gives a band at 3410 cm^{-1} (Le Fèvre, Maramba, and Werner 1953). However, deuteration moved this band to a position centred approximately at 2030 cm^{-1}, which shift clearly confirms that the original band is due to a hydroxyl group. In the 6μ region (Fig. 2*I*) there is a band at 1612 cm^{-1} but the region is clear above this and indicates the absence of any diketo-form. The strong hydrogen bonding together with the lack of bands above 1612 cm^{-1} might suggest the presence of the dienol were it not for the fact that a lowering of the carbonyl frequency to this value also occurs with chloroform as solvent. In this case the mono-enol must be concerned since it is unlikely that the diketone would exist with the dienol in the absence of the mono-enol.

As mentioned previously dimedone was examined in order to determine the effect of the hydroxyl group on the mesomerism of the system C=C–C=O.

While piperitone was a suitable comparison compound for diosphenol, isophorone (3,5,5-trimethyl-2-*cyclo*hexene-1-one) has a structure nearly identical with dimedone and was therefore chosen in this case. The non-existence of the enolic form of dimedone in a neutral solvent, however, makes difficult a comparison with isophorone and diosphenol. It is seen that, if we omit chloroform, the carbonyl frequency in piperitone and the ethyl ether of dimedone are little affected by the solvent. Isophorone gives a band at 1670 cm^{-1} both in benzene solution and as a liquid (see Table 1).

TABLE 1

OBSERVED FREQUENCIES OF C=O AND C=C IN THE 6μ REGION

Solvent	Dimedone	Dimedone Ethyl Ether	Piperitone	Isophorone
Carbon tetrachloride	1733, 1713	1660, 1610	1668	1670
Benzene	1728, 1708	1660, 1610	1668	1670
Acetonitrile ..	1728, 1700; 1640, 1612	—	—	—
Dioxane	1705, 1650, 1615	1659, 1609	1666	—
Diethyl ether ..	1705, 1650, 1615	—	—	—
Pyridine	1636, 1604	—	1664	—
o-Dichlorobenzene	1710	—	—	—
Chloroform	1730, 1705, 1610	1641, 1601	1658	—
Solid or liquid ..	1612 (s.)	1657, 1604 (s.)	1666 (l.)	1670 (l.)

In the case of dimedone itself, however, the differences between solvents are larger, and this must obviously mean that by a mesomeric mechanism, changes in the intermolecular bonding of the hydroxyl group are affecting the carbonyl polarity and hence frequency (Walsh 1947). Under these circumstances it is not possible to differentiate between the effect of the solvent and the effect of the unbonded hydroxl such as might be observable in a neutral solvent.

A reduced effect is expected and is observed in the case of the ethyl ether of dimedone, for which no solvent effects can intervene. In this case there is a small difference of 10 cm^{-1} between isophorone and the ether in the same solvent and this sets a lower limit to the effect expected in dimedone itself. An upper limit of 20 cm^{-1} is set by comparison between dimedone (in dioxane) and isophorone. Hence considerations lead to the conclusion that the hydroxyl in the β-position to the carbonyl group exerts a definite effect on the mesomerism in the system C=C–C=O which effect is absent in diosphenol.

IV. ACKNOWLEDGMENT

The authors wish to express their thanks to Professor R. J. W. Le Fèvre for helpful suggestions.

V. References

Barnes, R. B., Gore, R. C., Liddel, U., and Williams, v. Z. (1944).—" Infrared Spectroscopy." p. 81. (Reinhold Publ. Corp.: New York.)

Beckett, C. W., Pitzer, K. S., and Spitzer, R. (1947).—*J. Amer. Chem. Soc.* **69**: 2488.

Crossley, A. W., and Renouf, N. (1908).—*J. Chem. Soc.* **93**: 640.

Davison, W. H. T. (1951).—*J. Chem. Soc.* **1951**: 2456.

Fox, J. J., and Martin, A. E. (1940).—*Trans. Faraday Soc.* **36**: 897.

Friedel, R. A. (1951).—*J. Amer. Chem. Soc.* **73**: 2881.

Gordy, W., and Stanford, S. C. (1940).—*J. Chem. Phys.* **8**: 170.

Gordy, W., and Stanford, S. C. (1941).—*J. Chem. Phys.* **9**: 204.

Hartwell, E. J., Richards, R. E., and Thompson, H. W. (1948).—*J. Chem. Soc.* **1948**: 1436.

Hukins, A. A., and Le Fèvre, R. J. W. (1949).—*J. Chem. Soc.* **1949**: 898.

Le Fèvre, R. J. W., Maramba, F., and Werner, R. L. (1953).—*J, Chem. Soc.* **1953**: (in press).

Meyer, K. H. (1911).—*Leibigs Ann.* **380**: 212.

Meyer, K. H. (1912).—*Ber. dtsch. chem. Ges.* **45**: 2843.

Oetjen, R. A., Kao, C. L., and Randall, H. M. (1942).—*Rev. Sci. Instrum.* **13**: 515.

Rasmussen, R. S., Tunnicliff, D. D., and Brattain, R. R. (1949).—*J. Amer. Chem. Soc.* **71**: 1068.

Walsh, A. (1947).—*A.R. Nat. Res. Coun., Ottawa* **44**: 45.

STUDIES ON THE FORMATION OF GRAPHITE–FERRIC CHLORIDE COMPLEXES: KINETICS OF FORMATION

By J. A. Barker* and R. C. Croft*

[*Manuscript received January* 21, 1953]

Summary

A study has been made of the kinetics of the diffusion of anhydrous $FeCl_3$ in graphite. It was found that this process can be represented for stages between 50 and 100 per cent. saturation of the graphite and at temperatures in the range 200 to 350 °C by a relation of the type

$$\frac{\partial c}{\partial t} = D\left(\frac{\partial^2 c}{\partial r^2} + \frac{1}{r}\frac{\partial c}{\partial r}\right),$$

providing the diffusion coefficient D is assigned several values for concentrations of occluded $FeCl_3$ above and below a critical concentration. The value of the latter was found to be about two-thirds the saturation concentration of $FeCl_3$ in graphite, this value apparently being the point at which open hexagonal packing of intercalated ferric ions is complete and a closer hexagonal packing commences. Values of the activation energies of occlusion for concentrations above and below two-thirds saturation were found from the relations of corresponding values of diffusion coefficients to temperature. The small difference between these activation energies which were of the order of 2 to 3 kcal is attributed to a cancelling of effects, thus the energy necessary to separate carbon lamellae in early stages of occlusion is offset in later stages by hindrance imposed on diffusing molecules by those already occluded. Reduction of particle size of graphite accelerated the occlusion of $FeCl_3$.

I. Introduction

The complexes which are formed when graphite is heated with anhydrous $FeCl_3$ are typical lamellar compounds of carbon. As the name suggests, these compounds owe their existence to the ability of graphite to occlude various other substances (Br, O, Rb, Cs, and some anions) in the spaces between the carbon layer planes of which it is composed. However, the graphite-$FeCl_3$ complexes are of particular interest because they may have useful applications in connection with the chemical processing of minerals, as, for example, in the removal of iron from the chlorination products of ferruginous bauxites, which has been discussed by one of us in a previous paper (Croft 1952). The examination and development of these possible applications, however, require a thorough knowledge of the properties of graphite-$FeCl_3$ complexes and also of the processes by which they are formed. Although the properties and structures of the complexes have been studied in considerable detail by several investigators whose work is reviewed below, no previous attempts have been made to elucidate their formation processes.

* Division of Industrial Chemistry, C.S.I.R.O., Melbourne.

The expansion of graphite which occurs when this substance reacts with anhydrous $FeCl_3$ was first observed by Thiele (1932) and later was investigated by Rüdorff and Schulz (1940) who found that the phenomenon was due to the formation of layer lattice-type compounds in which single planes of ferric chloride molecules occupy the interlamellar spaces of the graphite crystal. It was shown that the complex obtained by heating graphite with $FeCl_3$ at temperatures between 200 and 309 °C contains 72 per cent. $FeCl_3$ after excess of the latter reactant is removed by sublimation. They also claimed that another complex is obtained when the reaction is conducted at temperatures between 325 and 409 °C. After separation of unreacted $FeCl_3$ by sublimation this second complex contained 31–37 per cent. $FeCl_3$. The remarkable stability of both complexes is evident from the fact that extraction with any of a number of solvents only reduces the amounts of $FeCl_3$ in each from 72 and 31–37 per cent. to 56 and 31 per cent. respectively. The $FeCl_3$ remaining in either complex after solvent extraction cannot be recovered by the action of boiling aqueous acids or alkalis. However, heating to above 500 °C expels all the $FeCl_3$ as such from both complexes. X-ray diffraction patterns obtained by Rüdorff and Schulz (1940) showed that, although the carbon layer planes of the graphite crystal are moved apart, they are not disrupted by penetration of $FeCl_3$ molecules into the spaces between them. The patterns also revealed that the complex prepared at temperatures below 309 °C $FeCl_3$ is intercalated in all interlamellar spaces of the graphite crystal, whereas the complex prepared in the range 325 and 409 °C contains $FeCl_3$ only in every third space. X-ray examination conducted by Wooster (1937) and Rüdorff and Schulz (1940) indicated that the $FeCl_3$ molecules occluded in these interplanar spaces are arranged in an orderly manner both relative to each other and to the carbon atoms in the layer planes above and below them. However, the X-ray data do not determine the actual arrangement of the ferric chloride in the planes. A good summary of the X-ray data is given by Riley (1945).

The present paper describes investigations of the mechanism by which $FeCl_3$ is intercalated in graphite and gives an account of studies on the kinetics of formation of graphite-$FeCl_3$ complexes. An investigation of the equilibria between complexes, graphite and $FeCl_3$ under various conditions, is being conducted at present.

II. Experimental

The South Australian graphite which was used in these experiments has been shown by Mathieson (personal communication 1952) to consist of well-developed crystals possessing the same structure as Ceylon and Madagascar graphites. It was obtained in a pure state from flotation concentrates by treating the latter with concentrated HCl and HF alternately until the ash content was reduced to less than 0·5 per cent. This purified material was then ground and screened, fractions between 208 and 295μ and 43 and 74μ being retained.

Anhydrous $FeCl_3$ was prepared from analytical reagent grade iron wire by direct reaction with dry chlorine.

(*a*) *Preparation and Treatment of Reaction Tubes*

Each reaction tube was prepared as follows: A 2-ft length of Pyrex glass tubing, 0·5 in. internal diameter, was constricted at points 3 and 11 in. from one end. A weighed sample of graphite was introduced into the compartment formed by these constrictions and a weighed quantity of iron wire was pushed into the middle of the longer open section of the tube. Dry chlorine gas was passed through the loaded tube at room temperature until all air had been displaced. The section of the tube containing iron wire was then heated to 300 to 350 °C. This temperature was low enough to avoid the formation of $FeCl_2$, but $FeCl_3$ formed readily and sublimed into the graphite compartment which protruded from the furnace. When chlorination was complete, the section of the tube containing graphite and sublimed $FeCl_3$ was sealed-off under vacuum. The volume of all tubes was between 28 and 30 ml.

Reaction tubes were heated in an electric muffle for definite times at pre-selected temperatures which were controlled to within $\pm 0{\cdot}5$ °C. In order to reduce temperature gradients in the muffle and to facilitate the rapid removal of tubes, the latter were slid into mild steel tubes set horizontally in the side of a box of the same material. The open ends of the tubes, of which there were 12, projected $\frac{1}{4}$ in. and were covered by an asbestos-lined metal lid hinged to the top of the box which was filled with flake graphite. Rapid withdrawal of reaction tubes was effected by means of fine wires attached to them before heating.

After heating, unreacted $FeCl_3$ was separated from the graphite-$FeCl_3$ complex either by washing with hydrochloric acid or by sublimation. In the first method hot N HCl was used and washing on a vacuum filter was continued until the filtrate showed no reaction with NH_4CNS. The complete effectiveness of washing in this manner is confirmed by the fact that only very small amounts of $FeCl_3$ could be further extracted by prolonged digestion of washed complexes with 6N HCl.

Separation by sublimation was effected by tapping the contents to one end of the reaction tube and inserting that end in a tube furnace controlled at the temperature of formation for the complex and fitted with a mild steel lining tube. Free $FeCl_3$ sublimed in the end of the reaction tube projecting from the furnace. Graphite-$FeCl_3$ complexes which had been separated from unreacted $FeCl_3$ by sublimation were also acid washed as described above in order to determine absorbed $FeCl_3$.

(*b*) *Velocity of Sorption*

In experiments to determine the rate of intercalation of $FeCl_3$ at various temperatures, 0·5 g samples of graphite were used in each reaction tube. The weight of iron wire chlorinated in each case was 0·8 to 0·9 g. Theoretically the yield of $FeCl_3$ should have been five times the weight of graphite, but losses due to $FeCl_3$ being carried on by the gas stream reduced this ratio to 4 to 1. The temperatures selected for these tests, namely 200, 250, 285, 300, and 350 °C, cover most of the range in which preliminary tests showed that $FeCl_3$ is readily intercalated in graphite to form stable complexes. They also extend over two

ranges, namely, 200 to 309 °C and 309 to 350 °C, in which according to Rüdorff and Schulz (1940) two complexes of different composition are formed. The amounts of $FeCl_3$ occluded in graphite after different periods of heating at each of the above temperatures were determined analytically and the data obtained used to construct the curves in Figure 1.

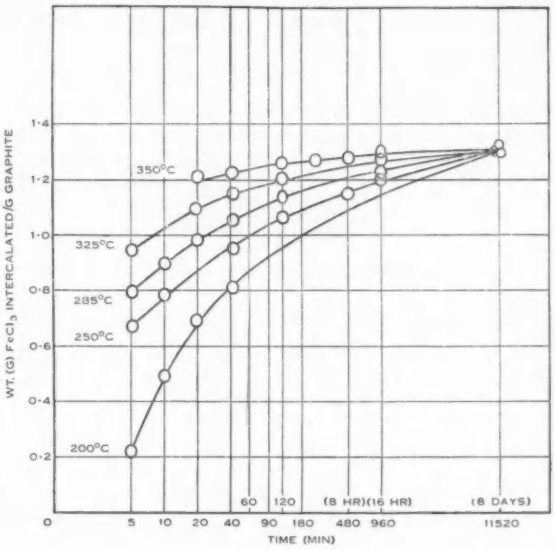

Fig. 1.—Rate of sorption of $FeCl_3$ in graphite in relation to time and temperature.

(c) *Effect of Particle Size of Graphite on Sorption Rate*

This was determined by heating 1 g samples of two different size fractions of the graphite with 3 to 4 g of $FeCl_3$ for various periods. All reactions were conducted at 250 °C. The two samples of graphite used were those in which the average particle sizes were 250 and 60μ respectively. The results of these experiments are shown graphically in Figure 2.

(d) *Analytical Methods*

The $FeCl_3$ in the complex was determined in the following manner. A weighed sample, previously dried to constant weight at 110 °C, was heated slowly to 600 °C in a stream of hydrogen chloride in a tube furnace and was maintained at that temperature for 20 min. Most of the $FeCl_3$ evolved during heating sublimed into a section of the analysis tube projecting from the furnace. Small amounts of $FeCl_3$ carried on by the gas stream were trapped in bubble towers, packed with glass beads and containing water. The analysis was terminated by decreasing the furnace temperature to 300 °C and flushing the

apparatus with dry nitrogen. The silica boat was then withdrawn, cooled, and reweighed. The $FeCl_3$ sublimate was dissolved in hot N HCl and combined with the contents of the bubble towers. Iron was determined in the usual manner by reduction with $SnCl_2$ and subsequent titration with standard $K_2Cr_2O_7$ solution.

Results obtained by this method agreed closely with those obtained by the Rüdorff and Schulz (1940) method which consisted of fuming samples to dryness with concentrated H_2SO_4 then ashing and determining iron in the residual ash.

The losses in weight of samples caused by heating complexes in hydrogen chloride were several per cent. higher than the amount of $FeCl_3$ found by either

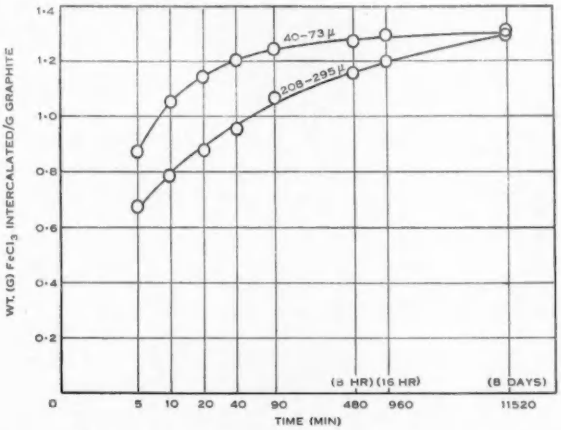

Fig. 2.—Effect of particle size of graphite on rate of sorption of $FeCl_3$.

of the analytical methods described above. Since the products obtained by heating washed complexes at temperatures below 200 °C in sealed glass tubes were found to consist mainly of water, these differences are attributed to the presence of small amounts of water in the samples. It was found possible to reduce the amount of this impurity by drying samples *in vacuo* over concentrated H_2SO_4 for long periods, or by oven drying of samples for several days. However, although both methods of drying reduced the associated water to 1 per cent. and sometimes less, it was never eliminated.

Each result shown in Figures 1 and 2 is a mean of four experiments for which the analytical data agreed to within 2 per cent.

III. Interpretation

The nature of the problem and of the results suggest that the reaction must be governed to a large extent by the rate of diffusion of ferric chloride into the interlamellar spaces of the graphite. The graphite particles are roughly disk-shaped, and the diffusion takes place only between the graphite layer planes.

The problem is therefore geometrically equivalent to one of diffusion into an infinite cylinder. Attempts to describe the data with a diffusion coefficient independent of concentration failed, as the reaction proceeded more rapidly in the early stages and more slowly in the final stages than could be predicted on such a basis. Factors other than diffusion (surface energy barriers etc.) would be expected to limit the reaction more in the early stages when diffusion is rapid than in the final stages when it is slow, and so could not explain these discrepancies. It was therefore assumed that the diffusion coefficient varied in some way with concentration. The actual mode of variation assumed is set out below.

(*a*) *Diffusion Coefficient Independent of Concentration*

The boundary value problem is

$$\frac{\partial c}{\partial t}=D\left(\frac{\partial^2 c}{\partial r^2}+\frac{1}{r}\frac{\partial c}{\partial r}\right),$$

$$c=0, \quad a>r\geqslant 0, \quad t=0,$$

$$c=c_0, \quad r=a, \qquad t>0.$$

The solution is (Carslaw and Jaeger 1947)

$$c/c_0=1-2\sum_{n=1}^{\infty}\exp\,(-\beta_n^2\theta)J_0(r\beta_n/a)/\beta_n J_1(\beta_n)$$

$$=F(r/a,\,\theta),$$

where β_n are the roots of $J_0(\beta)=0$, and $\theta=Dt/a^2$.

For the amount Q adsorbed at time t this gives

$$\frac{Q}{Q_\infty}=g(\theta), \quad \ldots\ldots\ldots\ldots\ldots\ldots\ldots \quad (1)$$

where

$$g(\theta)=1-4\sum_{n=1}^{\infty}\exp\,(-\beta_n^2\theta)/\beta_n^2.$$

The function $g(\theta)$ is plotted in Figure 3.

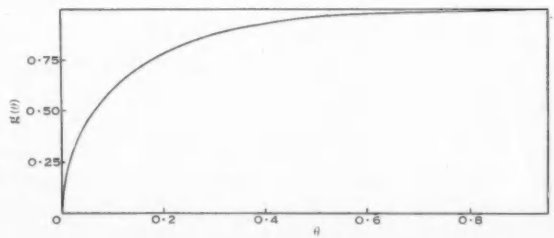

Fig. 3.—Function $g(\theta)$ for diffusion into cylinder.
$Q/Q_\infty=g(Dt/a^2)$.

In Table 1 we show values for Q/Q_∞ as determined experimentally at 200 °C compared with those calculated from equation (1). The constant D/a^2 was determined to give exact agreement at 90 min. The calculated values are too low in the early stages and too high in the later stages, showing that equation (1) does not give a satisfactory description of the data. The fact that the graphite particles are not all the same size would tend to remove this discrepancy, but in fact the possible range of particle sizes is too small to have an appreciable effect.

TABLE 1

COMPARISON OF EXPERIMENTAL VALUES WITH VALUES CALCULATED ASSUMING SINGLE DIFFUSION CONSTANT

Temperature, 200 °C; $D/a^2 = 0{\cdot}00166$

Time (min) ..	5	10	20	40	60	90	120	180	480	960
$Q/Q\infty$ (expt.) ..	0·169	0·377	0·531	0·623	0·665	0·705	0·735	0·769	0·838	0·885
$Q/Q\infty$ (calc.) ..	0·196	0·242	0·378	0·505	0·602	0·705	0·781	0·877	0·983	1·00

(*b*) *Diffusion Coefficient has a Constant Value* $D = D_1$ *up to a Certain Concentration* c_1, *and then Drops to a Lower Constant Value* $D = D_2$ *for* c *Greater than* c_1

The boundary value problem is

$$\frac{\partial c}{\partial t} = D_1\left(\frac{\partial^2 c}{\partial r^2} + \frac{1}{r}\frac{\partial c}{\partial r}\right), \qquad \text{when } c < c_1;$$

$$\frac{\partial c}{\partial t} = D_2\left(\frac{\partial^2 c}{\partial r^2} + \frac{1}{r}\frac{\partial c}{\partial r}\right), \qquad \text{when } c > c_1;$$

$$c = 0 \qquad a > r \geqslant 0, \qquad t = 0,$$

$$c = c_0 \qquad r = a, \qquad t > 0.$$

$D\partial c/\partial r$ is continuous.

An approximate solution of this problem, valid when $D_1 \gg D_2$, is

$$c/c_0 = xF(r/a,\ D_1t/a^2) + (1-x)F(r/a,\ D_2t/a^2),$$

$$Q/Q_\infty = xg(D_1t/a^2) + (1-x)g(D_2t/a^2), \quad \ldots\ldots\ldots\ldots\ (2)$$

where $x = c_1/c_0$ and the functions F and g are those already defined.

In equation (2) there are three constants, x, D_1/a^2, and D_2/a^2, to be determined from the experimental data. Since $D_1 \gg D_2$, $g(D_1t/a^2)$ is equal to unity in the later stages of the reaction. Thus x and D_2/a^2 were determined from the last few measurements at a given temperature—actually one guessed a value of x and calculated a value for D_2/a^2 from each of the last few points, choosing finally the value of x which made D_2/a^2 most nearly constant. Having determined x and D_2/a^2, D_1/a^2 was determined from one earlier point—actually the 20 min point was used in each case.

Table 2 shows values of the constants determined in this way for graphite of average particle size 250 μ. In Table 3 values of Q/Q_∞ calculated from equation (2) with these values of the constants are compared with the measured values. The agreement is reasonable except for the shortest times. For these times the heating and cooling lags are comparable with the reaction time, and the latter therefore becomes uncertain. The effect of factors other than diffusion (supply of ferric chloride vapour to the graphite, saturation of the graphite surface) would be relatively greater for these times.

TABLE 2

VALUES OF CONSTANTS

Temperature (°C)	x	D_2/a^2 (min^{-1})	D_1/a^2 (min^{-1})
200	0·66	0·000137	0·00860
250	0·75	0·000145	0·0133
285	0·81	0·000184	0·0159
325	0·87	0·000216	0·0206
350	0·93	0·000265	0·0300

(c) *Effect of Particle Size*

With smaller graphite particles the reaction proceeded more rapidly. For graphite of average particle size 60 μ, at 250 °C an attempt was made to determine constants as above. The results were $x=0\cdot75$ (the same value as for the larger particles); $D_1/a^2=0\cdot00052$ (3·6 times the value for the larger particles, whereas one would have expected about 20 times that value); no value could be found for D_1/a^2 (since $g(D_1t/a^2)$ was required to be greater than 1, which is impossible). Thus this theory does not describe quantitatively the effect of particle size. No pure diffusion theory could do this, for however the diffusion coefficient varies with concentration the time to reach a given concentration ought to be proportional to the square of the particle diameter, and this is not so. Thus Table 4 gives the ratios of the times required for large and small particles to reach specified concentrations; on a pure diffusion theory the ratio ought to be constant and equal to the square of the ratio of particle diameters, or about 20. The discrepancies may be due to differences of particle size distribution or surface roughness between the two samples. On the other hand they may indicate that with the small particles, when diffusion is rapid, the supply of ferric chloride is limited by some other factor, as, for example, rate of evaporation. In what follows we consider only graphite particles in a single size range (250 μ).

(d) *Effect of Temperature*

The logarithms of D_2/a^2 and D_1/a^2 are plotted against the reciprocal of the absolute temperature in Figures 4 and 5. The slopes of these plots correspond to activation energies of 3·1 kcal/mole for $c<c_1$, and 2·7 kcal/mole for $c>c_1$. The parameter x, or c_1/c_0, increases in linear fashion with temperature (Fig. 6).

TABLE 3

COMPARISON OF MEASURED AND CALCULATED QUANTITIES

Temperature (°C)	200		250		285		325		350	
t (min)	Q/Q_∞ (expt.)	Q/Q_∞ (calc.)	Q/Q_∞ (expt.)	Q/Q_∞ (calc.)	Q/Q_∞ (expt.)	Q/Q_∞ (calc.)	Q/Q_∞ (expt.)	Q/Q_∞ (calc.)	Q/Q_∞ (expt.)	Q/Q_∞ (calc.)
5	0·169	0·297	0·514	0·398	0·607	0·458	0·719	0·540		
10	0·377	0·403	0·598	0·628	0·663	0·603	0·783	0·705		
20	0·531	0·531	0·670	0·671	0·748	0·750	0·833	0·834	0·920	0·922
40	0·623	0·654	0·728	0·773	0·805	0·829	0·871	0·887	0·932	0·946
60	0·665	0·704	0·762	0·793	0·824	0·849	0·886	0·901	0·943	0·949
90	0·705	0·735	0·793	0·813	0·847	0·864	0·903	0·909	0·951	0·952
120	0·735	0·752	0·812	0·821	0·866	0·870	0·915	0·914	0·957	0·956
180	0·769	0·771	0·835	0·835	0·885	0·881	0·925	0·922	0·964	0·961
480	0·838	0·833	0·881	0·880	0·924	0·919	0·951	0·949	0·970	0·976
960	0·885	0·889	0·920	0·923	0·939	0·953	0·965	0·973	0·989	0·989

IV. Discussion

The above description in terms of a diffusion coefficient which changes abruptly to a smaller value at a certain value of the concentration seems to fit the experimental data quite well. In connection with similar problems Barrer

Table 4

RATIOS OF TIMES TAKEN BY LARGE PARTICLES AND BY SMALL PARTICLES TO REACH SAME CONCENTRATION

Q (g $FeCl_3$/g graphite) ..	0·9	1·0	1·05	1·1	1·2
$t(48–65)/t(300–375)$ ..	4·3	7·9	10·7	16·4	24·0

(1944, 1948) has discussed a picture in which the diffusion constant falls off linearly with concentration. Since the diffusion equation has not been solved, even approximately, for this case, and since our picture appears to have equal

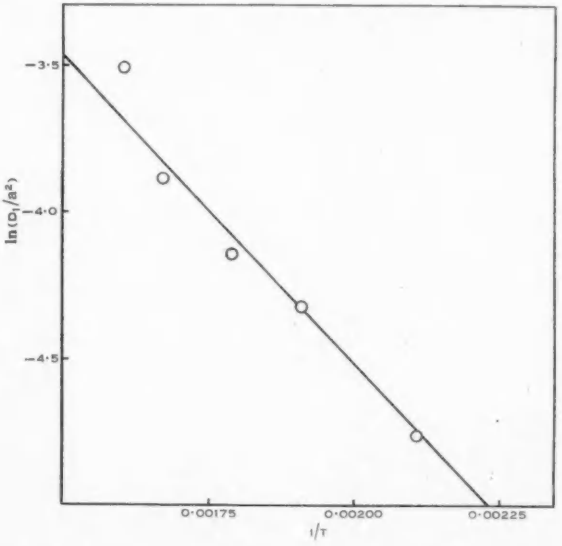

Fig. 4.—Temperature dependence of diffusion coefficient for low concentrations.

a priori appeal, we have not chosen to follow Barrer's picture. Some further considerations indicate that our picture is a reasonable one.

Having regard to the composition of the complex, the most probable structure is that shown in Figure 7, in which the ferric chloride occupies the points marked *A* and *B*. This structure gives one ferric chloride molecule to

$10\frac{2}{3}$ carbon atoms; the observed composition is about 1 to 10·2. Because of repulsive forces one might expect a tendency for the open hexagonal arrangement

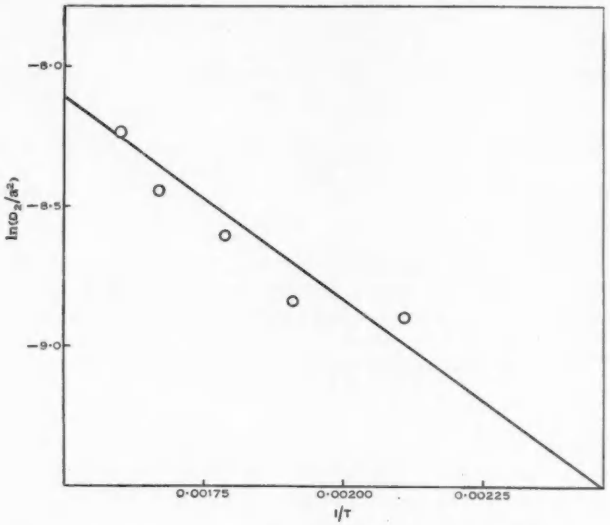

Fig. 5.—Temperature dependence of diffusion coefficient for high concentrations.

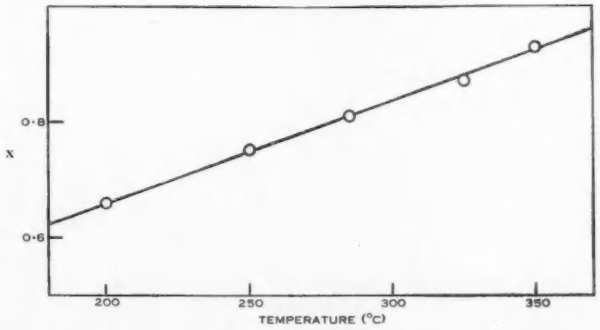

Fig. 6.—Temperature dependence of concentration c_1 at which diffusion coefficient changes ($x = c_1/c_0$).

indicated by the *A*-sites to fill first, the *B*-sites filling afterwards to give a close-packed hexagonal arrangement. There are twice as many *A*-sites as *B*-sites,

so that the A-lattice would fill when two-thirds of the final amount of $FeCl_3$ was intercalated.*

Thus if there is to be a change of diffusion coefficient one would expect it to occur when about two-thirds of the final amount of $FeCl_3$ is taken up, or rather more at higher temperatures since the preference for A-sites will then be less marked. This is just the behaviour we have found.

The activation energies for low concentrations (3·1 kcal) and high concentrations (2·7 kcal) differ surprisingly little. It may be that there is cancelling

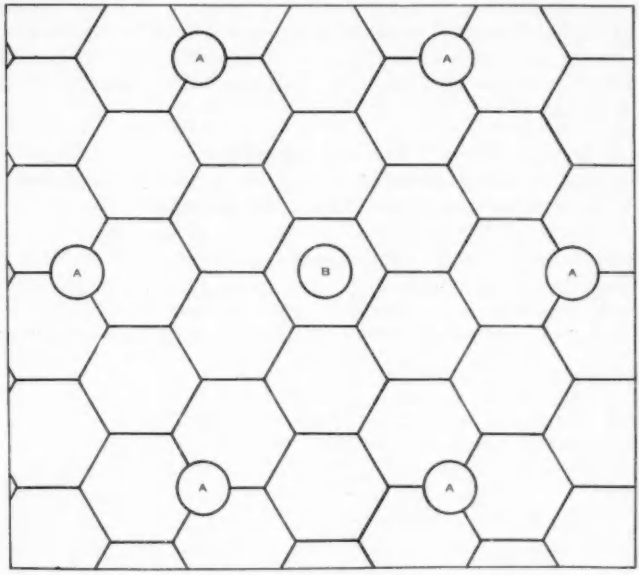

Fig. 7.—Suggested structure of graphite-$FeCl_3$ complex.

of two effects, since the early arrivals must force apart the graphite layer planes, and the later arrivals must squeeze between their predecessors. The large drop in diffusion constant is apparently due to a change in the probability factor, rather than a change in activation energy.

Investigation of the kinetics of sorption was limited to the range corresponding to 50 to 100 per cent. saturation of graphite, because of the high rate of occlusion of $FeCl_3$ at temperatures between 250 and 350 °C. Thus it was not possible to heat graphite-$FeCl_3$ mixtures for periods of less than 5 min owing to the fact that heating and cooling time lags became relatively large and could not be neglected even when the quantities of reactants were made small. Although

* There is one B-site for every hexagon on the A-lattice, each A-site is counted in three hexagons, and each hexagon involves six A-sites, and therefore there are two A-sites per B-site.

conducting experiments at temperatures below 200 °C would, because of the slower rates of diffusion at these temperatures, have permitted investigation of the initial stages of sorption, the small vapour pressure of $FeCl_3$ in this region would probably not have maintained saturation of graphite surfaces.

It is of interest to note that the fully intercalated complexes obtained with South Australian graphite contain 56–57 per cent. $FeCl_3$. This agrees with the composition of other complexes prepared below 310 °C, by Rüdorff and Schulz (1940) from a variety of graphites of natural and artificial origin. The fact, however, that complexes prepared from South Australian graphite at 350° C. after acid washing, also contain the same proportion of $FeCl_3$ suggests that Rüdorff and Schulz's method of removing unreacted $FeCl_3$ by sublimation partly decomposes the complex prepared at this temperature and explains why they found only 31 to 37 per cent. $FeCl_3$ in complexes which they prepared in the range 310 to 410 °C.

V. Acknowledgments

The authors wish to thank Dr. M. Winfield for helpful discussion, particularly in connection with the adsorption of $FeCl_3$ on graphite.

VI. References

Barrer, R. M., and Ibbetson, D. A. (1944).—*Trans. Faraday Soc.* **40**: 207.
Barrer, R. M., and Riley, D. W. (1948).—*J. Chem. Soc.* **1948**: 141.
Carslaw, H. S., and Jaeger, J. C. (1947).—"Conduction of Heat in Solids." (Oxford Univ. Press.)
Croft, R. C. (1952).—*J. Appl. Chem.* **2**: 557.
Riley, H. L. (1945).—*Fuel Lond.* **24**: 43.
Rüdorff, W., and Schulz, H. (1940).—*Z. Anorg. Chem.* **245**: 121.
Thiele, H. (1932).—*Z. Anorg. Allg. Chem.* **207**: 340.
Wooster, N. (1932).—*Z. Kristallogr.* **83**: 35.

A SYNTHESIS OF *O*-METHYLCRYPTAUSTOLINE IODIDE

By G. K. HUGHES,* E. RITCHIE,* and W. C. TAYLOR*

[*Manuscript received March* 12, 1953]

Summary

Two optically active forms of *O*-methylcryptaustoline iodide, one of them identical with the methyl ether of the natural alkaloid, have been synthesized.

I. INTRODUCTION

In a previous communication (Ewing *et al.* 1953) it was shown that cryptaustoline (I) and cryptowoline (II), the alkaloids of the bark of *Cryptocarya bowiei* (Hook.) Druce, were laevorotatory forms of simple ethers of dehydrolaudanosoline. Dehydrolaudanosoline itself was originally obtained by Robinson and Sugasawa (1932) and by Schöpf and Thierfelder (1932) by the oxidation of optically inactive laudanosoline and it should be noted that in the ring closure the nitrogen atom becomes asymmetric. The latter authors remarked that the oxidation proceeded so readily and smoothly that derivatives of dehydrolaudanosoline could reasonably be expected to occur naturally. It was therefore of

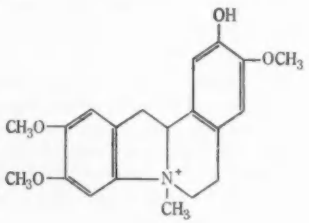

(I)

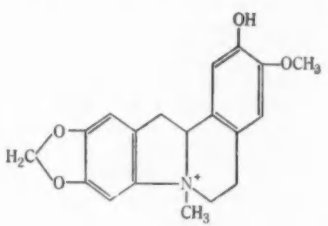

(II)

interest to examine the oxidation of *d*- and *l*-laudanosolines. It was found that *d*-laudanosoline hydrobromide obtained from *d*-laudanosine, gave on oxidation and complete methylation, optically pure *l*-cryptaustoline methyl ether, identical with the substance obtained from the natural alkaloid, whilst *l*-laudanosoline gave optically pure *d*-cryptoaustoline methyl ether. It is evident that in the ring closure the configuration of the asymmetric carbon atom determines the configuration of the nitrogen atom in the dehydrolaudanosoline, and this provides some support for Schöpf and Thierfelder's conjecture.

The identity of the synthetic product was established by comparison with material prepared from the natural alkaloid and by degrading each to the same

* Department of Organic Chemistry, University of Sydney.

laevorotatory methine-I and to the same optically inactive methine-II. Further an equimolecular mixture of the synthetic *d*- and *l*-methine-I was optically inactive and identical with methine-I prepared from optically inactive dehydrolaudanosoline.

II. Experimental

Melting points are uncorrected. Analyses are by Dr. K. W. Zimmerman, C.S.I.R.O. Microanalytical Laboratory.

(*a*) *Resolution of* dl-*Laudanosine.*—The base, synthesized by standard methods, was resolved by a modification of the method of Pictet and Athanasescu (1900). Laudanosine (14·1 g) and *l*-quinic acid (7·9 g) were dissolved in ethanol (15 c.c.) and ether added until a faint turbidity developed. On standing, and more readily on seeding, *l*-laudanosine quinate separated in clusters of leaflets. After three recrystallizations from ethanol-ether the product (7·1 g) had m.p. 132 °C (Pictet and Athanasescu give m.p. 120 °C). By decomposition with alkali in the usual way *l*-laudanosine was obtained and recrystallized from aqueous alcohol. It (4·1 g) had m.p. 89 °C, $[\alpha]_D^{24}$ −110±4° (*c*, 0·3 in ethanol). Pictet and Athanasescu recorded $[\alpha]_D^{15}$ −105° (*c*, 3 in ethanol).

By the addition of more ether to the mother liquor the salt of the *d*-base was obtained as long fibrous needles, which after two recrystallizations from ethanol-ether had m.p. 81–82 °C (yield 7·5 g). This salt was deliquescent, losing its crystalline form and changing to a clear glass on standing in air. Pictet and Athanasescu did not obtain it crystalline. On decomposition it gave *d*-laudanosine (4·4 g), m.p. 89 °C, $[\alpha]_D^{24}$ +107±4° (*c*, 0·3 in ethanol). Pictet and Athanasescu reported $[\alpha]_D^{15}$ +106° (*c*, 1·6 in ethanol) for the natural and $[\alpha]_D^{15}$ +98·7° (*c*, 1·86 in ethanol) for the synthetic base.

(*b*) d- *and* l-*Laudanosoline Hydrobromides.*—*d*- and *l*-Laudanosines were demethylated with hydrobromic acid (Schöpf and Thierfelder 1932). The hydrobromides dried overnight at 20 mm over calcium chloride (m.p. 125–128 °C, $[\alpha]_D^{24}$ +48±3° (*c*, 0·3 in water) and m.p. 125–127 °C, $[\alpha]_D^{24}$ −47·5±3° (*c*, 0·3 in water)) were evidently hydrated and were not analysed.

(*c*) d- *and* l-*Tetramethyldehydrolaudanosoline Iodides.*—The oxidations were effected with chloranil (Robinson and Sugasawa 1932) and the crude products methylated directly. *d*-Laudanosoline hydrobromide yielded *l*-tetramethyldehydrolaudanosoline iodide (40% overall) which crystallized from water in colourless rods. After drying overnight at 20 mm over calcium chloride the product had m.p. 80–84 °C, $[\alpha]_D^{28}$ −184±4° (*c*, 0·4 in water). Authentic *O*-methylcryptaustoline iodide recrystallized and dried in the same manner had m.p. 80–84 °C, $[\alpha]_D^{28}$ −186±4° (*c*, 0·4 in water).

The methine-I from the synthetic product formed colourless needles from ethanol, m.p. 101 °C, $[\alpha]_D^{26}$ −213±5° (*c*, 0·1 in ethanol) (Found : C, 71·0 ; H, 7·0 ; N, 4·0%. Calc. for $C_{21}H_{25}O_4N$: C, 71·0 ; H, 7·0 ; N, 3·9%). The methine-I from the natural product had m.p. 101 °C, alone or mixed with the above, $[\alpha]_D^{26}$ −215±5° (*c*, 0·1 in ethanol).

d-Tetramethyldehydrolaudanosoline iodide formed by oxidation of *l*-laudanosoline followed by methylation separated as colourless rods from water, m.p. 80–84 °C, $[\alpha]_D^{28}$ +184±4° (*c*, 0·4 in water). The related methine-I had m.p. 101 °C, $[\alpha]_D^{26}$ +212±5° (*c*, 0·1 in ethanol) (Found : C, 70·8 ; H, 6·8 ; N, 3·9%. Calc. for $C_{21}H_{25}O_4N$: C, 71·0 ; H, 7·0 ; N, 3·9%). When equal quantities of this and the above methine-I from synthetic *l*-tetramethyldehydrolaudanosoline iodide were crystallized from ethanol colourless leaflets, m.p. 126–127 °C, $[\alpha]_D^{26}$ 0° (*c*, 0·1 in ethanol) were obtained, identical with an authentic specimen prepared from optically inactive laudanosine.

The same methine-II, pale lemon prisms from ethanol, m.p. 108 °C, $[\alpha]_D^{26}$ 0° (*c*, 0·1 in ethanol) was obtained from *l*-methine-I, *d*-methine-I, *O*-methylcryptaustoline methine-I, and tetramethyldehydrolaudanosoline methine-I.

III. Acknowledgments

The authors are indebted to Professor A. J. Birch for his interest in this work and to Imperial Chemical Industries of Australia and New Zealand Ltd. for a scholarship awarded to one of them (W.C.T.).

IV. References

Ewing, Jean, Hughes, G. K., Ritchie, E., and Taylor, W. C. (1953).—*Aust. J. Chem.* **6**: 78.
Pictet, A., and Athanasescu, B. (1900).—*Ber. dtsch. chem. Ges.* **33**: 2346.
Robinson, R., and Sugasawa, S. (1932).—*J. Chem. Soc.* **1932**: 789.
Schöff, C., and Thierfelder, K. (1932).—*Liebigs Ann.* **497**: 22.

SHORT COMMUNICATIONS

PREPARATION OF AROMATIC SULPHONYL HALIDES*

By F. E. Jenkins† and A. N. Hambly†

In connection with a study now being made of the properties of sulphonyl halides (Jenkins 1952 ; Ham and Hambly 1953*a*, 1953*b*) a variety of aromatic sulphonyl chlorides and fluorides was required. One possible route for their synthesis involved the conversion of a substituted amine via the sulphinic acid to the sulphonyl chloride or fluoride.

The usual technique for the conversion of aromatic amines to sulphinic acids is that of Gattermann (1899), in which the amine (1 part) in dilute sulphuric acid solution is diazotized, the solution saturated with sulphur dioxide and then 5 to 6 parts of copper powder added with stirring. Several workers have recorded difficulties with this reaction in preparing *m*-substituted sulphinic acids.

Tröger and Hille (1903) found that the saturation of the solution of diazotized *m*-toluidine with sulphur dioxide gave a red precipitate, and practically no sulphinic acid on the addition of copper powder. Silvester and Wynne (1936) obtained a similar red by-product from 2,6-dichloro-*m*-toluidine while Todd and Shriner (1934) obtained only a 21 per cent. yield of *m*-chlorobenzenesulphinic acid, from *m*-chloraniline, compared with an 86 per cent. yield of the corresponding *o*-acid.

Gattermann in his original paper suggested a modification of the above procedure as especially suitable for naphthalene derivatives. We find that this modification, which differs from the preceding merely in the addition of the diazonium sulphate solution to a suspension of copper powder in diute sulphuric acid, which is kept saturated with sulphur dioxide, overcomes the difficulties met by the above workers. The sulphinic acid is readily separated as its insoluble ferric salt, which can then be converted to the sodium salt and halogenated to yield the sulphonyl chloride, bromide, or iodide (Thomas 1909).

The conversion of aromatic sulphonyl chlorides to fluorides by refluxing with excess of a saturated aqueous solution of potassium fluoride (Davies and Dick 1931, 1932) usually gives good yields without special precautions. However, the rate of hydrolysis of the product becomes more rapid when there are electron attracting substituents present (Walker 1950), and a series of experiments in the preparation of *p*-nitrobenzene sulphonyl fluoride showed that an optimum yield of 65 per cent. was obtained after 30 min. For the conversion of high

* Manuscript received March 23, 1953.

† Chemistry Department, University of Melbourne.

melting point, sparingly soluble, sulphonyl chlorides such as *p*-acetamidobenzene sulphonyl chloride to the corresponding fluoride the addition of dioxan to the reaction mixture is advantageous.

Experimental

(*a*) *Preparation of Sulphonyl Chlorides.*—(i) *m-Toluene Sulphonyl Chloride.* Freshly distilled *m*-toluidine (20 g) in sulphuric acid (40 ml H_2SO_4, 200 ml H_2O) was diazotized at 0 °C with sodium nitrite (16 g) in water (80 ml). Copper powder (40 g) was suspended in sulphuric acid (50 ml H_2SO_4, 200 ml H_2O), the mixture saturated with sulphur dioxide, and then the diazonium solution added with vigorous stirring while maintaining a current of sulphur dioxide.

The product was filtered, the insoluble residue washed three times with concentrated ammonia and the washings added to the filtrate which was made just acid to Congo red. Concentrated ferric chloride was then added until no more orange precipitate was formed, the ferric sulphinate filtered off and washed with a little alcohol. In a series of experiments in which the quantity of copper powder was varied from 20–80 g the yield of ferric sulphinate remained between 70 and 79% of the theoretical quantity.

TABLE 1

Substituted Benzene Sulphonyl Fluoride	Physical Constants	Yield (%)	Molecular Weight		
			Calculated	From Hydrolysis*	From Fluoride Estimation†
o-Methoxy- ..	M.p. 39–40 °C	42	190·2	190·1	190·7
m-Methyl- ..	B.p. 78·5–79 °C/1·4 mm, n_D^{25} 1·4909	85	174·3	174·2	173·7
p-Acetamido-‡	M.p. 176 °C	47	217·2	—	218·4
m-Chloro- ..	B.p. 69–70 °C/0·8 mm, n_D^{25} 1·5114	63	194·7	194·0	194·5
m-Bromo- ..	B.p. 90 °C/1 mm, n_D^{25} 1·5358	63	239·1	236·0	238·6
p-Nitro- ..	M.p. 77·5–78·5 °C (corr.)	65	205·2	203·2	204·8

* By back titration after hydrolysis with excess alkali in aqueous dioxan.

† By titration at pH 3 with thorium nitrate of solution from alkaline hydrolysis.

‡ Using aqueous dioxan (40 : 60) as solvent.

The orange precipitate was treated with excess sodium hydroxide solution (2N), the black hydrated iron oxide filtered off (with the aid of " Filtercel ") and the filtrate just neutralized with hydrochloric acid (2N). Chlorine was passed into this solution until no more oily sulphonyl chloride separated, the product was extracted with carbon tetrachloride and the extracts, after washing with water, dried over anhydrous $CaCl_2$. After the removal of the solvent on the water-bath the crude sulphonyl chloride was distilled under reduced pressure to yield *m*-toluene sulphonyl chloride (17·8 g, 50% based on *m*-toluidine), b.p. 77–78 °C/0·3 mm Hg (Found : S, 16·8 ; Cl, 18·7%. Calc. for $C_7H_7O_2SCl$: S, 16·8 ; Cl, 18·6%).

Treatment with concentrated ammonia gave *m*-toluene sulphonamide, m.p. 108·5–109·5 °C (cf. Hollemann and Caland 1911) (Found : N, 8·5 ; S, 18·4%. Calc. for $C_7H_9O_2NS$: N, 8·2 ; S, 18·7%).

(ii) Using the above general method, *o*-methoxybenzene sulphonyl chloride, m.p. 53·5–55 °C, 51% yield ; *m*-chlorobenzene sulphonyl chloride, b.p. 143–144 °C/12 mm Hg, 50% yield ; and *m*-bromobenzene sulphonyl chloride, b.p. 164 °C/14 mm Hg, 54% yield, were prepared.

(*b*) *Preparation of Sulphonyl Fluorides.*—(i) *By the Method of Davies and Dick.* The sulphonyl fluorides shown in Table 1 were prepared by refluxing the corresponding sulphonyl chloride with 100% excess of saturated potassium fluoride solution. The first three compounds have not been reported previously while *m*-chloro- and *m*-bromobenzene sulphonyl fluorides have been prepared only by the Sandmeyer reaction with *m*-aminobenzene sulphonyl fluoride (Steinkopf and Hübner 1934).

(ii) p-*Aminobenzene Sulphonyl Fluoride.*—*p*-Nitrobenzene sulphonyl fluoride (30 g) was reduced with granulated tin (40 g) and concentrated hydrochloric acid (200 ml), the latter being added slowly and the temperature being kept below 50 °C. When all the acid had been added the mixture was kept at 40–45 °C for 30 min and then decanted from residual tin. To the cold solution was added hydrated sodium acetate (450 g), the white precipitate filtered off and extracted with hot alcohol. The sulphonyl fluoride was precipitated from the alcoholic solution by addition of water and crystallized from light petroleum/chloroform as colourless needles, m.p. 72–73 °C (45%).

Acetylation with acetic anhydride in glacial acetic acid gave *p*-acetamidobenzene sulphonyl fluoride identical in m.p. and mixed m.p. with the product from *p*-acetamidobenzene sulphonyl chloride and potassium fluoride.

The authors express their thanks to Mr. G. J. Walker and Mr. J. H. Bradbury for assistance in some of the experimental work.

References

Davies, W., and Dick, J. H. (1931).—*J. Chem. Soc.* **1931** : 2104.
Davies, W., and Dick, J. H. (1932).—*J. Chem. Soc.* **1932** : 483.
Gattermann, L. (1899).—*Ber. dtsch. chem. Ges.* **32** : 1136.
Ham, N. S., and Hambly, A. N. (1953*a*).—*Aust. J. Chem.* **6** : 33.
Ham, N. S., and Hambly, A. N. (1953*b*).—*Aust. J. Chem.* **6** : 135.
Holleman, A. F., and Caland, P. (1911).—*Ber. dtsch. chem. Ges.* **44** : 2504.
Jenkins, F. E. (1952).—Thesis, University of Melbourne.
Silvester, W. A., and Wynne, W. P. (1936).—*J. Chem. Soc.* **1936** : 691.
Steinkopf, W., and Hübner, R. (1934).—*J. prakt. Chem.* **141** : 193.
Thomas, J. (1909).—*J. Chem. Soc.* **95** : 342.
Todd, H. R., and Shriner, R. L. (1934).—*J. Amer. Chem. Soc.* **56** : 1382.
Tröger, J., and Hille, W. (1903).—*J. prakt. Chem.* (ii) **68** : 297.
Walker, G. J. (1950).—Thesis, University of Melbourne.

A NEW SOURCE OF TARAXEROL*

By W. J. Dunstan,† G. K. Hughes,‡ and N. L. Smithson‡

In the course of an examination of *Litsea dealbata* Nees (a member of the family Lauraceae) the dried, milled bark was extracted with ethanol in a Wester extraction apparatus. Small crystals separated from the concentrated alcohol, purification of which gave 0·17 per cent. of colourless needles (I) giving an intense red-violet Liebermann-Burchard test suggesting it may be a triterpene. The molecular weight and analysis of I were consistent with this conclusion and comparison of its physical properties and derivatives showed it to be identical with taraxerol, previously obtained by Burrows and Simpson (1938) from the roots of *Taraxacum officinale* Weber (dandelion). A preliminary note of this finding was made by Dunstan, Smithson, and Hughes (1947). Subsequently, Koller *et al.* (1950) carried out structural investigations on taraxerol and showed that alnulin and tiliadin are identical with it. Skimmiol isolated by Takeda (1941) from *Skimmia japonica* Thunb. was noted by Takeda and Yoshiki (1941) as showing much similarity to taraxerol. The preparation of the ketone, taraxerone, by Koller *et al.* (loc. cit.) and comparison with skimmione (described by Takeda loc. cit.) shows their similar identity is beyond doubt.

Experimental

(*a*) *Isolation.*—The dried, milled bark of *L. dealbata* (5·5 kg) was extracted with 95% ethanol by continuous percolation. Concentration of the extract to small volume caused the separation of small colourless crystals with a small quantity of tarry matter. The crystals were washed with light petroleum, which removed much of the tar, and then recrystallized from light petroleum (chloroform-ethanol mixture 1 : 1 was also suitable) yielding colourless needles of I; (9 g, 0·17%); m.p. 269–270 °C, $[\alpha]_D^{15}$ +4·0° (*c*, 0·85 in chloroform) (Found: C, 84·3; H, 11·5%; M (camphor), 422. Calc. for $C_{30}H_{50}O$: C, 84·4; H, 11·8%; M, 426). Taraxerol has m.p. 269–271 °C, $[\alpha]_D$ 0° (*c*, 1·30 in chloroform) (Koller *et al.* loc. cit.).

(*b*) *Acetylation.*—The acetyl derivative of I was prepared in the usual way from I (0·3 g); acetic anhydride (6 ml); glacial acetic acid (1 ml) and fused sodium acetate (0·5 g) with 2 hr refluxing. Recrystallization from ethanol-benzene mixture (3 : 1) gave colourless needles, m.p. 294–296 °C, $[\alpha]_D^{18}$ +9·1° (*c*, 1·04 in chloroform) (Found: C, 81·8; H, 11·1%. Calc. for $C_{32}H_{52}O_2$: C, 82·0; H, 11·2%). Taraxeryl acetate has m.p. 296–297 °C, $[\alpha]_D^{18}$ +8·4° (*c*, 1·56 in chloroform).

(*c*) *Benzoylation.*—I (0·2 g) was dissolved in dry pyridine (3 ml) and benzoyl chloride (0·5 g) added and the mixture warmed 1 hr on the water-bath. Recrystallization from chloroform-ethanol mixture (1 : 1) gave colourless needles, m.p. 281 °C, $[\alpha]_D^{18}$ +33° (*c*, 0·21 in chloroform) (Found: C, 83·5; H, 10·2%. Calc. for $C_{37}H_{54}O_2$: C, 83·8; H, 10·3%). Taraxeryl benzoate has m.p. 282–284 °C, $[\alpha]_D^{11}$ +35° (*c*, 2·0 in chloroform). The melting points are uncorrected and the data for taraxerol and derivatives are from Burrows and Simpson (loc. cit.) except where noted.

* Manuscript received September 15, 1952.

† School of Applied Chemistry, N.S.W. University of Technology, Broadway, Sydney.

‡ School of Chemistry, University of Sydney.

Thanks are due to Miss J. Fildes and Dr. E. Challen for the semi-micro-analyses and to Mr. L. J. Webb, Division of Plant Industry, C.S.I.R.O., for the supply of plant material.

References

BURROWS, S., and SIMPSON, J. C. E. (1938).—*J. Chem. Soc.* **1938** : 2042.
DUNSTAN, W. J., HUGHES, G. K., and SMITHSON, N. L. (1947).—*Nature* **160** : 577.
KOLLER, E., HIESTAND, A., DIETRICH, P., and JEGER, O. (1950).—*Helv. Chim. Acta* **33** : 1050.
TAKEDA, K. (1941).—*J. Pharm. Soc. Japan* **61** : 117.
TAKEDA, K., and YOSHIKI, S. (1941).—*J. Pharm. Soc. Japan* **61** : 506.

AUSTRALASIAN MEDICAL PUBLISHING CO. LTD.
SEAMER AND ARUNDEL STS., GLEBE, SYDNEY